COMPLEX ZONING PATTERNS AND RARE EARTH ELEMENT VARIATIONS ACROSS TITANITE CRYSTALS FROM THE HALF DOME GRANODIORITE, CENTRAL SIERRA NEVADA, CALIFORNIA

Janelle Elizabeth Bauer

A thesis submitted to the faculty at the University of North Carolina at Chapel Hill in partial fulfillment of the requirements for the degree of Master of Science in the Department of Geological Sciences.

Chapel Hill
2015

Approved by:

Allen F. Glazner

Drew S. Coleman

Larry K. Benninger

ABSTRACT

Janelle Elizabeth Bauer: Complex zoning patterns and rare earth element variations across titanite crystals from the Half Dome Granodiorite, Central Sierra Nevada, California
(Under the direction of Allen F. Glazner)

Titanite is a common accessory phase in igneous rocks and is particularly abundant in the Half Dome Granodiorite of Yosemite National Park, California. Holding a large proportion of trace elements, such as rare earth elements, makes titanite an important phase because of the influence of temperature, pressure, oxygen fugacity, and liquid composition on trace-element partitioning. Equilibrium crystallization and fractional crystallization have been used to explain the distribution of elements in titanite. However, backscattered electron images of titanite reveal complex zoning patterns that correlate with rare earth element concentrations. Transects across the centers of titanite crystals further emphasize the fluctuating chemistry of titanite and its complex crystallization. The geochemical and textural evidence from titanite show that simple fractional crystallization models cannot explain the distribution of rare earth elements throughout the crystals.

ACKNOWLEDGEMENTS

I would like to thank my advisor, Allen Glazner, for his guidance his invaluable assistance. My committee members, Drew Coleman and Larry Benninger, also provided excellent advice. Thank you to Jon Munnikhuis for his assistance with field work, as well as Nick Foster for help with electron microprobe work, and Luca Fedele for help with laser ablation work. This research was supported by the Martin Fund and the Sigma Xi Grant-in-Aid of Research.

TABLE OF CONTENTS

LIST OF TABLES

LIST OF FIGURES

LIST OF ABBREVIATIONS AND SYMBOLS

BSE	backscattered electron
C_i^{melt}	concentration of element *i* in melt
$C_i^{mineral}$	concentration of element *i* in mineral
C_O	concentration in original liquid
C_R	concentration in residual crystals
D_i	partition coefficient of element *i*
d	bulk partition coefficient
F	weight fraction of melt remaining
fO_2	oxygen fugacity
i	element
κ	diffusivity
LA-ICPMS	laser ablation-inductively coupled plasma mass spectrometer
R	correlation coefficient
REE	rare earth element
SEM	scanning electron microscope
TIS	Tuolumne Intrusive Suite
t	time

INTRODUCTION

Accessory minerals make up but a small proportion of igneous rocks, but their significance far outweighs their abundance. Phases such as titanite, monazite, and zircon can hold a significant proportion of trace elements such as rare earth elements (REE), U, Th, and Zr (Gromet and Silver 1983). Intensive parameters such as temperature, pressure, oxygen fugacity (fO_2), and liquid composition influence trace-element partitioning (e.g., Mahood and Hildreth 1983; Green and Pearson 1986; Paterson and Stephens 1992). Therefore, studying how elements are distributed into these accessory phases is important in determining the petrogenesis of igneous rocks.

Titanite is a particularly important accessory phase because of its large appetite for important trace elements such as REE, Y, and Zr (Gromet and Silver 1983) and because of its utility in U-Pb geochronology (Frost et al. 2000). Titanite is a widespread accessory mineral in many silicic igneous rocks (Deer et al. 1982), and is particularly abundant in the Half Dome Granodiorite of Yosemite National Park, California (Fig. 1), where it occurs in euhedral crystals that can reach ~10 mm in longest dimension (Fig. 2). In this study, I investigate the complex zoning patterns found in these crystals.

Partitioning of non-stoichiometric elements between crystals and liquid is governed by the thermodynamics of the relevant exchange reaction and is typically assumed to follow Henry's Law (Watson 1976). Equilibrium crystallization, in which crystals are assumed to freely exchange with the liquid throughout crystallization, and fractional crystallization, where they are immediately removed upon crystallization, are end-members that are commonly used to explain

element partitioning (e.g. Albarede and Bottinga 1972; Whitney and Stormer 1985). In this study I analyzed titanite crystals from the Half Dome Granodiorite to quantify patterns of trace-element variation. The complex zoning patterns and REE concentrations are reflective of the conditions in which they crystallized because of the influence of temperature, fO_2, and melt composition on partitioning of Y, Zr, and REE.

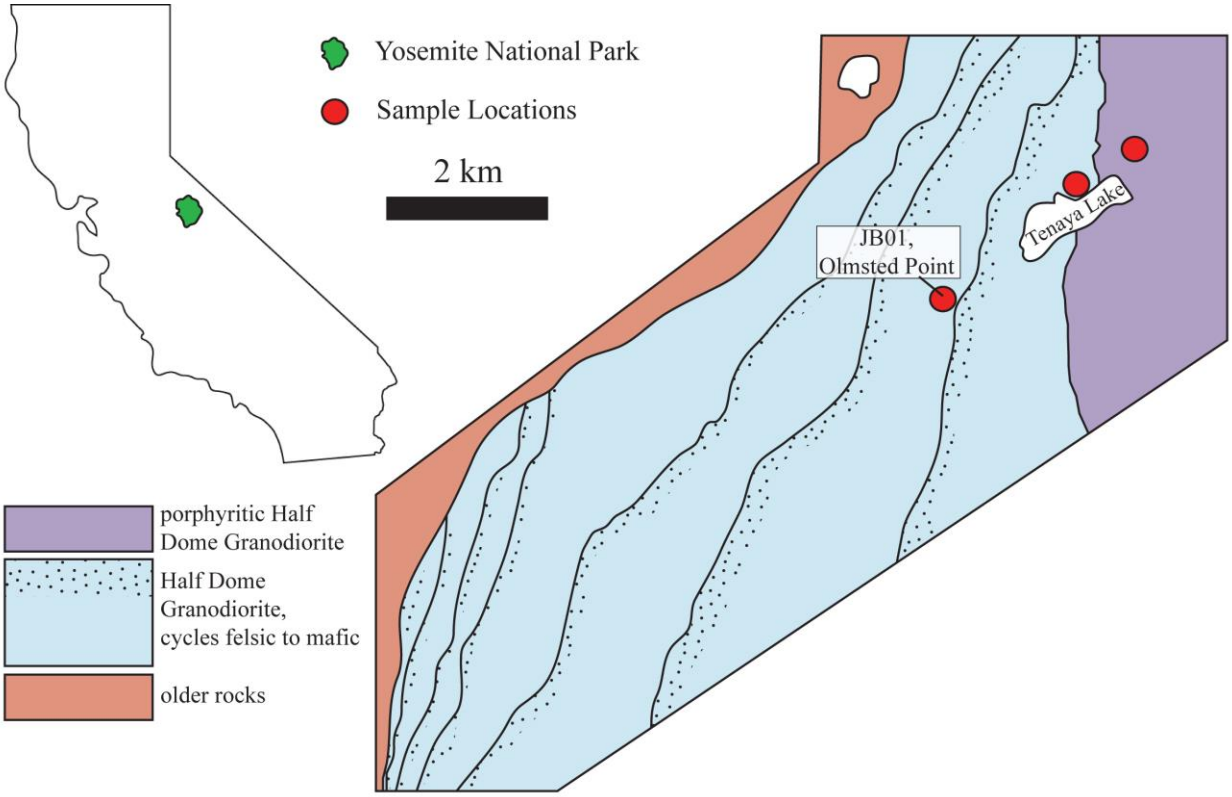

Figure 1. Sample location map, modified from Coleman et al. (2012). All samples were taken from the Half Dome Granodiorite of the TIS in Yosemite National Park, California. Samples from Olmsted Point can be seen in Fig. 2.5. The Half Dome Granodiorite has several cycles, grading felsic to mafic from western contacts.

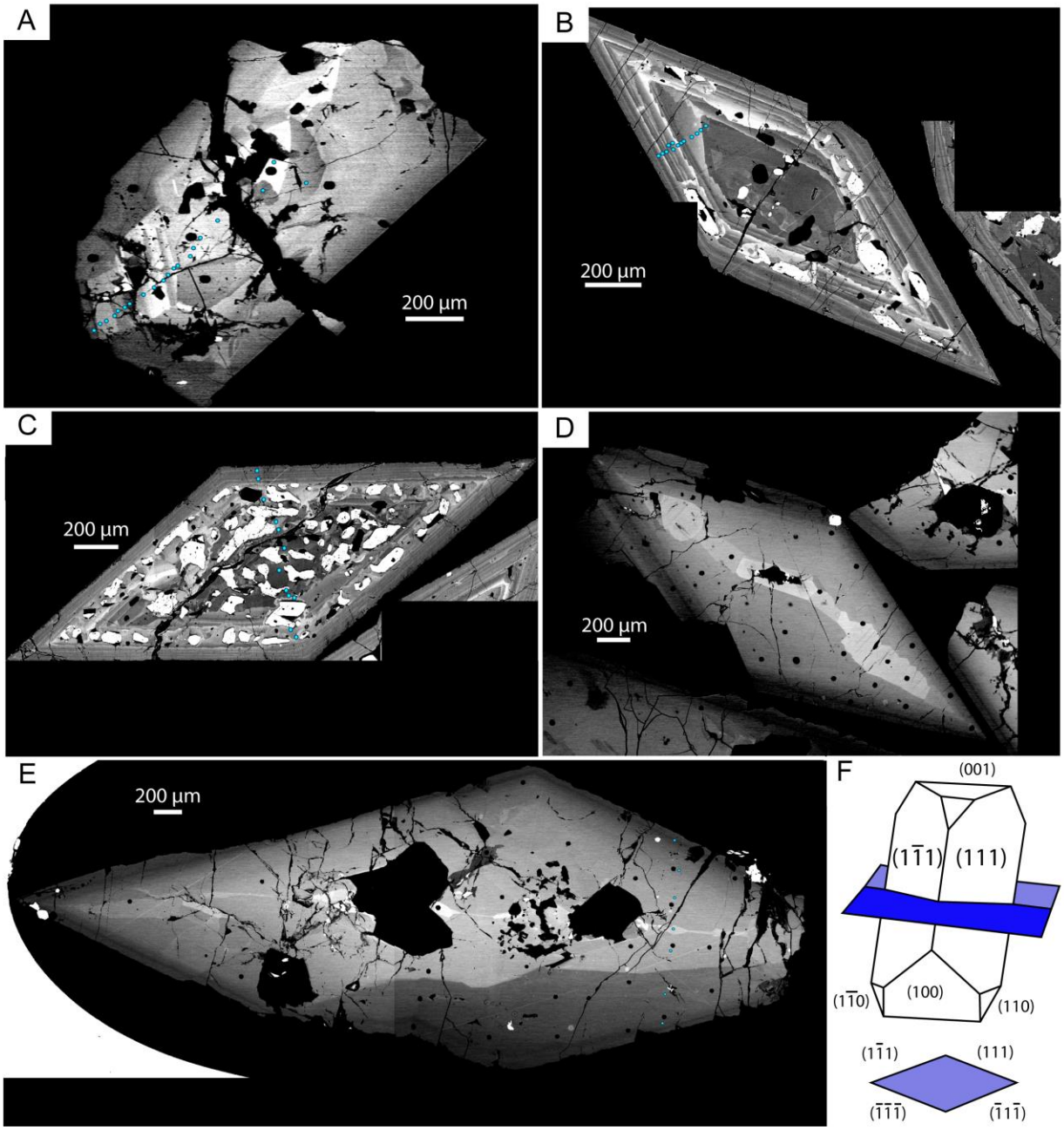

Figure 2. Representative backscattered electron images of titanite crystals, cut through the center, parallel to {111}, from the Half Dome Granodiorite. **a** Titanite crystal shows a bright core, and patchy zoning. There is a small section of oscillatory zoning in the southwest corner. **b** A titanite crystal with a dark center, indicating a depletion in REE. The core is surrounded by concentric, oscillating zones. There are a couple of zones that have inclusions of oxides. There is also slight sector zoning in some of the rings. **c** This titanite crystal has a large relative number of inclusions, mostly oxides (ilmenite, anatase, pyrophanite, and magnetite). There is a dark, patchy core, surrounded by concentric, oscillating zones. **d** Titanite crystal with a bright core (high REE concentration). It is sector zoned, grading to a darker rim. **e** Large (~1 cm along the long axis) titanite crystal that has patchy sector zones. The south edge of the crystal is dark and does not mirror the other side. **f** Crystal drawing modified from Paterson and Stephens 1992, of a typical euhedral titanite, dominated by the {111} form. The cross section shows orientation of titanite a-e.

Partition coefficients

The distribution of an element i between mineral and melt is represented by the partition coefficient (D):

$$D_i = \frac{C_i^{mineral}}{C_i^{melt}} \quad (1)$$

where C is the concentration of an element in weight units. These values are determined experimentally or from natural mineral-glass pairs (McIntire 1963). Phenocryst and groundmass are either analyzed in bulk, homogenizing any differences in chemistry from core to rim (Mahood and Hildreth 1983; Colombini et al. 2011), or spot analyses are averaged (Green and Pearson 1986; Tiepolo et al. 2002; Bachmann et al. 2005). However, mineral/groundmass partition coefficients are not true equilibrium values because disequilibrium zoning in titanite is common (Paterson and Stephens 1992).

Titanite has high partition coefficients for Zr, Y, Hf, and REE, with distinct differences between natural and experimentally grown crystals (Fig. 3a). D values determined for natural samples are extremely high, especially for REE, where they commonly exceed 100 (Bachmann et al. 2005; Ackerson 2011; Colombini et al. 2011); experimentally determined values are typically an order of magnitude lower (Green and Pearson 1986; Tiepolo et al. 2002).

Several factors influence partition coefficients of REE in titanite. D values for REE increase with decreasing temperature, water content of the liquid, and increasing pressure, fO_2, and silica content of the liquid (Mahood and Hildreth 1983; Green and Pearson 1986; Wones 1989). For example, Green and Pearson (1986) showed that in a system with 70 wt % SiO_2 at 7.5 kbar, D_{Sm} increases from ~20 to ~35 as temperature decreases from 1100 to 900 ºC. These parameters affect partition coefficients because they influence melt polymerization and lattice strain in titanite (Mahood and Hildreth 1983; Blundy and Wood 2003; Prowatke and Klemme 2005).

Elements that substitute into the crystal with the least amount of stress are preferred over those elements that are a poorer fit.

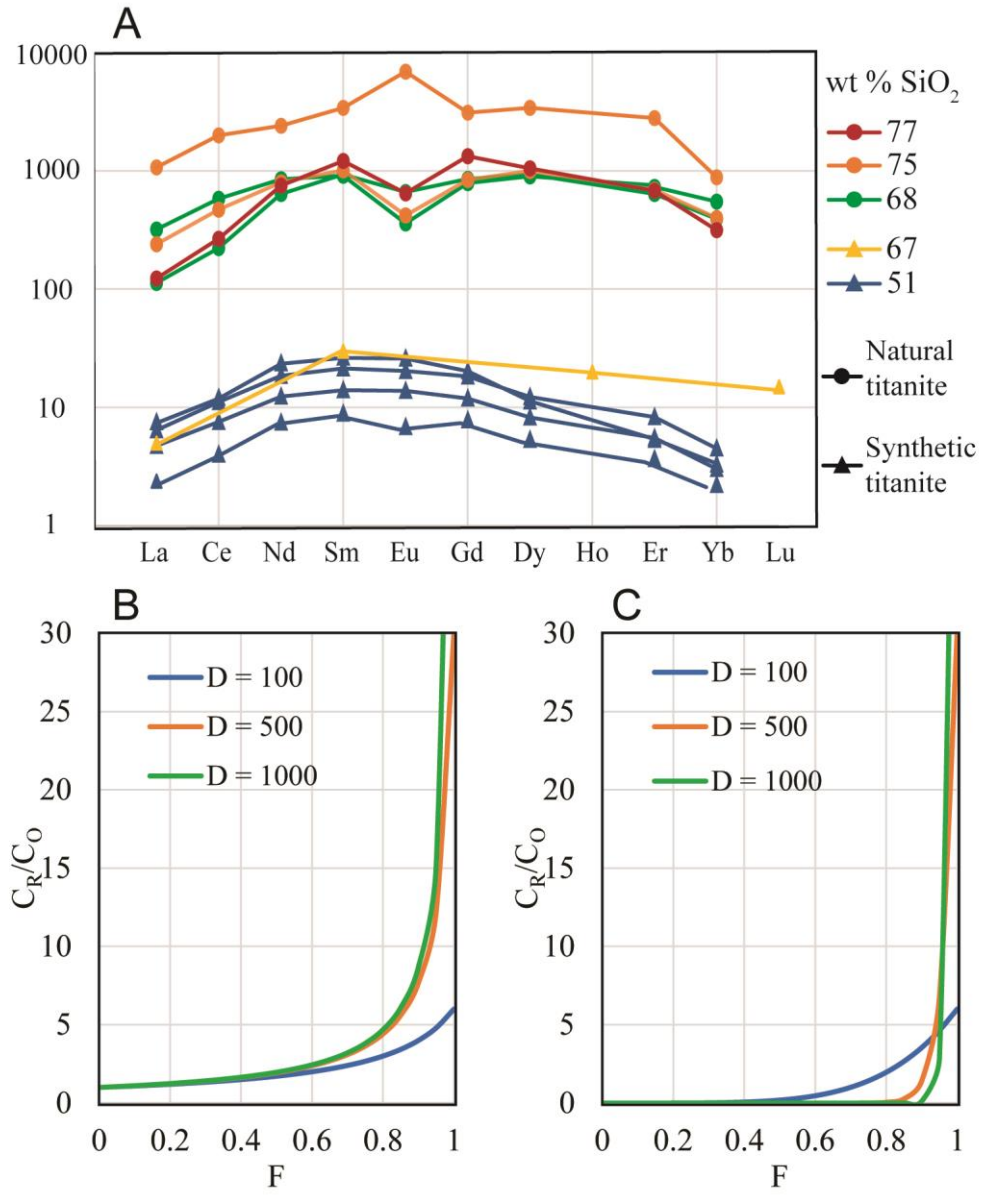

Figure 3. a Representative partition coefficients of REE for titanite determined using natural titanite (Bachmann et al. 2005; Ackerson 2011; Colombini et al. 2011) and synthetic titanite (Green and Pearson 1986; Tiepolo et al. 2002) at various wt % SiO_2. **b** Equilibrium crystallization of a trace element in titanite at D values of 100, 500, and 1000. **c** Fractional crystallization of a trace element in titanite at D values of 100, 500, and 1000. Representative D values were chosen based on average natural titanite partition coefficients (Bachmann et al. 2005; Ackerson 2011; Colombini et al. 2011).

Trace element variation during crystallization

Equilibrium crystallization and fractional crystallization are two end members that model how an element partitions into a solid as the liquid crystallizes. These models assume that the partition coefficients are constant throughout crystallization. Equilibrium crystallization involves complete equilibrium between all phases, and the variation in concentration in the crystals is given by (Rollinson 1993):

$$\frac{C_R}{C_O} = \frac{D}{[D+F(1-D)]} \quad (2)$$

C_R: average concentration of an element in the crystal in weight units

C_O: concentration in the original liquid

F: weight fraction of melt remaining

Fig. 3b shows variations in concentration of a trace element in titanite under equilibrium crystallization at various high D values. Equilibrium crystallization requires that the element have the same concentration throughout the crystal. However, the concentrations of REE are not homogenous throughout titanite crystals (Paterson and Stephens 1992; Piccoli et al. 2000), so this requirement is not met.

Titanite will retain zoning over long periods of time because elements such as REE and Zr diffuse slowly (Fig. 4). An estimate of the length scales over which diffusion can erase zoning is given by characteristic diffusion distance, defined as $\sqrt{\kappa t}$ where κ is diffusivity and t is time. In 1 m.y. at temperatures of 700-800 ºC, these distances are ~1 μm for Nd and ~10-60 μm for Zr, using diffusivity values from Cherniak (2010); thus, these elements are effectively immobile via diffusion over geologic timescales, leading to exquisite preservation of zoning (Fig. 2).

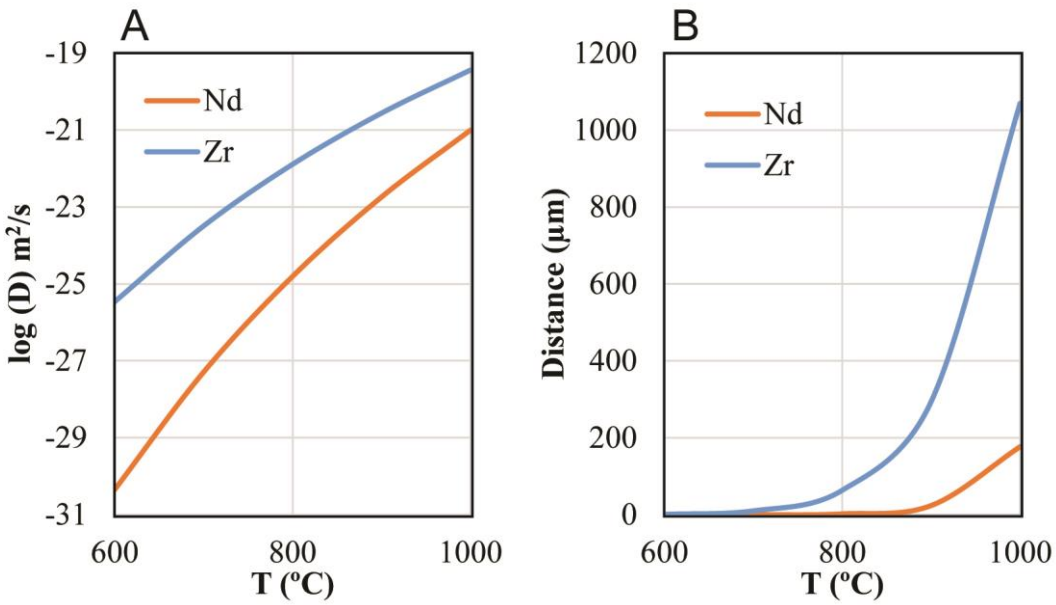

Figure 4. a Diffusivities of Nd and Zr in titanite versus T (modified from Cherniak 2010). **b** Distance (µm) that Nd and Zr will diffuse in 1 m.y. at temperatures of 600-1000 ºC. Diffusivities are from Cherniak (2010).

Fractional crystallization (equation 3) describes the situation where crystals are effectively removed from the site of formation after crystallization (Rollinson 1993), and this process has been used to model situations where only the surface of the crystals is in communication with the melt (Gast 1968).

$$\frac{C_R}{C_O} = DF^{(D-1)} \qquad (3)$$

Fractional crystallization predicts that the concentration of an element with large *D* will decrease drastically after initial crystallization (Fig. 3c)—far faster than during equilibrium crystallization. However, in backscattered electron (BSE) images, titanite shows complex continuous, discontinuous, patchy, oscillatory, and sector zoning (Fig. 2). Because brightness is positively correlated with Fe, Y, Zr, and REE concentration (Paterson and Stephens 1992; Piccoli et al. 2000; this study), such zoning indicates that there is not a dramatic decrease in REE from core-to-rim as predicted by surface equilibrium and fractional crystallization. Clearly,

partitioning of these elements into titanite is more complicated than simple equilibrium or fractional crystallization models can account for.

Crystallization conditions

Titanite is involved in many reactions involving Ti and Ca in igneous rocks. Titanite crystallization is favored by relatively high fO_2 (Lipman 1971; Whitney and Stormer 1985; Nakada 1991), which drives the following reaction to the left (Wones 1989):

$$titanite + magnetite + quartz = hedenbergite + ilmenite + O_2 \quad (4)$$

$$3CaTiSiO_5 + 2Fe_3O_4 + 3SiO_2 = 3CaFeSi_2O_6 + 3FeTiO_3 + O_2$$

Colombini et al. (2011) found that titanite in the Peach Springs Tuff of California and Arizona is commonly found in high-silica glasses (~76 wt % SiO_2) in the presence of quartz, suggesting that it is a late-crystallizing phase. Frost et al. (2000) also suggested that titanite is a late-crystallizing phase in calc-alkaline plutonic rocks that can form during hydration of pyroxene to amphibole. Decreasing temperature and increasing water fugacity drive the following reaction to the left:

$$ferroactinolite + titanite + ulvöspinel = hedenbergite + ilmenite + H_2O \quad (5)$$

In some volcanic rocks, titanite crystals are rimmed with ilmenite, which may indicate mixing with more mafic magma before eruption (Nakada 1991; Colombini et al. 2011). Ilmenite is an indication of decreasing fO_2 and increasing temperature (equations 4 and 5).

Titanite

Titanite is a common primary and secondary accessory mineral in volcanic and plutonic systems. The structure of titanite, which is monoclinic with a $P2_1/a$ space group, influences which elements can be incorporated (Paterson and Stephens 1992). It has TiO_6 corner-sharing octahedral chains and isolated SiO_4 tetrahedra, with bridging 7-fold coordinated Ca polyhedra

(Ribbe 1982; Deer et al. 1982). Ionic radius, charge, and bonding between these elements control element substitution. These properties vary with pressure and temperature, and therefore partition coefficients can change as conditions of crystallization change (Green 1994).

Titanite is dominated by the {111} form, which is parallel to the long axis, and has minor faces that include {001}, {100}, {102}, and {110} (Paterson and Stephens 1992). The distribution of elements into titanite is not equal between forms. Changing melt conditions interfere with crystal-interface kinetics and cause disequilibrium partitioning to occur (Watson and Liang 1995). There is preferential incorporation of Ti, Nb, and REE onto minor {100} forms, and Ca, Al, and Fe on the {111} form (Paterson and Stephens 1992; Green 1994). This causes sector zoning (Fig. 2). Sector zoning is important when considering partition coefficients because elements will not be equally distributed between faces (Paterson and Stephens 1992).

Many elements can substitute into titanite as long as charge balance is maintained. Typical substitutions are listed in Table 1. These substitutions introduce several strong correlations among the elements in typical natural titanite crystals; for example, Paterson and Stephens (1992) found that Ca^{2+} and Ti^{4+} negatively correlate with REE^{3+} and Y^{3+}.

Table 1. Site specific substitutions and coupled substitution in titanite (Sahama 1946; Smith 1970; Coombs et al. 1976; Higgins and Ribbe 1976; Deer et al. 1982; Paterson and Stephens 1992; Piccoli et al. 2000; Olin and Wolff 2012).

Site	Substituting Elements
Ti	Mg, Al, Fe^{3+}, Fe^{2+}, V, Cr, Nb, Sn, Mo, Ta, W
Ca	Na, Sr, Mn, Ba, REE
Si	Al
O	OH, F, Cl
$2Ti^{4+}$	$(Al^{3+}, Fe^{3+}) + (Nb^{5+}, Ta^{5+})$
$Ti^{4+} + O^{2-}$	$(Al^{3+}, Fe^{3+}) + (OH^{-}, F^{-})$
$Ca^{2+} + Ti^{4+}$	$Na^{+} + (Nb^{5+}, Ta^{5+})$ $(REE^{3+}, Y^{3+}) + (Al^{3+}, Fe^{3+})$

Half Dome Granodiorite

The Half Dome Granodiorite (Fig. 1) is a member of the Late Cretaceous Tuolumne Intrusive Suite (TIS) of Yosemite National Park, California (Bateman 1992). The TIS becomes progressively younger inward and was emplaced from about 95-85 Ma (Coleman et al. 2004). The Half Dome Granodiorite is one of the five mapped units of the TIS and was emplaced from about 93-89 Ma. Coleman et al. (2012) interpreted cyclic compositional layering in the granodiorite to reflect migration of late-stage silicic liquids during repeated episodes of emplacement. Titanite is an important accessory phase in the TIS and is particularly prominent in the Half Dome Granodiorite, which is well exposed in the glaciated terrain of Yosemite National Park.

METHODS

Seven samples were collected from the granodiorite in three locations (Fig. 1). Samples were reduced by a jaw crushing into pieces no more than a few cm across. Individual large, intact, euhedral titanite crystals were removed from the crush, mounted in specific orientations (generally perpendicular to the {111} faces) in epoxy, and polished through to their centers so that all sections show full core-to-rim variation. A Tescan VEGA 5130 scanning electron microscope (SEM) was used for BSE imaging.

A JEOL JXA-8530F electron microprobe (EMP) at Fayetteville State University was used for additional BSE imaging and for analysis of major elements, Zr, La, Ce, Nd, and Gd. REE were standardized using rare earth orthophosphate Smithsonian Microbeam Standards (Jarosewich 2002); Zr and Hf were standardized with zircon. Operating conditions included an accelerating voltage of 15 kV, a probe current of $7x10^{-8}$ A, and beam diameter of 1 µm. Data were reduced using ZAF correction. An Agilent 7500ce ICPMS and 193 nm Geolas laser ablation inductively coupled mass spectrometry system (LA-ICMPS) at Virginia Polytechnic Institute and State University were used to analyze major elements as well as REE using glass standard NIST SRM 610 and a spot size of 24 µm. Reproducible and accurate results have been demonstrated using SRM 610 and this instrument (Heinrich et al. 2003). Spot locations for EMP and LA-ICPMS were chosen in order to acquire data for all BSE brightness levels—to see differences in light versus dark areas and to examine compositional differences within zones of the same brightness. Several transects across grains were also mapped to examine core-to-rim variations. BSE brightness values (256-level grayscale, with 0 as black and 255 as white) for all

spot locations were determined by SEM. ICPMS data were reduced using AMS data reduction software (Mutchler et al. 2008).

RESULTS

BSE images

Titanite crystals cut through their centers from the Half Dome Granodiorite display complex continuous, discontinuous, oscillatory, and sector (fir-tree) zoning in BSE (Fig. 2). Different crystals from the same sample display highly variable zoning patterns and varying proportions of inclusions (Fig. 5; see supplementary material for full set of crystal images). In most crystals, bright patchy zones and sector zones dominate the core and are surrounded by darker rims. Small-scale oscillatory zones rim some crystals but are not as prevalent. Individual crystals contain ~5-40 vol% inclusions of other minerals (Fig. 6) including oxides (magnetite; ilmenite with anatase or rutile and pyrophanite), K-feldspar, plagioclase, quartz, allanite, apatite, zircon, and biotite—all the significant minerals in the rock except hornblende. Some inclusions have dark BSE zones around their borders (Fig. 6b). Inclusions tend to be in the cores of crystals, but some crystals have oxides near or at the rim. In some crystals, ilmenite occurs around oscillatory zoned rims as small inclusions.

Titanite in situ in probe sections from Gray (2003), not necessarily cut through their centers, do not show any significant patterns. Euhedral crystals are seen neighboring plagioclase, K-feldspar, quartz, biotite, hornblende, and oxides (see supplementary material for images). Oscillatory zoning and sector zoning is seen in crystals bounded by all of these phases, as well as varying proportions of inclusions.

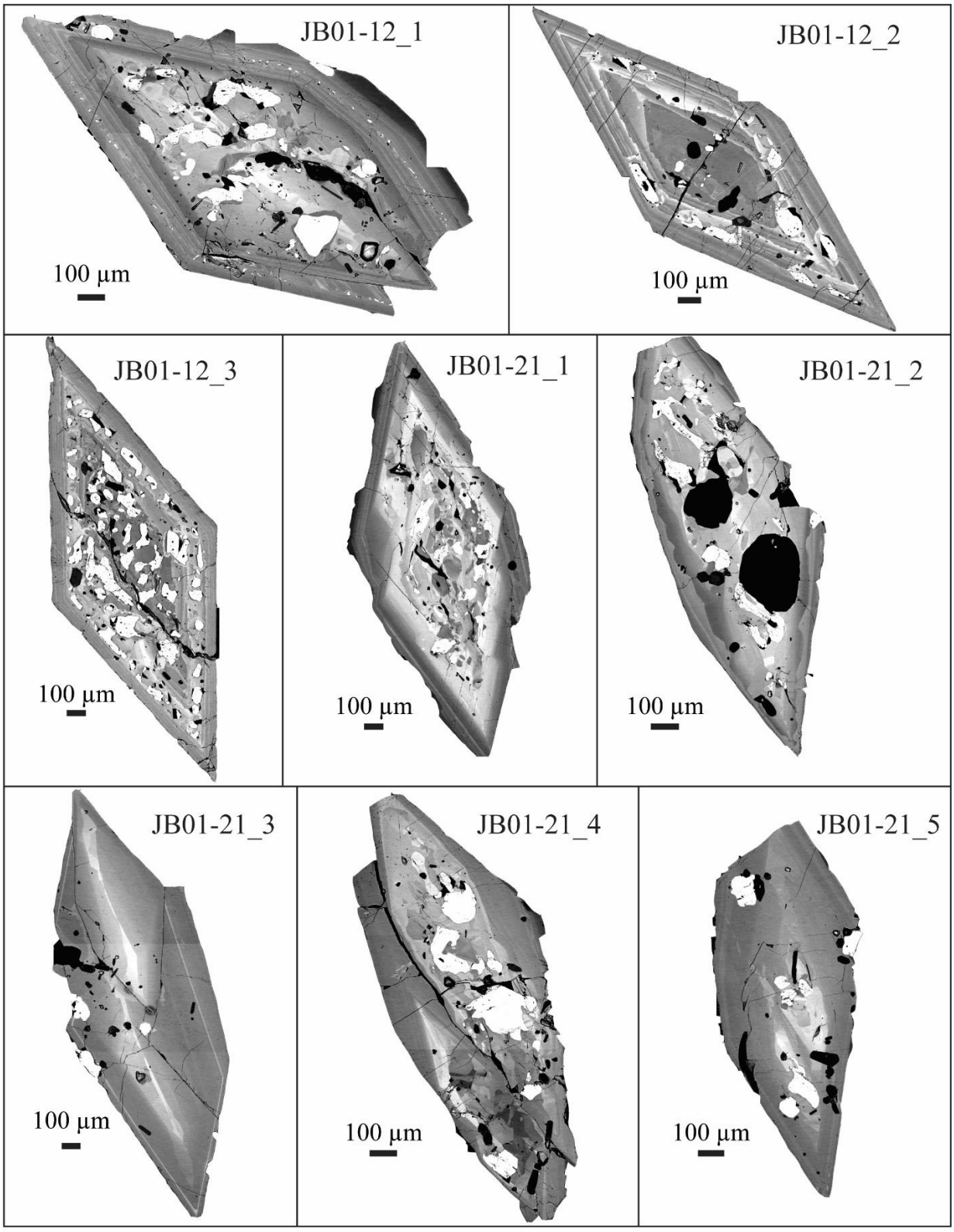

Figure 5. BSE images of titanite crystals from the same sample JB01 (located at Olmsted Point, Yosemite National Park, see Fig. 1). Crystals are parallel to the {111} form and cut through the center. They show varying levels of inclusions and different zoning patterns.

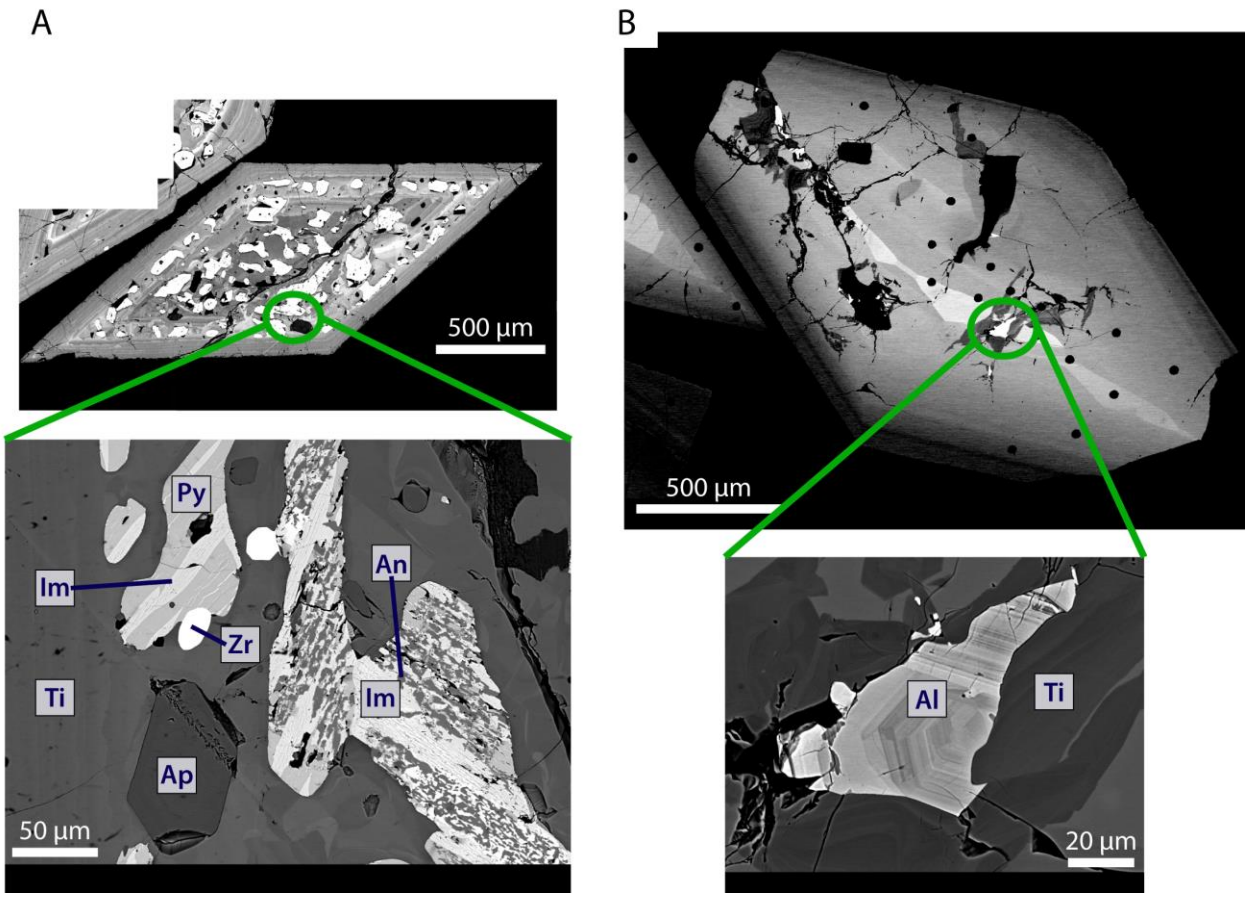

Figure 6. Titanite (Ti) crystals from the Half Dome Granodiorite can have up to ~40 % inclusions of other minerals. These minerals include: ilmenite (Im), anatase (An), zircon (Zr), pyrophanite (Py), apatite (Ap), allanite (Al), magnetite biotite, hornblende, quartz, K-feldspar, and plagioclase. **a** This titanite has ~40 % inclusions. In the inset image, ilmenite is altering to anatase and pyrophanite. It also has inclusions of apatite and zircon. **b** This titanite crystal has ~20 % inclusions. Large inclusions of quartz and feldspars appear black in BSE. The inset image shows a highly zoned allanite inclusion, with a dark zone around its border.

Compositional zoning

Several major trace elements were analyzed with both an EMP and LA-ICPMS on the same crystals. These data are in general agreement with each other, although EMP analyses of Gd have poor precision (Fig. 7). Fig. 8 shows the correlation matrix between major element oxides, trace elements, and brightness. Mg and Al are negatively correlated with Ti and Ca, and positively correlated with Fe, Ce, Pr, Nd, Gd, and brightness. Elements that substitute into titanite, such as Fe and REE, are negatively correlated with Ca and Ti (Table 1). Scatterplots

(Fig. 9) show strong positive correlations between Mg, Al, Fe, and brightness; Ca and Ti show strong negative correlations with Mg, Al, Fe, and brightness.

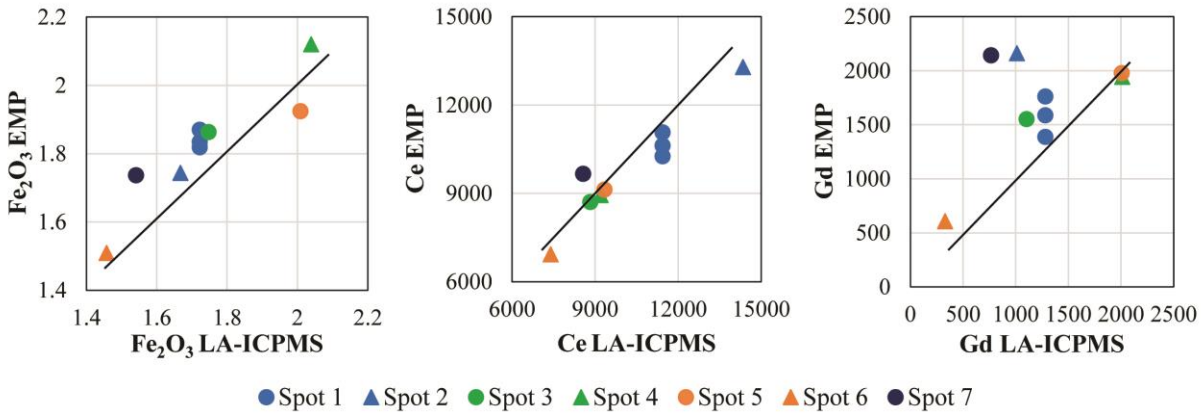

Figure 7. Comparison of LA-ICPMS and EMP data for three elements. In each Fe_2O_3 (wt %), Ce (ppm), and Gd (ppm) were analyzed with LA-ICPMS and EMP on the same titanite crystals, near the same spots. Analyses for most elements are consistent between instruments. Scatter in Gd is probably a result of poor counting statistics and low signal/background with EMP analyses. Diagonal 1:1 lines are shown.

	Na_2O	MgO	Al_2O_3	SiO_2	CaO	TiO_2	MnO	Fe_2O_3	Y	Zr	La	Ce	Pr	Nd	Gd	Brightness
Na_2O	1.00															
MgO	0.17	1.00														
Al_2O_3	0.01	0.63	1.00													
SiO_2	-0.07	-0.37	-0.27	1.00												
CaO	-0.43	-0.65	-0.55	0.11	1.00											
TiO_2	-0.22	-0.64	-0.75	0.02	0.71	1.00										
MnO	-0.38	0.24	0.03	-0.03	0.08	-0.06	1.00									
Fe_2O_3	0.00	0.70	0.81	-0.30	-0.60	-0.85	0.22	1.00								
Y	0.36	0.67	0.69	-0.42	-0.82	-0.72	-0.09	0.64	1.00							
Zr	0.16	0.33	0.20	-0.23	-0.42	-0.37	0.03	0.42	0.27	1.00						
La	0.28	0.21	-0.02	-0.17	-0.38	-0.30	-0.03	0.30	0.09	0.84	1.00					
Ce	0.40	0.61	0.36	-0.34	-0.76	-0.65	-0.01	0.62	0.59	0.47	0.65	1.00				
Pr	0.40	0.69	0.54	-0.42	-0.85	-0.74	-0.02	0.70	0.80	0.69	0.64	0.85	1.00			
Nd	0.42	0.74	0.63	-0.45	-0.89	-0.78	-0.03	0.71	0.93	0.40	0.34	0.82	0.92	1.00		
Gd	0.38	0.67	0.65	-0.43	-0.81	-0.70	-0.07	0.61	0.99	0.27	0.09	0.58	0.79	0.94	1.00	
Brightness	0.40	0.52	0.39	-0.24	-0.72	-0.67	-0.07	0.56	0.69	0.43	0.43	0.72	0.77	0.78	0.69	1.00

Figure 8. Correlation matrix of major oxides (wt %), trace elements (ppm), and brightness (grayscale values 0-255, 0 = black, 255 = white). Positive correlations are in red and negative correlations are in blue. There are high positive correlations between the trace elements and Fe_2O_3. There are strong negative correlations with CaO, TiO_2 and the trace elements.

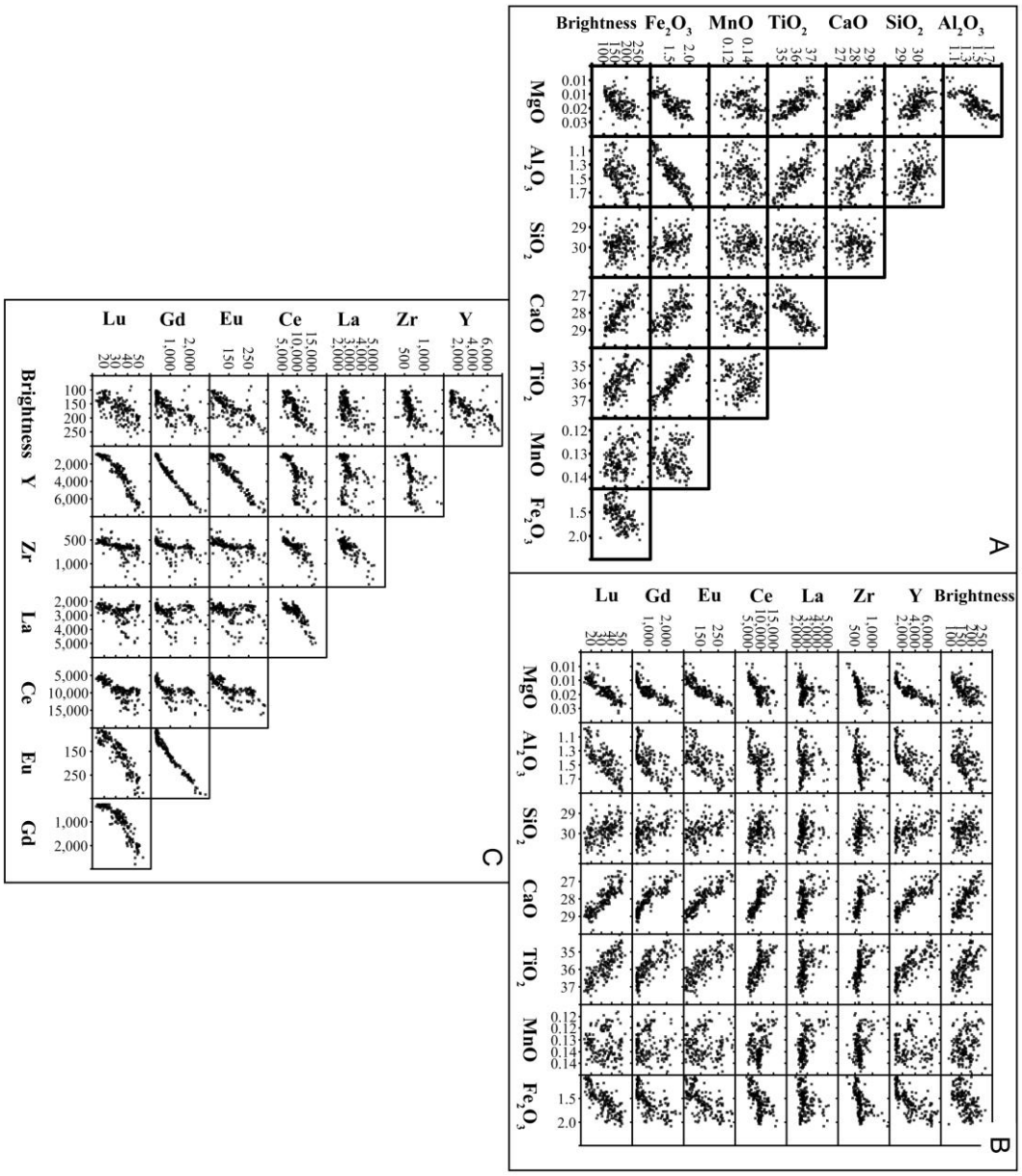

Figure 9. a Major element oxide analyses (wt %) from LA-ICPMS and brightness from BSE images show strong positive and negative correlation with each other. There is no correlation between SiO_2 and CaO, TiO_2, and MnO. **b** Trace element analyses (ppm) from LA-ICPMS and brightness from BSE images show some very strong positive correlations among the REE. Eu, Gd, and Y are strongly positively correlated with each other. **c** Major oxides (wt %) and trace elements (ppm) from LA-ICPMS are compared to one another.

Compatible trace elements Y, Zr, and REE show little correlation with Si. Al, Fe, and brightness are all positively correlated, and Ca and Ti negatively correlated, with Zr, Y, and the REE. The REE are mostly positively correlated with one another and brightness. La and Ce are

not as correlated as the middle REE and Y with each other. Y is highly positively correlated with the REE, with an average correlation coefficient (*R*) of ~0.9. Zr is also positively correlated with the REE, but weakly, with an average *R* of ~0.3. Brightness is largely a function of Fe, Y, and REE concentration (Fig. 10); higher concentrations of these elements yields brighter zones in BSE. Owing to strong positive correlations among these elements, it is not possible to sort out their relative contributions to brightness variations.

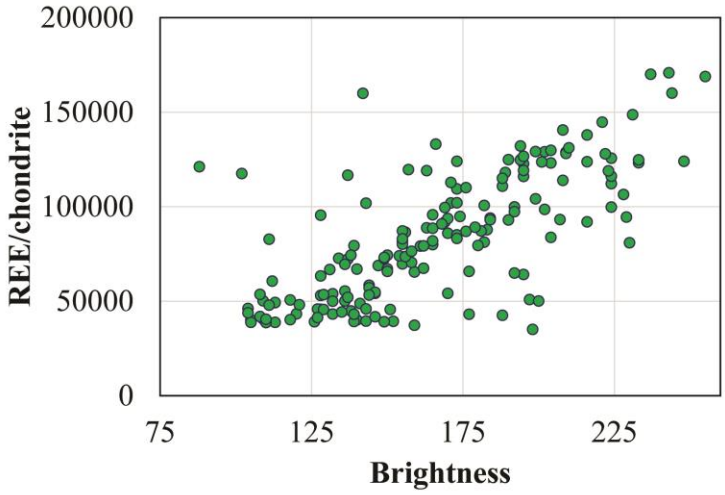

Figure 10. 173 LA-ICPMS spot analyses show that there is a strong positive correlation between brightness in BSE and the sum of all REE.

Chondrite-normalized (Sun and McDonough 1989) REE data are highly variable (Fig. 11a) with light REE reaching concentrations of ~10,000-20,000 times chondrite, declining to ~500-3000 times chondrite for heavy REE. Concentrations of all REE in a single crystal typically decrease by a factor of ~2 from core to rim, consistent with a general core-to-rim darkening in BSE.

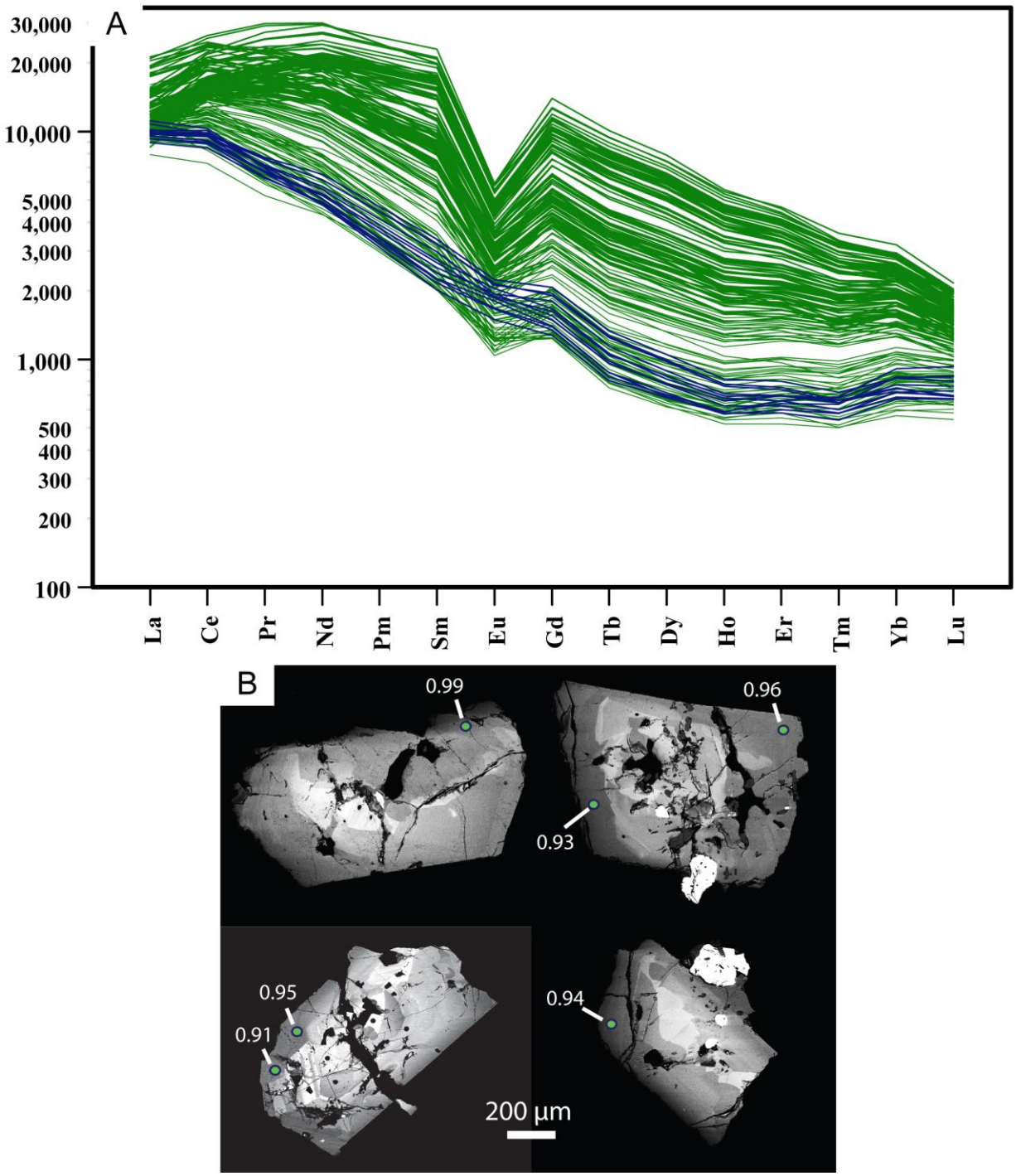

Figure 11. a Chondrite-normalized REE patterns (Sun and McDonough 1989) from LA-ICPMS analyses with a 24 µm spot size. Light REE reach concentrations of ~10,000x chondrite, declining to ~1,000x chondrite for heavy REE. Most patterns have a negative Eu anomaly (shown in green), but there are 27 titanite analyses with a flat Sm-Eu-Gd profile (shown in blue). **b** The BSE images show 4 titanite samples that have high Eu/Eu* values. All such spots are in dark, depleted zones around crystal rims.

Several transects across titanite crystal zones and within zones were analyzed by EMP (Fig. 12). Titanite crystals chosen for these transects have variable zoning patterns, but REE concentrations are highly correlated with brightness. Most crystals have cores that are relatively enriched in REE, Zr, and Y (Fig. 12 a, c-e). However, some crystals with dark cores have REE-depleted centers (Fig. 12 b and f). From core to rim, changes in REE concentrations mimic the BSE zoning pattern of the crystal; e.g., crystals with oscillatory BSE zoning have transects with oscillatory concentrations of REE. Within each transect, Fe, Zr, Y, La, Ce, Nd, and Gd followed the same trends, with higher concentrations on brighter spots (Fig. 12). Si and Ca are negatively correlated with La, Ce, Nd, Gd, and Fe. The REE and Y are more tightly correlated than Fe and Zr in all transects.

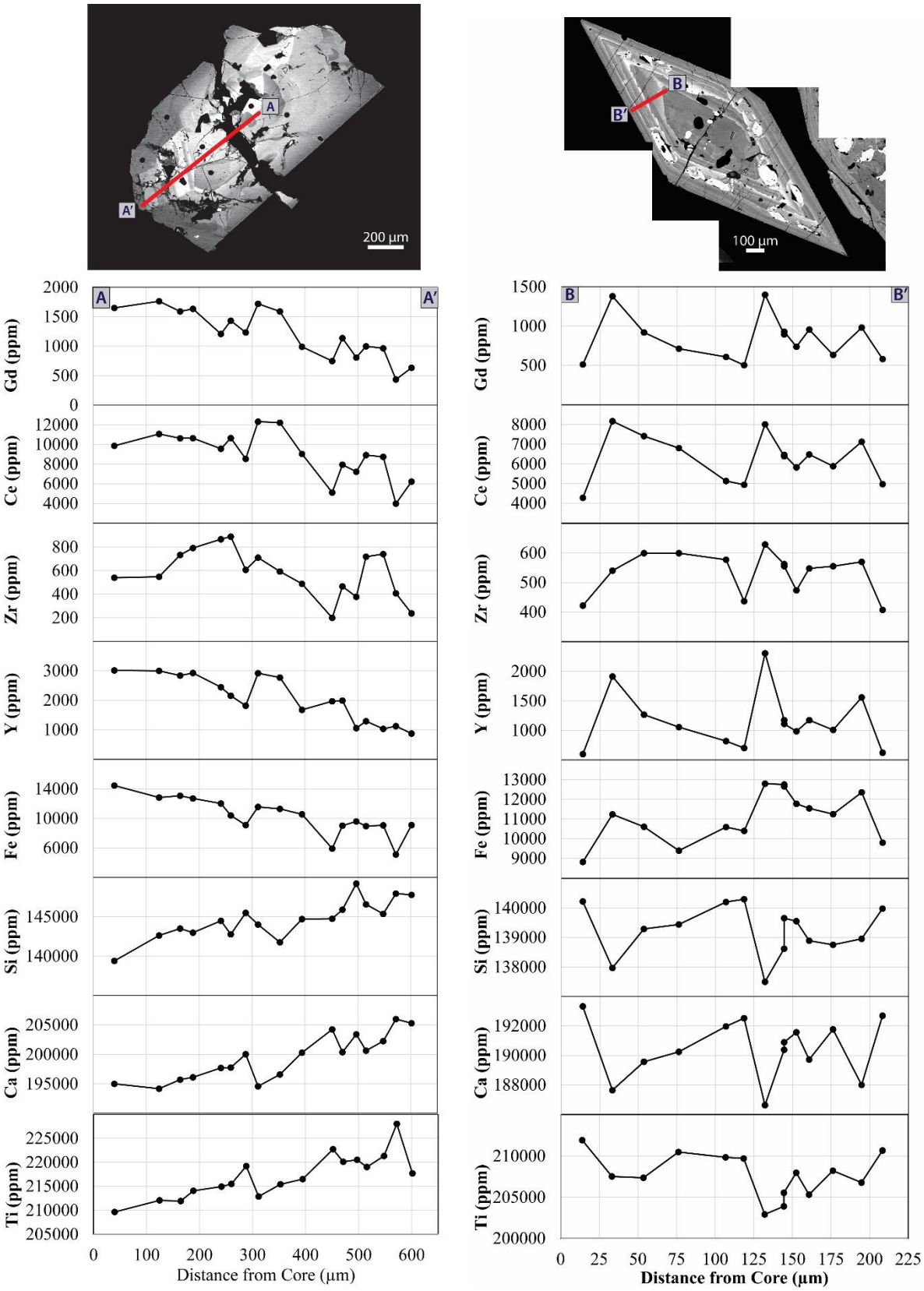
A
A′
200 µm
B
B′
100 µm
Gd (ppm)
Ce (ppm)
Zr (ppm)
Y (ppm)
Fe (ppm)
Si (ppm)
Ca (ppm)
Ti (ppm)
Distance from Core (µm)

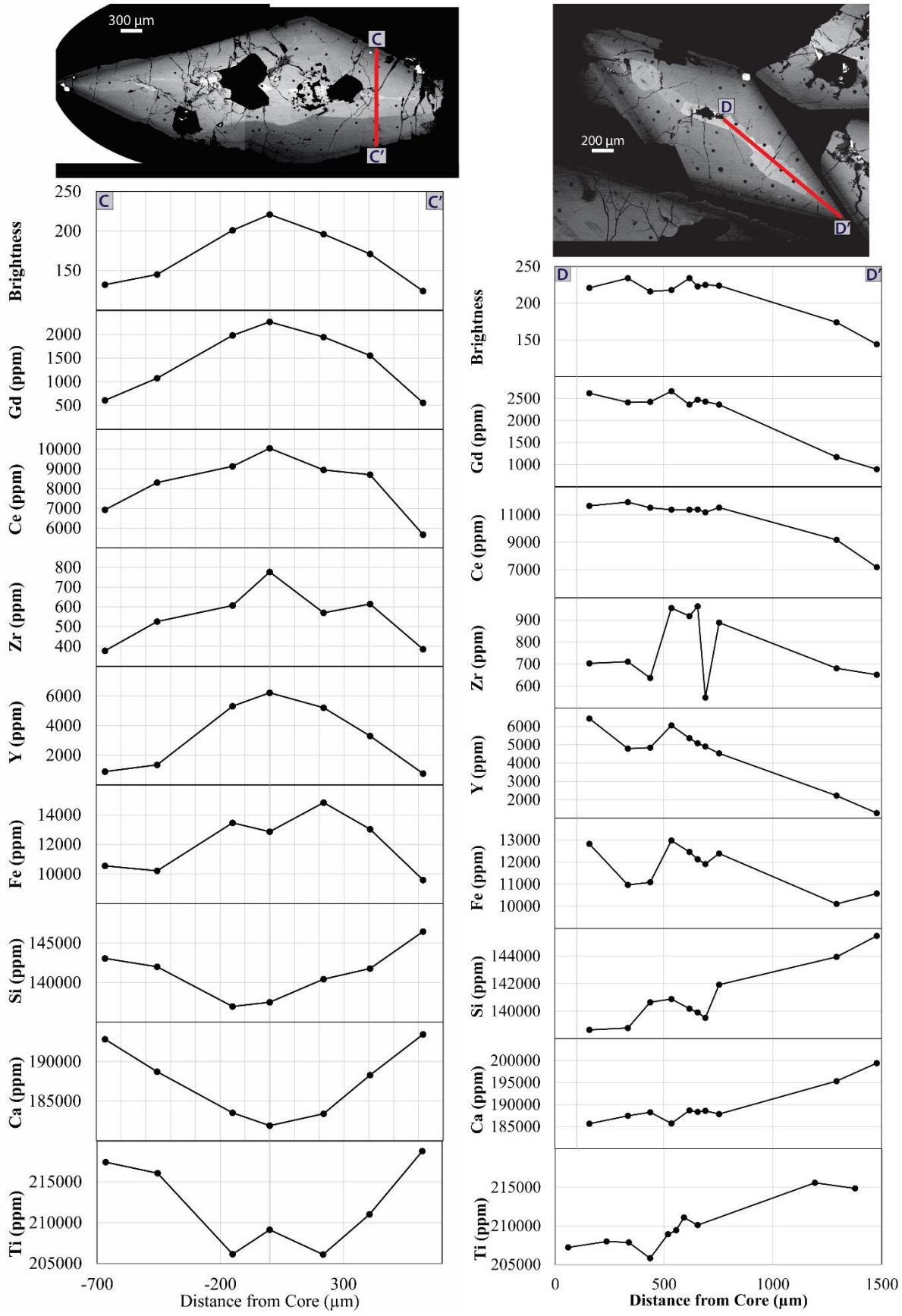
300 µm
C
C′
200 µm
D
D′
Brightness
Gd (ppm)
Ce (ppm)
Zr (ppm)
Y (ppm)
Fe (ppm)
Si (ppm)
Ca (ppm)
Ti (ppm)
Distance from Core (µm)
Distance from Core (µm)

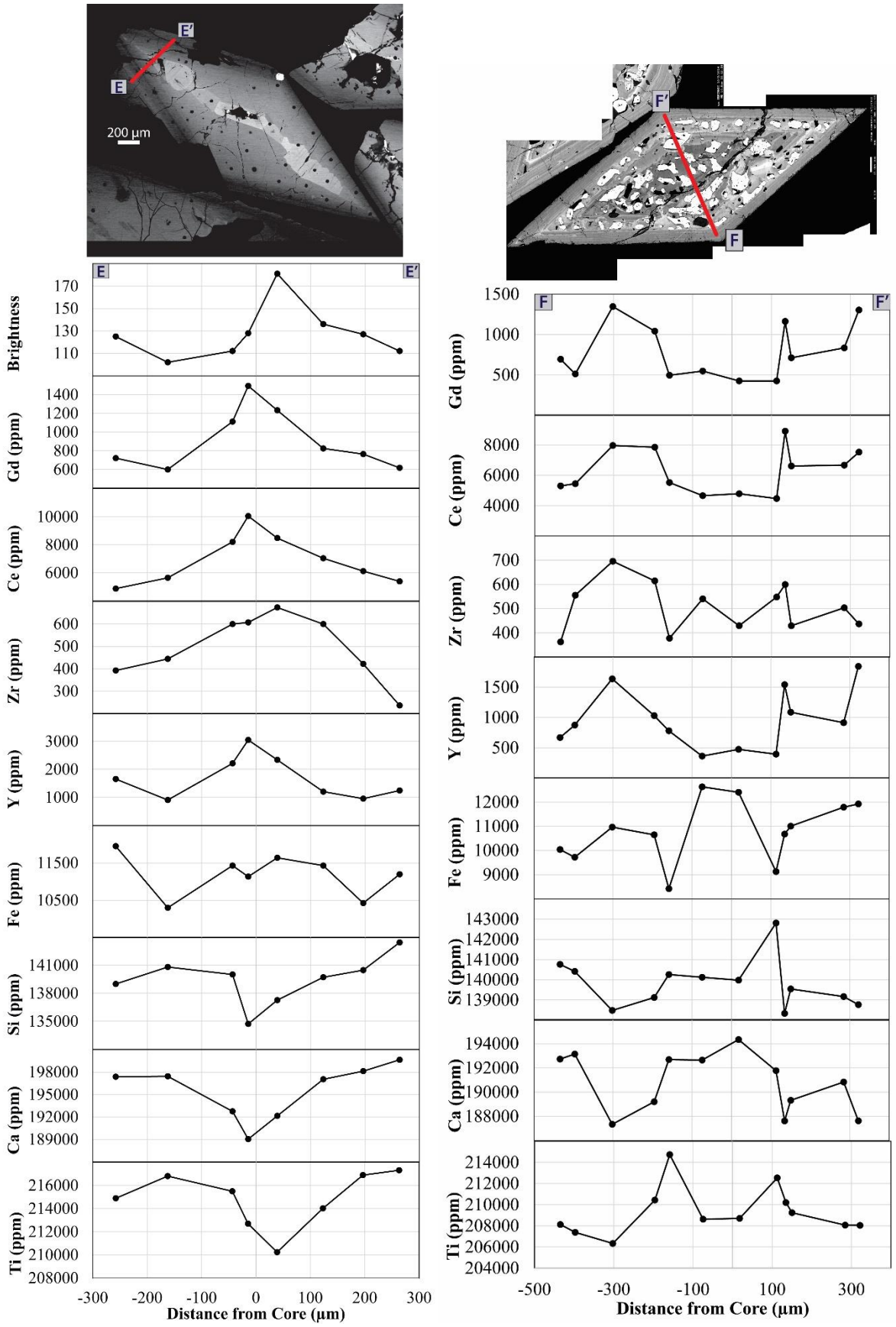
E
E′
200 µm
F
F′
Brightness
Gd (ppm)
Ce (ppm)
Zr (ppm)
Y (ppm)
Fe (ppm)
Si (ppm)
Ca (ppm)
Ti (ppm)
Distance from Core (µm)

Figure 12. Core to rim transects of titanite crystals using EMP analyses. There is a positive correlation between brightness, Gd, Ce, Zr, Y, and Fe. These elements and brightness are negatively correlated with Ti, Ca, and Si. There is an overall decrease in trace element concentration and Fe from core to rim. The concentration of trace elements mimics the brightness in BSE, and the other major elements follow an opposite trend.

Eu anomaly

Most patterns have a negative Eu anomaly (defined as $Eu/Eu^* = Eu_{norm}/\sqrt{[Sm_{norm}*Gd_{norm}]}$; Taylor and McLennan 1985), with Eu/Eu* averaging 0.48. Analyses with negative Eu anomalies are also enriched in REE, with light REE values up to ~30,000 times chondrite (Fig. 11 a). However, 27 LA-ICPMS spot analyses have a relatively flat Sm-Eu-Gd segment. These spots have an average Eu/Eu* of 0.85, and occur in 9 crystals from all 3 locations in the granodiorite. Spots with shallow Eu anomalies are located on the rims of crystals in dark BSE zones (Fig. 11b). In general, the Eu anomaly becomes deeper as overall REE concentrations increase.

DISCUSSION

Understanding variations in REE, Zr, and Y concentrations between and within crystals is important to understanding the complex zoning patterns seen in BSE images of titanite cut through their centers. The following discussion relates geochemical and textural data from titanite crystals from the Half Dome Granodiorite to models of crystallization.

Partitioning of elements into titanite

There is a large spread in REE concentrations, even within individual crystals (Figs. 9, 10, 11, 12). Complex zoning patterns coupled with highly variable REE concentrations could indicate fluctuating partition coefficients. For example, the cores of the titanite crystals are relatively enriched in REE, Zr, and Y. Given D values on the order of 100-1000 (Green and Pearson 1986; Tiepolo et al. 2002; Bachmann et al. 2005; Ackerson 2011; Colombini et al. 2011), both equilibrium and fractional crystallization models predict that trace element concentrations should plummet to negligible values in the early stages of crystallization (Fig. 3). However, typical overall core-to-rim decreases are only about a factor of 2 (Fig. 12). Equilibrium crystallization and fractional crystallization assume constant crystallization conditions and constant partition coefficients, as well as titanite crystallization throughout the entire solidification of the pluton, which is not likely.

Fig. 13 shows the brightness values across several transects from rim to core. These values further emphasize the fluctuating chemistry of titanite. Each crystal has small-scale oscillatory zoning around the rim, but the cores are different. Most crystals show an overall decrease in brightness from core to rim.

Glazner and Johnson (2013) hypothesized that K-feldspar megacrysts in the TIS owe their growth to long periods of thermal cycling and fluid pulses as the TIS was constructed over several million years. The condensed equivalent volume of water released by crystallization of water-rich granitic magma can be 10 vol % or more of the magma volume (Glazner et al. 2011). Addition of water to a magma depolymerizes a melt, which decreases *D*s for REE in titanite (Mahood and Hildreth 1983). Increasing temperature also decreases *D*s (Green and Pearson 1986). Therefore, influxes of fresh magma and associated water could cause partition coefficients to decrease, followed by recovery to higher values as the magma cools and water bleeds off.

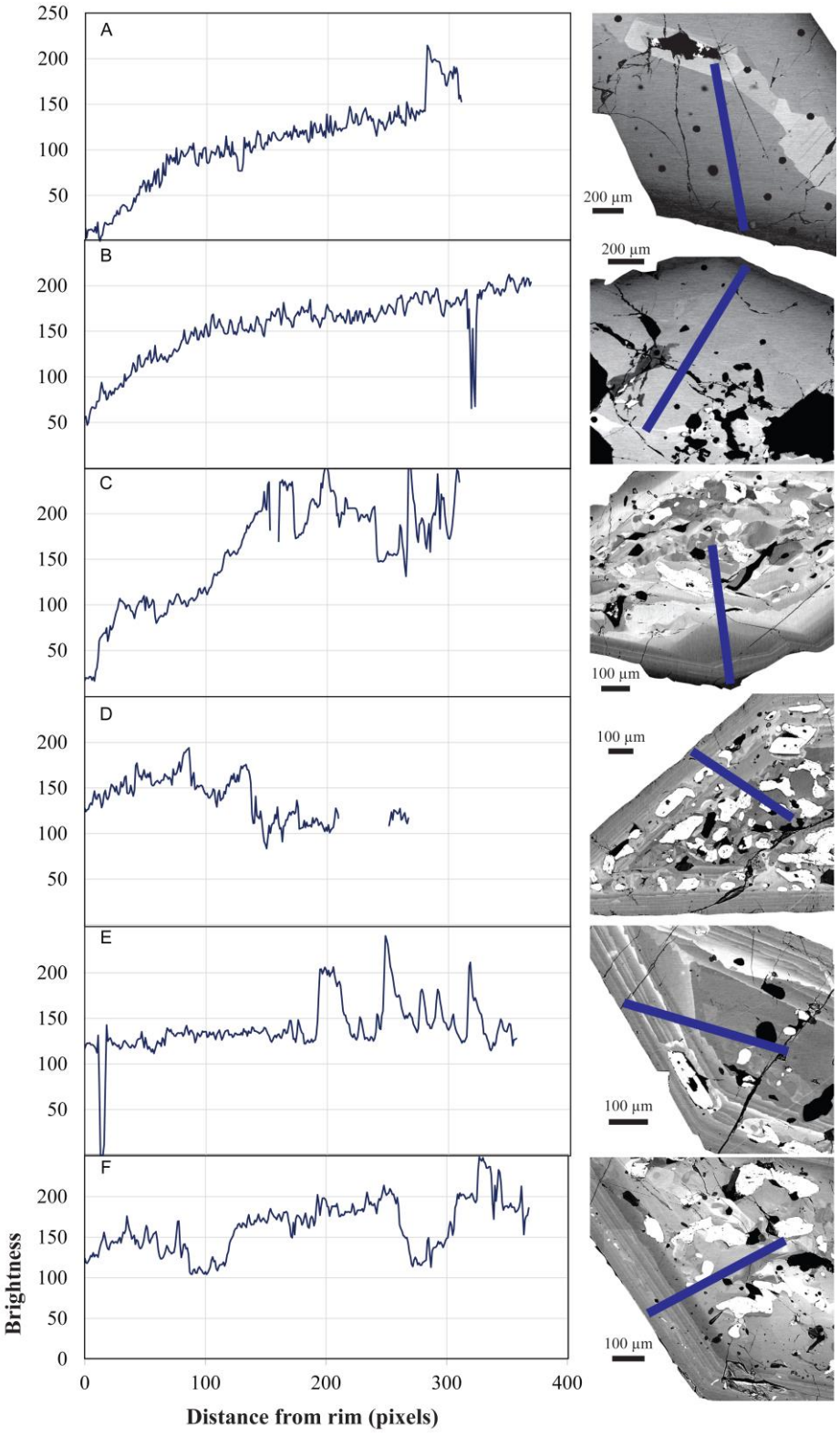

Figure 13. Transects from rim to core showing brightness variations, from 0-250. Values close to 0 are black and values close to 250 are white. All crystals show oscillating values at the rims, but in the core, each crystal is different. **a b c** show a steady decrease in brightness from core to rim; **d** shows a steady decrease; **e** and **f** show patterns that oscillate, but are flat overall.

The assemblage ilmenite + hedenbergite is favored over titanite + magnetite + quartz (Eq. 4) at higher temperatures and lower fO_2 (Lipman 1971; Wones 1989; Piccoli et al. 2000). Emplacement of a more mafic magma should decreases fO_2 (increasing temperature decreases fO_2) and stabilize ilmenite (Lipman 1971; Piccoli et al. 2000), which is a common inclusion in titanite crystals from the Half Dome Granodiorite. When the system cools, titanite stabilizes as fO_2 increases (Frost et al. 2000). Relatively higher fO_2 also increases the partition coefficients for REE in titanite (Green and Pearson 1986).

Sector zoning is seen in titanite (Fig. 2), and is caused by the chemical disequilibrium between the {111} face and the {100} face as the crystal grows (Paterson and Stephens 1992). In BSE images, titanite has bright sector zones and dark sector zones. Fir-tree zones (Fig. 2) are common in titanite crystals from the Half Dome Granodiorite. These are caused by the alternation of crystallization on the minor {100} form and two faces of the {111} form (Paterson and Stephens 1992). The magnitude of the fir-tree zone is related to the growth rate of the crystal faces. Each face either grew simultaneously at different rates, or grew at different times (Paterson and Stephens 1992). Growth rates are influenced by temperature, pressure, and melt composition. Local fluctuations of crystallization conditions can cause sector zoning, as well as fluctuations throughout the whole magma. In order to form different patterns in the same sample, there may have been fluctuating melt conditions locally, affecting each crystal differently. Sector zoning also influences coupled substitutions. REE and Ti prefer to crystallize on the {100} form, whereas Ca, Al, and Fe prefer to crystallize on the {111} form (Paterson and Stephens 1992).

Principal component analysis was performed in order to examine correlations among compositional variables. I used MgO, Al_2O_3, SiO_2, CaO, TiO_2, Fe_2O_3, Y, Ce, Gd, Eu, Lu, and brightness in this analysis; the full set of REE was not used because of their inherent self-

correlation. Eigenvector principal component 1 holds 67.6% of the variance; SiO_2, CaO, and TiO_2 have positive principal component 1 loadings, whereas the rest of the variables are negative (Fig. 14). The coupled substitutions of Al + Fe, 2 REE, and REE + Y for Ca + Ti is shown by their groupings on the loading plot. SiO_2 does not substitute readily with any of these variables, and therefore sits alone. The trace elements and brightness have similar values. The coupled substitutions of Al + Fe, 2 REE, and REE + Y for Ca + Ti are also seen in titanite crystals from volcanic rocks analyzed by Ackerson (2011).

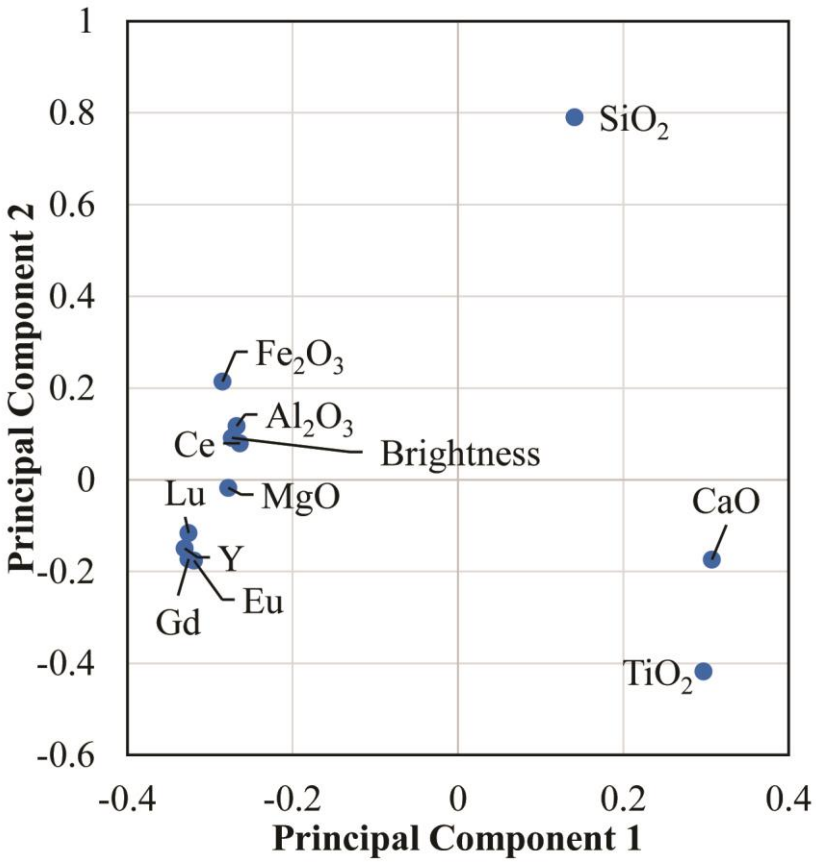

Figure 14. A principal component 1 vs principal component 2 plot of the loadings shows correlations between the variables.

Eu anomaly

The negative Eu anomaly seen in titanite with enriched REE patterns can be explained by plagioclase fractionation (Graham and Ringwood 1971). Plagioclase has a relatively high D for Eu^{2+} (3; Bachmann et al. 2005), whereas Ds for the other REE are on the order of 0.01-0.4. Decreasing fO_2 increases the Eu^{2+}/Eu^{3+} ratio, preferentially incorporating Eu into plagioclase (Drake and Weill 1975; Cicconi et al. 2012). Outer parts of some titanite crystals have relatively high Eu/Eu* value, as well as an overall depleted REE pattern. Flat Sm-Eu-Gd patterns on dark BSE rims have been attributed to metamorphic origin (Gao et al. 2012). If titanite is a late crystallizing mineral, the rims might be crystallizing when the pluton is solid, when it is under metamorphic conditions during thermal cycling.

Fractional crystallization

Titanite in the Half Dome Granodiorite has complex zoning (Figs. 2, 5, 6, 11, 12, 13), and diverse patterns are seen in crystals from the same sample, cut through the center (Fig. 5). Using fractional crystallization from equation 3, the concentrations of REE were modeled in titanite (equation 5):

$$C_R = D[C_O(F^{(d-1)})] \quad (5)$$

The bulk D (d) was calculated using partition coefficients from Bachmann et al. (2005), and is the weighted sum of the D values from all phases present in the system. The average weight fraction of titanite (1 wt %) and initial REE concentrations (taken as the average from the Half Dome Granodiorite) from Gray (2003) were used. The concentration of Ce and Gd in titanite were modeled at different fractions of melt (F), from $F = 0.9$ to $F = 0.1$. This model (Fig. 15) shows that even with a small percentage of titanite, REE concentration dramatically decreases after initial concentration. The initial concentration in this model is comparable to measured

values from titanite cores (Fig. 12), but transects measured by EMP do not show such dramatic decreases in concentration. There is no way that the complex zoning patterns in titanite can be explained with fractional crystallization.

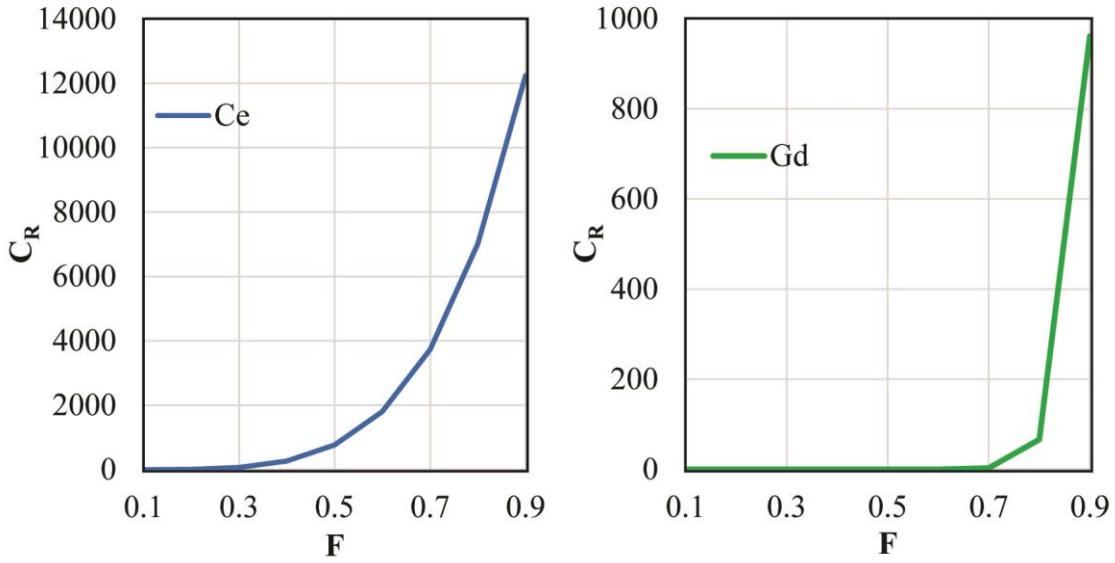

Figure 15. Fractional crystallization (equation 3) was modified to show the concentration of Ce and Gd in titanite from $F = 0.9$ to $F = 0.1$ using equation 5.

Watson and Müller (2009) developed a growth model to show how crystallization occurs under disequilibrium conditions. The growing surface of the crystal affects the local concentration of the liquid, and therefore affects subsequent concentrations in the crystal. Fluctuating partition coefficients and diffusion-controlled zoning is more likely than fractional crystallization to create sector zoning (Paterson and Stephens 1992; Watson and Liang 1995) and the complex patterns seen in titanite. Diffusion-controlled zoning that depends on growth kinetics has also been observed and modeled in plagioclase (Allègre et al. 1981; L'Heureux and Fowler 1996).

Plutonic titanite versus volcanic titanite

Modified fractional crystallization still does not model the actual concentrations in a titanite crystal. Ackerson (2011) attributed discrete oscillatory zones in volcanic titanite to be a result of diffusion-controlled partitioning. Some volcanic titanite crystals that have thicker zones, similar to those in plutonic titanite crystals, may be zoned due to thermal cycling (Ackerson 2011). However, some crystals from the Half Dome Granodiorite have discrete oscillatory zones on the rims. This might indicate disequilibrium zoning in plutonic titanite as well, where crystals grow more rapidly than the rate at which elements are incorporated into the crystal, creating a diffusion profile. Therefore, early crystallization might have been affected by thermal cycling, but towards the end of crystallization, some titanite had diffusion-controlled zones.

One explanation for neighboring crystals with different zoning patterns, such as those in Fig. 5, is clustering after growth in different parts of a magma body (Vogt 1921; Wiebe 1968; Vance 1969). Such gathering could be produced by crystal settling (Beane and Wiebe 2012). Alternatively, chaotic mixing via forced convection can produce widely divergent flow lines, separating crystals that grew near each other and bringing together ones that grew separately (Perugini et al. 2012). Either origin could explain the wide diversity in zoning patterns seen in titanite crystals from the same hand sample, but they require crystallization of titanite relatively early in the magma's crystallization history, before the effective viscosity rises to levels that preclude crystal settling or forced convection. Rigid lockup generally occurs when the crystal fraction reaches 50 ± 20 vol% (Petford 2003).

Because of the geochemical and textural evidence from volcanic rocks, the crystallization of plutonic titanite is better understood. In some volcanic rocks, titanite is euhedral and contains ilmenite inclusions around the rims (Whitney et al. 1985; Colombini et al. 2011; Pamukcu et al.

2013). Colombini et al. (2011) interpreted ilmenite rims as evidence of transient hotter conditions and decreasing fO_2 at the end of its crystallization (equation 4), possibly as a result of magma recharge which increased the melt fraction and facilitated eruption. Titanite crystallization in the Peach Springs Tuff coincided with a high-silica melt (72-77 wt% SiO_2) and high phenocryst percentage (30%) (Colombini et al. 2011; Pamukcu et al. 2013). Titanite is therefore likely a late-crystallizing mineral in the tuff.

In the Fish Canyon Tuff, there is a higher phenocryst percentage (45%) and eruption is attributed to thermal rejuvenation by emplacement of more mafic magma (Bachmann et al. 2005). Dissolution of feldspars and quartz suggest an assemblage with even higher crystallization before eruption (Bachmann et al. 2005), and therefore rigid lockup. Different zoning patterns in the same hand sample arriving by forced convection is ruled out because a crystal-rich magma does not permit significant differential movement of crystals.

CONCLUSIONS

The complex zoning patterns in BSE images coupled with the large variation in REE concentrations have provided insight into the crystallization of titanite. The conclusions from this study include:

1. Plutonic titanite has high concentrations of important trace elements, such as Y, Zr, and REE. These elements are distributed in the crystal by coupled substitutions to maintain charge balance. Fluctuating crystallization conditions due to thermal cycling may influence how these elements are distributed into the crystal. Instead of dramatically decreasing from core to rim, as fractional crystallization predicts, trace elements decrease by a factor of ~2.
2. Changes in fO_2 affect the partitioning of Eu into titanite. Negative Eu anomalies are caused by plagioclase partitioning, whereas flat Sm-Eu-Gd profiles with relatively low REE concentrations may be caused by metamorphic conditions during thermal cycling near the end of crystallization.
3. The zoning patterns, REE concentrations, and coupled substitutions in volcanic titanite are just as complex as those in plutonic rocks. Differences between them have been described, including smaller oscillatory zoning in volcanic titanite and relatively higher REE concentrations in volcanic titanite. However, the Half Dome Granodiorite has some titanite crystals with smaller, oscillatory zones. Some have large patchy zones in the core, with dark, thick rims. There are also crystals with sector zoning in the core, with dark, thick rims. Other crystals have the same core patterns, but discrete, small oscillatory

zones around the rims. This might indicate that some crystals were influenced by thermal cycling (no small oscillatory zones) whereas others grew with disequilibrium zoning.

4. Crystals in the same sample with different zoning patterns may be caused by locally varying crystallization conditions. It also could be an effect of late crystallization and the proximity to other mineral phases that will influence partitioning of REE into titanite.

APPENDIX A: TITANITE BSE IMAGES

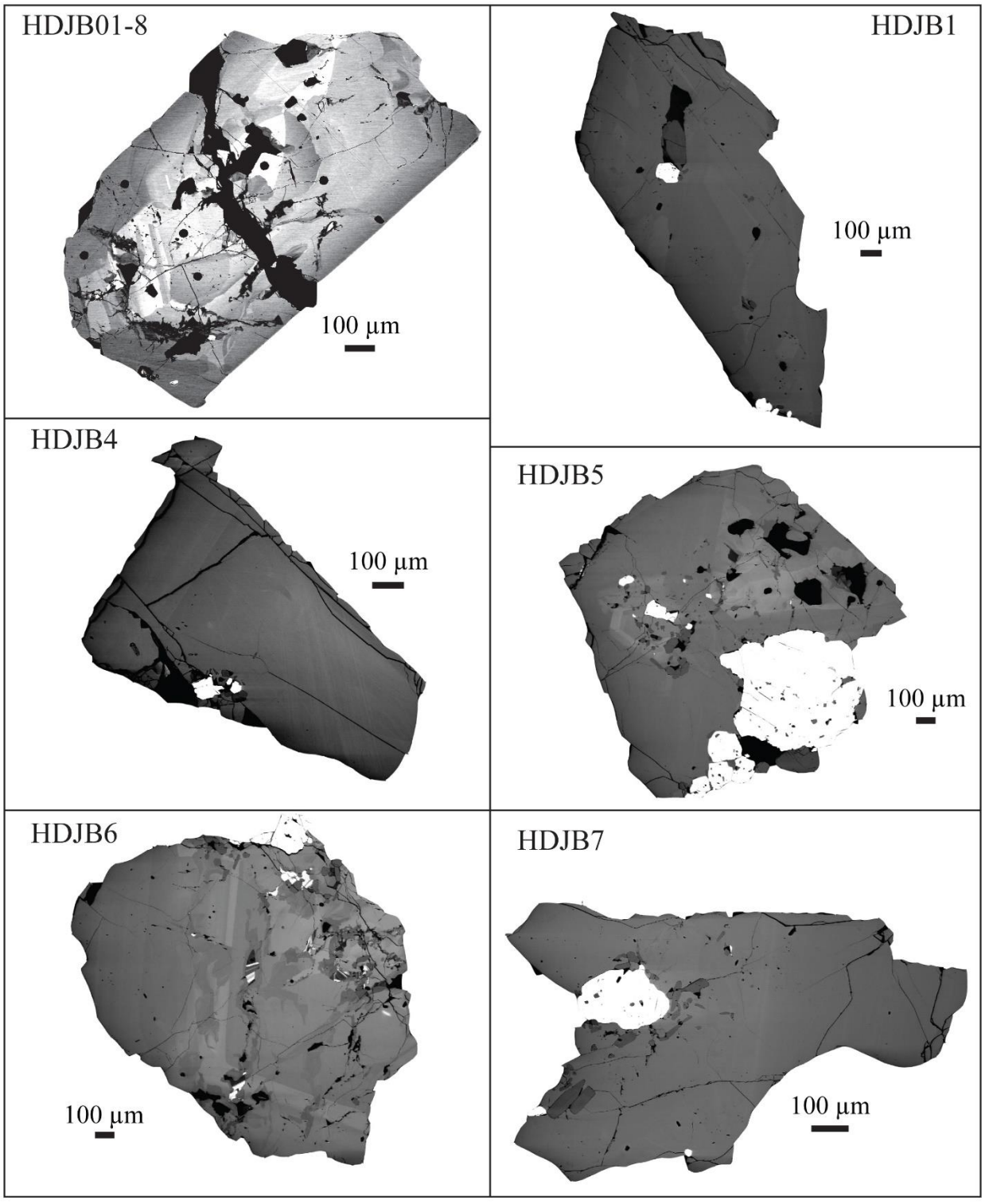

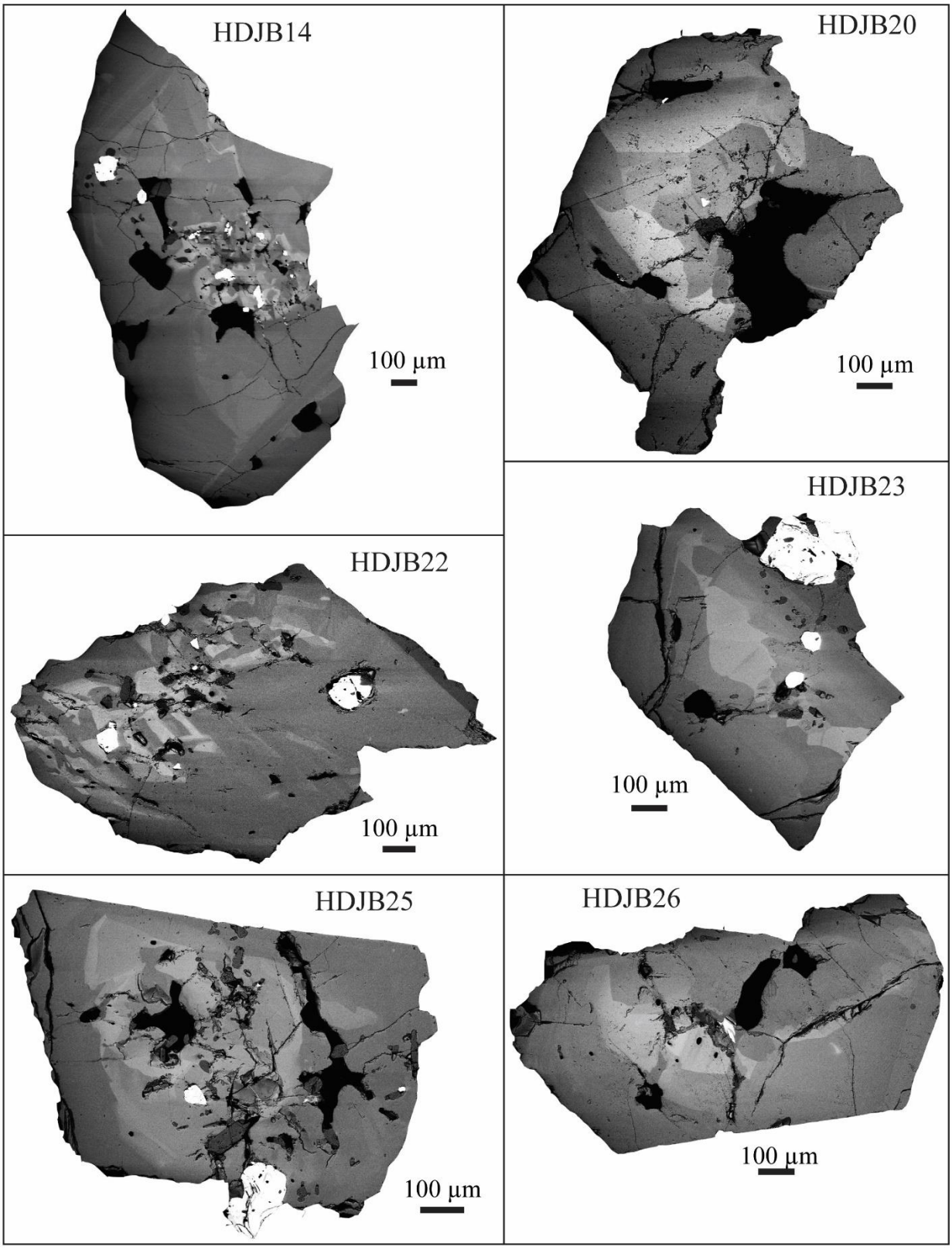
HDJB14
100 µm
HDJB20
100 µm
HDJB23
100 µm
HDJB22
100 µm
HDJB25
100 µm
HDJB26
100 µm

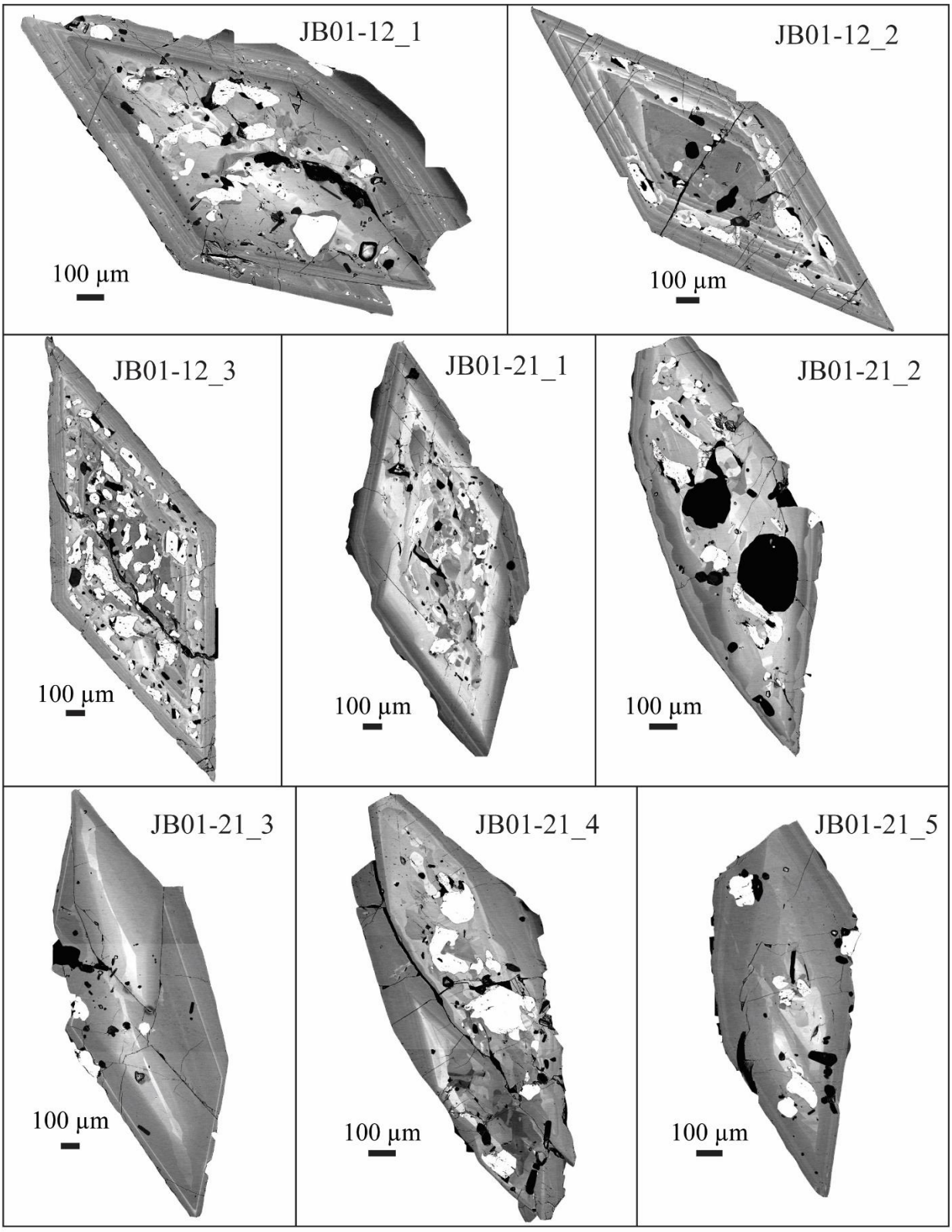
JB01-12_1
100 µm
JB01-12_2
100 µm
JB01-12_3
100 µm
JB01-21_1
100 µm
JB01-21_2
100 µm
JB01-21_3
100 µm
JB01-21_4
100 µm
JB01-21_5
100 µm

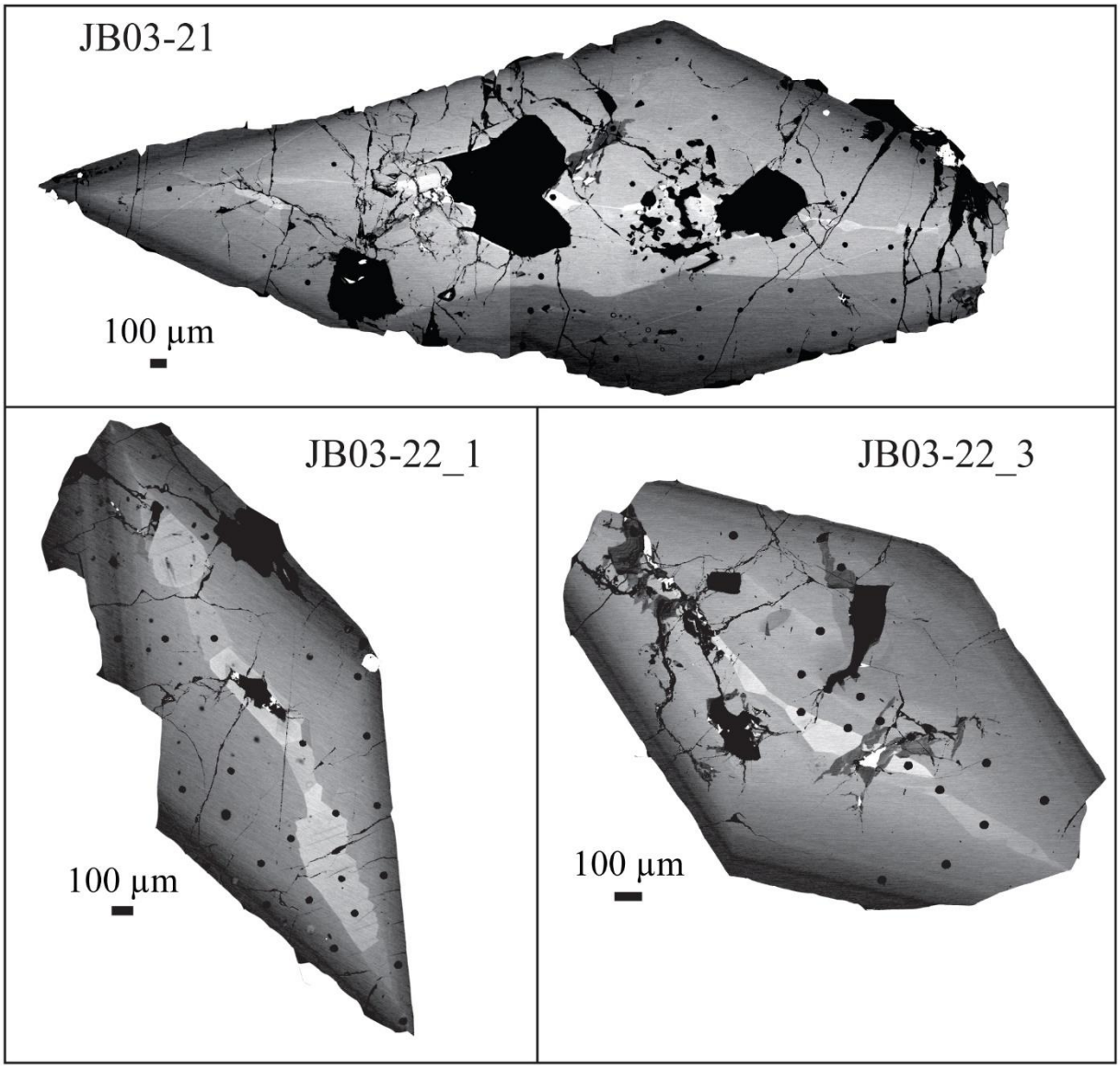

Backscattered electron images of titanite crystals, mostly cut through the center, parallel to {111}, from the Half Dome Granodiorite. HDJB01-8; HDJB1, 4, 5, 6, 7, 14, 20, 22, and 23 are randomly oriented.

APPENDIX B: TITANITE IN THIN SECTIONS FROM GRAY (2003).

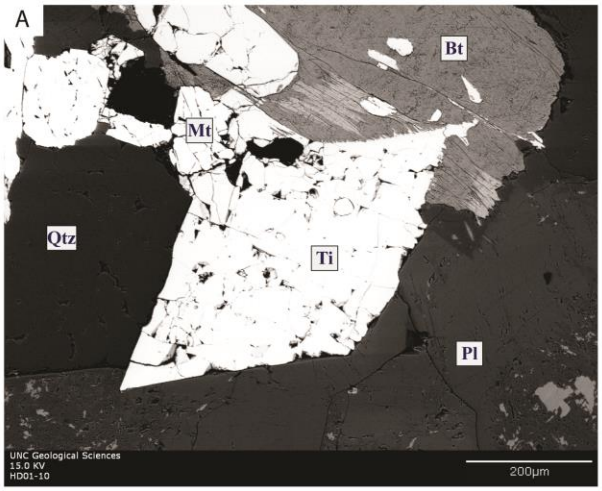

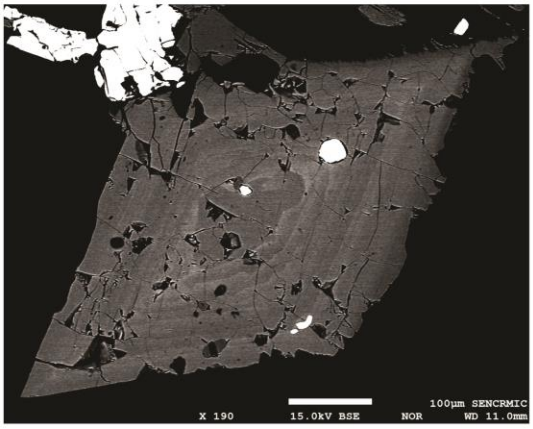

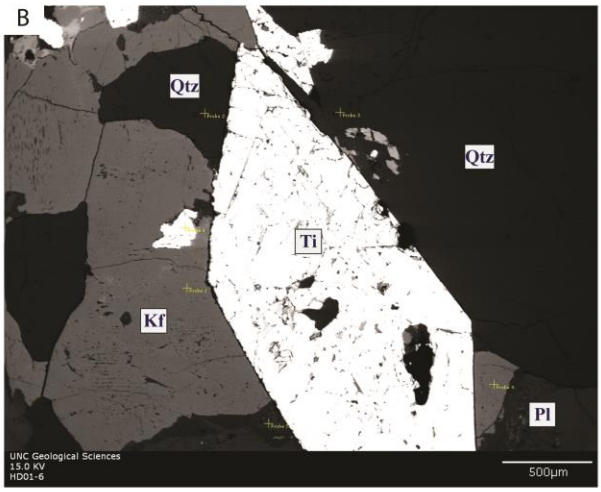

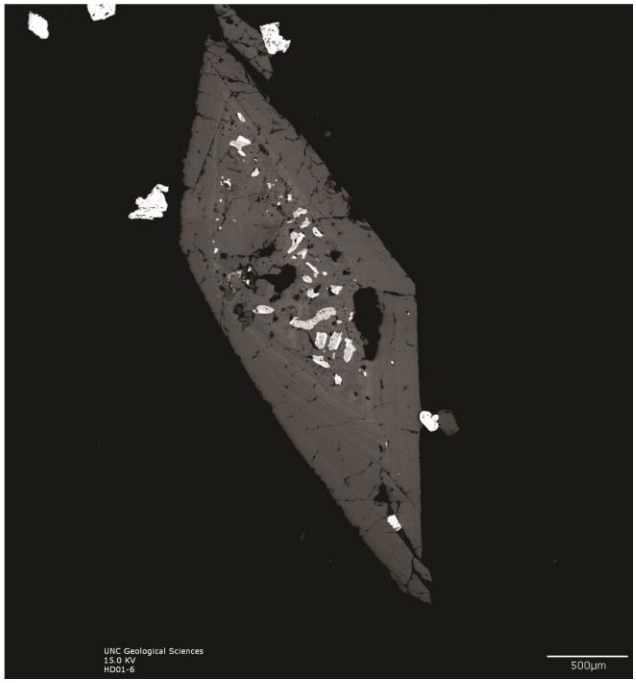

Ti	Titanite	Bt	Biotite
Qtz	Quartz	Hb	Hornblende
Kf	K-feldspar	Mt	Magnetite
Pl	Plagioclase	Ap	Apatite

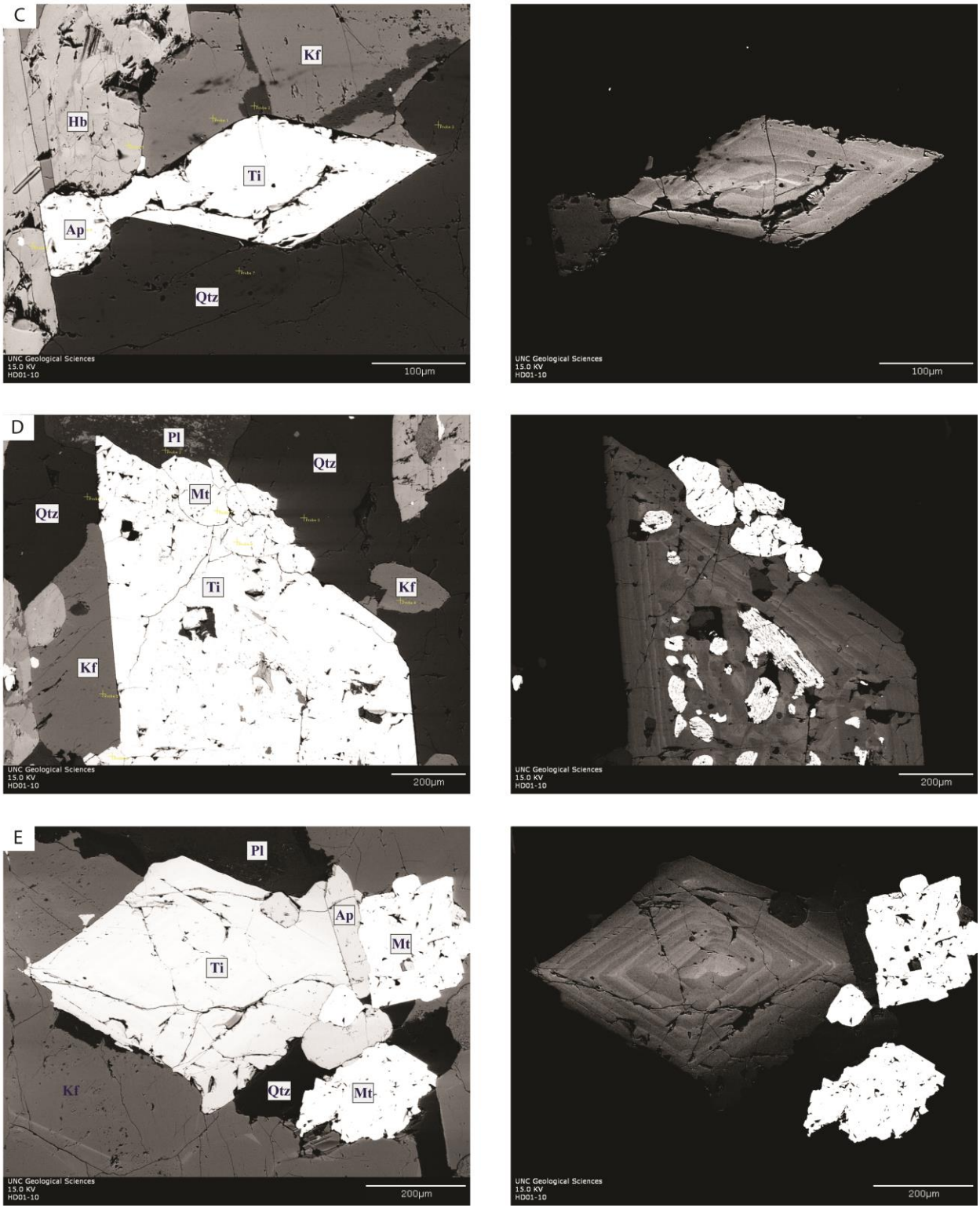
C
Kf
Hb
Ti
Ap
Qtz
UNC Geological Sciences
15.0 KV
HD01-10
100µm
UNC Geological Sciences
15.0 KV
HD01-10
100µm
D
Pl
Qtz
Mt
Qtz
Ti
Kf
Kf
UNC Geological Sciences
15.0 KV
HD01-10
200µm
UNC Geological Sciences
15.0 KV
HD01-10
200µm
E
Pl
Ap
Mt
Ti
Kf
Qtz
Mt
UNC Geological Sciences
15.0 KV
HD01-10
200µm
UNC Geological Sciences
15.0 KV
HD01-10
200µm

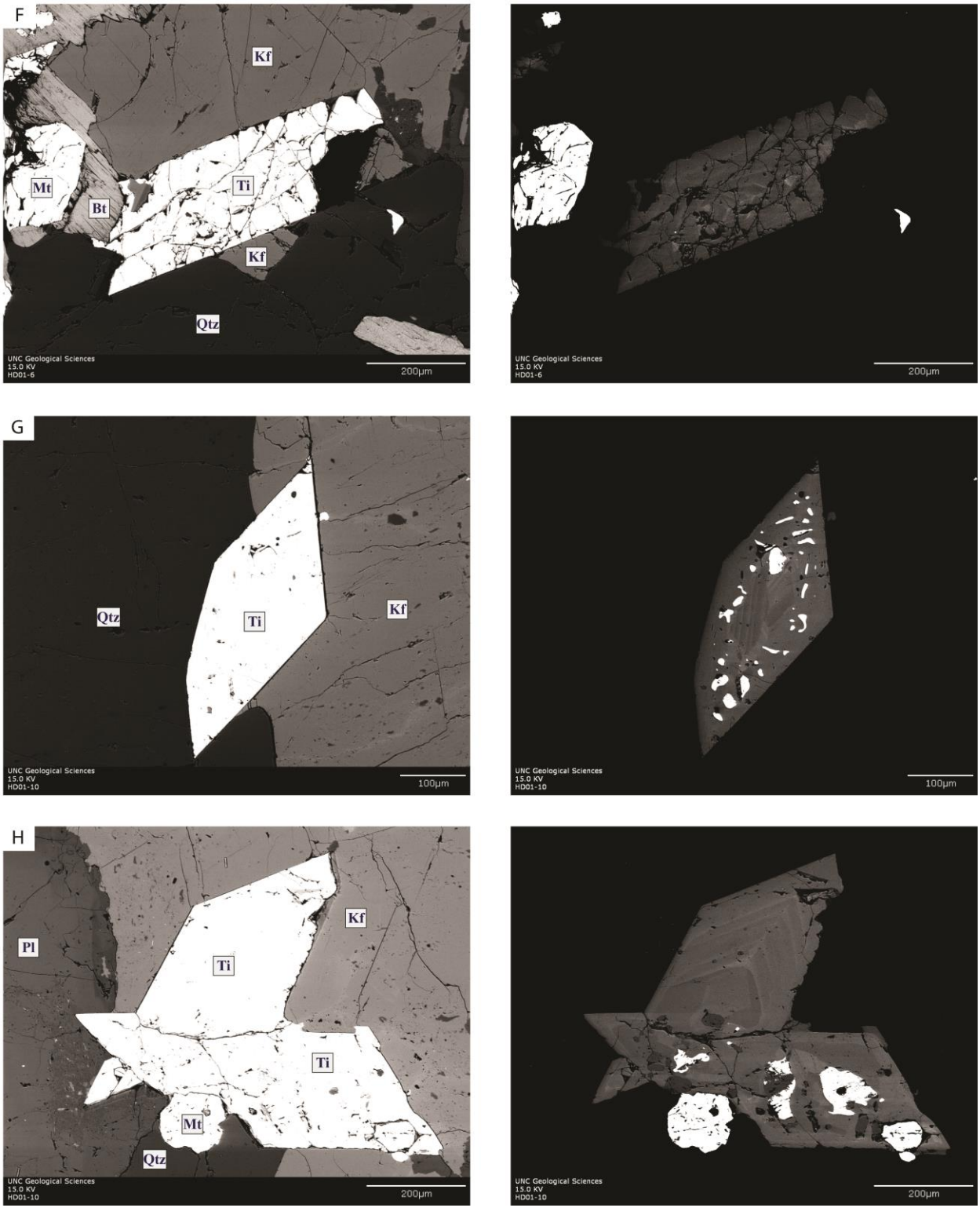

Backscattered electron images of probe slides showing titanite *in situ* from Gray (2003). Left column shows phases surrounding titanite crystals. Right column shows titanite zoning and inclusions. Images that are next to each other show the same titanite crystals, with different brightness and contrast settings. All slides are from the Half Dome Granodiorite.

APPENDIX C: LA-ICPMS MAJOR AND TRACE ELEMENT DATA

Sample	MgO wt %	Al_2O_3 wt %	SiO_2 wt %	CaO wt %	TiO_2 wt %	MnO wt %	Fe_2O_3 wt %
HDJB1-1	0.01200648	1.31126998	29.035774	29.698231	36.808673	0.1487739	1.471019712
HDJB1-2	0.01104709	1.20391718	30.765922	28.511505	36.318074	0.1523875	1.508326216
HDJB1-3	0	1.20761795	35.535462	26.558889	33.932027	0.1489306	1.541378088
HDJB1-4	0.0115688	1.25667388	29.399564	29.69834	36.748743	0.1423542	1.291604929
HDJB1-5	0.01179344	1.2223829	30.414932	28.742147	36.413398	0.1313347	1.277253575
HDJB1-6	0	1.19683211	32.365335	27.763785	35.538686	0.1343588	1.269994824
HDJB4-1	0.01177376	1.30193037	29.911075	29.650795	36.089844	0.1553343	1.50258771
HDJB4-2	0.01155652	1.25540982	30.166437	28.981817	36.420249	0.1503925	1.468999475
HDJB4-3	0	1.32208697	31.637235	29.049537	35.421426	0.152454	1.458918081
HDJB4-4	0.01476976	1.3167615	29.846694	29.729569	36.280002	0.1366293	1.412411582
HDJB4-5	0.01503091	1.43541144	30.875212	28.711819	35.681128	0.130961	1.667681779
HDJB4-6	0.01516976	1.2800633	33.353748	27.805415	34.803209	0.1330891	1.251132374
HDJB5-1	0.01228617	1.27314567	30.613086	29.385363	35.807067	0.144702	1.30985232
HDJB5-2	0.01266622	1.18128635	31.816283	28.550386	35.617413	0.1374753	1.221058002
HDJB5-3	0.01342969	1.10616813	35.710126	26.823449	33.726951	0.136801	1.1636112
HDJB5-4	0.0102531	1.20800365	30.639214	29.419094	35.785249	0.1513907	1.274481141
HDJB5-5	0.01851477	1.33230094	31.815722	27.198272	34.133166	0.1328801	1.604213485
HDJB5-6	0	1.26977278	35.084058	26.316446	33.214111	0.1273864	1.467937828
HDJB6-1	0.01458119	1.15904162	30.397785	29.568156	36.010511	0.1404919	1.243170735
HDJB6-2	0.01085434	1.193808	32.317409	28.5806	34.883403	0.1569304	1.46258624
HDJB6-3	0	1.14527361	37.090738	26.28022	33.000482	0.1447781	1.43354885
HDJB6-4	0.01254969	1.06289869	30.715507	28.940484	35.714027	0.1550825	1.325505691
HDJB6-5	0.02002425	1.48539297	31.963571	27.369117	33.819966	0.1358244	1.816190252
HDJB6-6	0	1.24569553	34.800426	27.229821	34.414174	0.0816265	0.618320327
HDJB7-1	0.01246974	1.32067082	28.476156	30.157046	36.899855	0.1525428	1.403918139
HDJB7-2	0.01270206	1.34025404	30.396954	28.929309	36.223548	0.150738	1.415370522
HDJB7-3	0	1.37055739	30.814052	29.538925	36.063485	0.1420661	1.317172498
HDJB7-4	0.0059081	1.41904809	29.908885	30.439869	36.657218	0.1199469	1.248965579
HDJB7-5	0.01108876	1.33257013	29.601074	29.254013	36.814192	0.1396312	1.282272156
HDJB7-6	0.01408238	1.04095301	31.675004	28.176961	36.243783	0.1293314	1.029567621
HDJB14-1	0.01232957	1.2204011	29.909576	29.509028	36.316237	0.1374754	1.23786995
HDJB14-2	0.00940067	1.21613416	31.151652	29.378858	35.964728	0.1523794	1.277653714
HDJB14-3	0.01290518	1.12481517	32.492702	28.864217	35.170005	0.1475884	1.209343744
HDJB14-4	0.01397069	1.09230659	29.935974	29.742999	36.484581	0.1386468	1.040072224
HDJB14-5	0.01178997	1.14009958	31.157231	28.631994	36.144368	0.1320148	1.131137433
HDJB14-6	0	1.06885012	32.314498	28.241812	35.321343	0.1312011	1.105475932
HDJB17-1	0.0064702	1.38169348	30.200528	30.442363	36.349662	0.1218875	1.276670665
HDJB17-2	0.00547758	1.36539572	31.212749	29.652155	36.320269	0.109225	1.178599687
HDJB17-3	0	1.32296526	31.999433	29.397396	35.961317	0.1045298	1.097536575
HDJB17-4	0.01334284	1.19497008	29.875179	29.531021	36.526814	0.1349547	1.147773569
HDJB17-5	0.0124837	1.24997499	30.626911	28.926821	36.175606	0.1338259	1.224408009
HDJB17-6	0	1.26887121	34.800582	26.86424	34.222356	0.1385021	1.30924705
HDJB20-1	0.01387791	1.17730515	30.20687	28.961356	37.002628	0.1341878	1.092821625
HDJB20-2	0.01401537	1.0252834	29.830329	28.825609	37.107001	0.1238489	1.134790362
HDJB20-3	0.01733615	1.27614584	29.754369	27.773461	35.875414	0.1214405	1.514064015
HDJB20-4	0.01768863	1.31937618	29.803671	27.714997	35.666757	0.1224913	1.560715372
HDJB20-5	0.01621065	1.45568159	30.177477	28.654716	36.074976	0.12776	1.607653166
HDJB20-6	0.01867864	1.35081121	29.923534	27.588171	35.497518	0.1282716	1.638898081
HDJB20-7	0.01807015	1.46299295	29.740399	28.228545	35.509251	0.1240661	1.806045745
HDJB20-8	0.01491521	1.13633299	29.666305	28.997433	37.322699	0.1296434	1.132131489
HDJB20-9	0.01608893	1.01608878	29.767851	29.034496	37.232564	0.1285078	1.08638973
HDJB20-10	0.01890945	1.42302743	29.814102	27.432188	35.027248	0.1239109	1.732333406
HDJB20-11	0.01890661	1.49725696	29.705771	27.651758	34.934584	0.1273432	1.808109299
HDJB20-12	0.01437435	1.11378492	30.584799	28.454097	36.783069	0.1274443	1.044806643

Sample	MgO wt %	Al_2O_3 wt %	SiO_2 wt %	CaO wt %	TiO_2 wt %	MnO wt %	Fe_2O_3 wt %
HDJB21-1	0.01819641	1.69025459	28.617578	28.29747	35.816663	0.1216173	1.964638887
HDJB21-2	0.01862226	1.47761262	28.665554	27.387012	35.83443	0.1179903	1.665293358
HDJB21-3	0.01564964	1.37455026	28.844455	28.903763	37.216698	0.1239756	1.502454737
HDJB21-4	0.02267472	1.70674654	28.845094	26.43046	34.669371	0.1211962	1.967276026
HDJB21-5	0.01511075	1.10057903	28.567988	29.32825	37.891394	0.1229467	1.142260642
HDJB21-6	0.0237945	1.72499185	28.131456	26.995364	34.760178	0.1228569	2.083577476
HDJB21-7	0.01983771	1.60863443	29.13679	28.459722	35.871452	0.1228973	1.917875158
HDJB21-8	0.01788046	1.6486563	29.373937	28.254421	35.568122	0.1242832	2.001863966
HDJB21-9	0.0197595	1.62117443	29.576867	28.251421	35.597979	0.1251328	1.984297341
HDJB21-10	0.01640842	1.09761566	29.50422	28.854972	37.506121	0.1304893	1.110905964
HDJB22-1	0.0137212	1.27341453	30.127807	28.757175	36.638502	0.1316259	1.352384637
HDJB22-2	0.0145551	0.9882373	30.405874	28.666852	37.161057	0.1277294	1.090322693
HDJB22-3	0.01440464	1.25005721	30.514536	28.754409	36.629137	0.1338431	1.249806119
HDJB22-4	0.01244488	1.21553212	30.262916	29.004004	36.725914	0.1404437	1.184645635
HDJB22-5	0.01390313	1.17082521	30.56592	28.710643	36.760334	0.1317509	1.091581425
HDJB22-6	0.01773473	1.36133944	30.174285	27.699377	35.567435	0.1240118	1.56615858
HDJB22-7	0.01317948	1.0849234	30.050384	28.520859	36.46509	0.1393626	1.260064357
HDJB22-8	0.01567246	1.06400683	30.447437	28.450961	36.728333	0.1274245	1.124921238
HDJB23-1	0.01770814	1.597003	30.245086	28.111621	35.30017	0.1262303	1.878143149
HDJB23-2	0.01735088	1.57610129	30.397219	27.557616	34.941338	0.1254382	1.862270066
HDJB23-3	0.01758047	1.62778959	30.285418	27.614249	35.204445	0.1241886	1.90199114
HDJB23-4	0.01747417	1.6401019	30.234738	27.765094	35.102242	0.1259706	1.968828594
HDJB23-5	0.01902754	1.56401749	30.20064	26.831734	35.0601	0.1236504	1.645222619
HDJB23-6	0.01775783	1.58963254	29.848632	28.449402	35.653625	0.1257456	1.815386012
HDJB23-7	0.01433728	1.17038276	28.679599	30.747059	35.46692	0.1245949	1.295304534
HDJB23-8	0.01728522	1.31355574	30.248585	27.334504	35.556154	0.1244861	1.561752081
HDJB23-9	0.01512788	1.27153388	30.498279	28.70572	36.737713	0.131258	1.198936036
HDJB23-10	0.01655853	1.47362918	30.239807	28.83925	35.912122	0.1296718	1.69379745
HDJB24-1	0.01305342	1.30443041	30.827314	28.783655	36.199865	0.1370286	1.230824434
HDJB24-2	0.01305328	1.30498895	30.535325	28.8433	36.311222	0.1297012	1.313366436
HDJB24-3	0.01969109	1.43304054	31.006312	27.705725	34.929155	0.1305052	1.851909646
HDJB24-4	0.01821877	1.39148552	30.505803	27.454554	35.088898	0.1261641	1.722569948
HDJB24-5	0.01874274	1.34932196	30.566104	26.731089	34.935028	0.1215739	1.667816525
HDJB24-6	0.01893085	1.41269126	30.886541	27.535662	35.243317	0.1255155	1.626958285
HDJB25-1	0.01378552	1.22522025	31.49028	28.250466	36.26406	0.1323979	1.187066057
HDJB25-2	0.01420954	1.19465911	31.076859	27.535661	35.413448	0.1262775	1.418373543
HDJB25-3	0.0180538	1.50578	30.094028	27.823096	35.231123	0.1239809	1.762235687
HDJB25-4	0.01734622	1.57992381	30.123005	27.601249	35.054599	0.1257578	1.812368112
HDJB25-5	0.01756947	1.46033958	30.700805	27.77224	35.233099	0.1254907	1.683916371
HDJB25-6	0.01689073	1.30004262	29.482352	28.704536	35.556996	0.1216617	1.504240151
HDJB25-7	0.01766736	1.41933549	30.474331	27.687125	35.311581	0.1246905	1.698678385
HDJB25-8	0.01419037	1.23272892	30.95169	28.64597	36.30483	0.1384206	1.215748565
HDJB26-1	0.01427214	1.25503105	30.022884	29.100058	36.557745	0.1299965	1.309806003
HDJB26-2	0.01483169	1.01273357	30.5752	28.537977	36.992263	0.1313725	1.084181684
HDJB26-3	0.01511087	1.05170445	29.883133	28.94845	37.168158	0.1296397	1.096295152
HDJB26-4	0.01451324	1.01212632	30.677132	28.592656	36.8097	0.1310632	1.064150388
HDJB26-5	0.01940962	1.42526141	30.061504	27.036634	34.858893	0.1220478	1.781961559
HDJB26-6	0.01847573	1.45660942	29.432488	28.255643	35.564568	0.1236344	1.641071775
HDJB26-7	0.019461	1.46182081	29.955705	27.180965	34.696862	0.1219619	1.860604817
HDJB26-8	0.03506965	1.27524562	30.151008	28.691614	36.247244	0.1253188	1.446935391
HDJB26-9	0.0156713	0.9909551	29.960768	28.981777	37.225225	0.129653	1.064311632
HDJB26-10	0.01611613	1.09885495	30.07721	28.630031	36.725543	0.1234718	1.193979406
JB03-21_1	0.01690737	1.47355909	29.747799	29.075613	36.047233	0.1355238	1.47282566
JB03-21_2	0.02308973	1.77203161	29.944459	27.673504	34.423001	0.139239	1.942958554

Sample	MgO wt %	Al_2O_3 wt %	SiO_2 wt %	CaO wt %	TiO_2 wt %	MnO wt %	Fe_2O_3 wt %
JB03-21_3	0.01898673	1.39565463	29.945112	28.644094	35.958801	0.1366813	1.440399395
JB03-21_4	0.02075538	1.72054235	30.427116	27.801531	34.895023	0.14215	1.747990844
JB03-21_5	0.02312499	1.85357218	29.454899	27.690393	34.49236	0.1378158	2.039561631
JB03-21_6	0.02252671	1.84092482	29.643614	27.60866	34.415428	0.1382724	2.008822403
JB03-21_7	0.01586734	1.39857104	30.1474	28.960463	35.990373	0.1336111	1.457498388
JB03-21_8	0.02235261	1.84085449	29.854496	27.515379	34.50481	0.1381272	1.973001474
JB03-21_9	0.02289712	1.79176635	29.501623	27.567486	34.485644	0.1366207	1.978605713
JB03-21_10	0.01950714	1.3044579	30.64281	28.186033	35.797419	0.1362065	1.38515316
JB03-21_11	0.01433893	1.3630779	30.803286	28.888977	35.914551	0.1313192	1.4201943
JB03-21_12	0.02359867	1.74990921	29.474744	27.906757	34.952548	0.1379993	1.851097832
JB03-21_13	0.02094018	1.7263686	30.842733	26.94599	34.043909	0.1434327	1.921495626
JB03-21_14	0.01782978	1.38775874	30.355916	28.580927	35.888295	0.1382541	1.445545206
JB03-21_15	0.01508194	1.35453411	30.201979	28.989087	36.197119	0.1326046	1.389912329
JB03-21_16	0.01764362	1.48416948	29.963683	28.564245	36.358232	0.1371709	1.457461158
JB03-21_17	0.00570823	1.27762623	29.52891	28.560683	37.115258	0.0927958	0.75720242
JB03-21_18	0.024265	1.80206165	30.097842	26.981633	34.366684	0.1406059	1.972760693
JB03-21_19	0.01395825	1.30064916	30.24562	28.904709	36.59327	0.131353	1.357589333
JB03-21_20	0.02657548	1.63075469	28.909458	26.645317	34.843897	0.1321378	1.814075487
JB03-21_21	0.02276541	1.74695131	29.303512	27.403781	35.170183	0.1367395	1.844026847
JB03-21_22	0.01583216	1.35611368	29.432396	28.716882	36.883852	0.1334728	1.371249784
JB03-21_23	0.01225458	1.45651933	29.230625	29.275494	37.075235	0.1393556	1.347829613
JB03-21_24	0.02229656	1.82551831	30.090189	27.051697	34.741018	0.1360064	1.94166176
JB03-21_25	0.02027091	1.5654094	29.428433	28.584138	36.153008	0.1404719	1.519807887
JB03-21_26	0.02029081	1.31954902	29.267025	28.05917	36.33376	0.1346556	1.457952356
JB03-22_2_1	0.01335214	1.39014849	29.789023	29.290251	36.486678	0.1383237	1.485928745
JB03-22_2_2	0.01487067	1.31895163	30.166645	29.043285	36.387375	0.1341618	1.414420238
JB03-22_2_3	0.01861837	1.20670276	30.021422	28.170947	36.332564	0.1344501	1.328401877
JB03-22_2_4	0.01559225	1.36411619	29.835136	28.994725	36.57989	0.1347447	1.446829289
JB03-22_2_5	0.01883171	1.25339115	29.660153	27.890223	36.302984	0.132582	1.372667689
JB03-22_2_6	0.02042852	1.41358745	29.926119	28.281247	35.917783	0.1404401	1.532055522
JB03-22_2_7	0.01390416	1.36325596	29.361096	29.785607	36.186933	0.1358096	1.410746962
JB03-22_2_8	0.01754794	1.45441042	30.073904	28.536366	36.059507	0.1382677	1.451092785
JB03-22_2_9	0.01942413	1.47025071	29.756367	28.200925	35.779837	0.1389056	1.621561608
JB03-22_2_10	0.02130433	1.47161434	30.051869	27.754857	35.693851	0.1379853	1.634312779
JB03-22_2_11	0.01552751	1.41467081	30.121867	28.995436	36.332127	0.1354295	1.422493534
JB03-22_2_12	0.0172737	1.45954424	29.930659	28.814004	36.23843	0.1390478	1.511173808
JB03-22_2_13	0.02089056	1.6274466	29.774422	28.094813	35.437724	0.1415001	1.756903463
JB03-22_2_14	0.02351253	1.70889903	29.602952	27.6659	34.877439	0.1415924	1.879408135
JB03-22_2_15	0.01971353	1.50695103	30.077449	28.153327	35.80672	0.1402175	1.59203765
JB03-22_2_16	0.01890155	1.59010682	29.743535	28.219578	35.739453	0.1414162	1.645029964
JB03-22_2_17	0.02257814	1.75763555	29.598068	27.759431	34.941774	0.1417262	1.922432619
JB03-22_2_18	0.01965443	1.43227325	29.703412	28.428708	36.034661	0.1390138	1.546050661
JB03-22_2_19	0.01679432	1.41764194	29.754648	28.838994	36.462617	0.1370312	1.527043387
JB03-22_3_1	0.02047047	1.59651694	28.952218	28.200321	36.247871	0.1352575	1.640606696
JB03-22_3_2	0.02205161	1.68781782	28.988819	27.158541	35.600203	0.132582	1.778192925
JB03-22_3_3	0.02050928	1.54710335	29.167959	28.058364	36.569772	0.1359386	1.541270755
JB03-22_3_4	0.01597128	1.40392436	29.70411	28.5623	36.873616	0.1295995	1.436191649
JB03-22_3_5	0.02069942	1.63280227	29.056794	27.816078	35.949896	0.1336844	1.717583336
JB03-22_3_6	0.02355465	1.70649386	28.901731	27.514363	35.265013	0.1341938	1.861251119
JB03-22_3_7	0.0232353	1.54513152	28.970281	26.611691	35.209106	0.1274401	1.767198828
JB03-22_3_8	0.01470612	2.04566854	31.236248	27.661718	35.757656	0.0536973	0.86724608
JB03-22_3_9	0.01734613	1.44721407	29.032692	27.638091	36.420931	0.1187921	1.33477868
JB03-22_3_12	0.01903796	1.30044703	29.252773	27.726302	36.486662	0.1289353	1.378637913
JB03-22_3_13	0.02029909	1.4939557	29.748354	27.01146	35.589151	0.1304012	1.596283722

Sample	MgO wt %	Al_2O_3 wt %	SiO_2 wt %	CaO wt %	TiO_2 wt %	MnO wt %	Fe_2O_3 wt %
JB03-22_3_14	0.02124046	1.36747334	28.973813	27.394516	36.013624	0.1287086	1.501333371
JB03-22_3_15	0.01504873	1.27309493	29.536644	28.039596	36.907499	0.119517	1.164760944
JB03-22_3_16	0.02088315	1.55950863	29.5683	27.941201	36.027983	0.1360025	1.588260188
JB03-22_4_1	0.01542621	1.39667114	29.915926	28.468988	36.759906	0.1310883	1.409674619
JB03-22_4_2	0.01939891	1.24262957	29.173644	27.867031	36.683845	0.1299514	1.365735666
JB03-22_4_3	0.01906687	1.44017301	29.500978	28.293085	36.719787	0.131711	1.358049172
JB03-22_4_4	0.0172838	1.40646754	29.541819	28.595836	36.910624	0.1296995	1.414990388
JB03-22_4_5	0.01969123	1.5262211	29.874145	27.823914	36.110026	0.1349251	1.569708551
JB03-22_4_6	0.02248735	1.38733902	29.325262	26.975824	35.859121	0.1299403	1.606102219
JB03-22_4_7	0.0199856	1.61611347	29.831416	27.564298	35.753665	0.1335214	1.668320963
JB03-22_4_8	0.02253211	1.79374778	29.169008	27.297957	35.211989	0.1323257	1.910961711
JB03-22_4_9	0.02237846	1.63332027	29.713566	26.44307	34.950492	0.1303002	1.789818389
JB03-22_4_10	0.01843285	1.34241125	30.695123	27.45536	36.322045	0.1339827	1.373066558
JB03-22_1_1	0.01459128	1.23046951	30.694562	28.146226	36.466472	0.1327301	1.278014404
JB03-22_1_2	0.01699942	1.42153321	30.396565	28.268159	36.259355	0.1326123	1.485062029
JB03-22_1_3	0.02021629	1.36002749	29.821604	27.171043	35.704889	0.1313281	1.534714236
JB03-22_1_4	0.01884149	1.45235793	29.819552	28.377977	36.397387	0.1346525	1.409543419
JB03-22_1_5	0.01848862	1.45684913	29.94183	28.240885	36.254718	0.1352413	1.440001016
JB03-22_1_6	0.01984195	1.38367083	30.06863	26.738794	35.539627	0.1304675	1.575042468
JB03-22_1_7	0.02004141	1.64421561	30.263708	27.522703	35.445432	0.1355709	1.721410939
JB03-22_1_8	0.0146026	1.35549717	30.167036	28.594916	36.694325	0.1304615	1.387779195
JB03-22_1_9	0.01913759	1.45921893	29.920914	28.237559	36.354019	0.1357954	1.396162522
JB03-22_1_10	0.02245243	1.49651695	29.688259	26.742202	35.284726	0.1312126	1.647673277
JB03-22_1_11	0.02193192	1.67648632	29.609451	27.650504	35.449262	0.1378622	1.817524536
JB03-22_1_12	0.01978345	1.60126214	29.714885	27.914995	35.938974	0.1381484	1.616109669
JB03-22_1_13	0.01977256	1.5034086	29.666702	28.077299	36.402854	0.136588	1.445942581
JB03-22_1_14	0.02134676	1.56484728	29.582595	26.721368	35.421894	0.1330164	1.485492403
JB03-22_1_15	0.01967735	1.58663789	29.883276	27.510059	35.581597	0.1357807	1.706919802
JB03-22_1_16	0.02052184	1.51488387	29.804988	28.06767	36.165195	0.1382467	1.541603655
JB03-22_1_17	0.0189131	1.51102606	29.42153	28.298472	36.439442	0.1375458	1.459510233
JB03-22_1_18	0.02218971	1.38983735	29.293677	27.079568	35.811847	0.1313628	1.62929473
JB03-22_1_19	0.02072043	1.66646714	29.723101	27.686346	35.589277	0.1362842	1.737937434
JB03-22_1_20	0.01188282	1.35346956	30.031971	28.741523	36.918227	0.1277784	1.369961284
JB03-23_1_1	0.01471542	1.30756439	29.825266	28.995839	36.699139	0.1325073	1.41567853
JB03-23_1_2	0.02046522	1.36434336	29.810064	28.214728	35.986556	0.1366693	1.477195201
JB03-23_1_3	0.00901495	0.96652889	30.437788	29.127811	36.999075	0.1321223	1.046275981
JB03-23_1_4	0.00919382	1.06087462	30.29672	28.714377	36.696114	0.1376125	1.183434427
JB03-23_1_5	0.02115989	1.70142241	29.527816	27.578539	35.178731	0.1386561	1.880448814
JB03-23_1_6	0.0213512	1.71249286	29.642639	27.702649	35.140857	0.1392036	1.920745081
JB03-23_1_7	0.02069686	1.34391453	29.473472	27.69198	35.826396	0.132611	1.509718092
JB03-23_1_8	0.0220647	1.55094243	29.942062	27.355679	34.982042	0.1356964	1.771828135
JB03-23_1_9	0.01734073	1.38878427	30.853091	27.792451	35.771711	0.1346262	1.433610001
JB03-23_1_10	0.02226068	1.45747136	29.375705	27.498282	35.7922	0.1351531	1.429355322
JB03-23_1_11	0.02083486	1.68054679	29.902862	27.970351	35.221652	0.1391889	1.849495113
JB03-23_2_1	0.02104541	1.3308053	29.968758	27.334684	35.567827	0.1347993	1.559151288
JB03-23_2_2	0.0258173	1.57396341	29.399964	26.73397	34.599361	0.1333745	1.825386696
JB03-23_2_3	0.02374833	1.75497698	29.384641	27.733269	34.66181	0.1379706	2.04682916
JB03-23_2_4	0.02130041	1.3605871	29.720982	27.450066	35.44529	0.136235	1.632046779
JB03-23_2_5	0.02173435	1.50091193	30.026502	26.920976	35.075513	0.1329792	1.513490838
JB03-23_2_6	0.02340417	1.62244444	29.71238	27.424273	35.061748	0.1363038	1.772929351
JB03-23_2_7	0.02368289	1.4404261	29.510719	27.391913	35.262443	0.134977	1.65202051
JB03-23_2_8	0.02104797	1.44065447	29.83478	27.890436	35.640023	0.1368794	1.60298242
JB03-23_2_9	0.01042987	1.01609425	30.566686	28.274154	36.720897	0.1361493	1.181338383
JB03-23_2_10	0.01889419	1.47450507	30.375569	28.355295	35.720518	0.1390284	1.510430834

Sample	Y ppm	Zr ppm	La ppm	Ce ppm	Pr ppm	Nd ppm	Sm ppm	Eu ppm
HDJB1-1	1276.69	384.66	2243.94	5793.08	619.47	2206.74	388.27	63.16
HDJB1-2	1706.24	377.69	2059.61	4939.94	569.79	2441.85	510.78	68.01
HDJB1-3	1170.71	315.37	1707.41	3591.56	410.77	1714.99	343.39	51.62
HDJB1-4	1099.05	417.13	2214.79	5733.81	609.36	2035.77	301.36	59.77
HDJB1-5	1061.05	491.27	2837.47	7261.41	722.72	2461.84	340.66	92.84
HDJB1-6	1146.45	504.22	2647.51	6746.49	757.02	2545.38	330.66	82.53
HDJB4-1	1371.00	355.59	1892.17	5087.61	546.45	2042.05	403.21	59.95
HDJB4-2	1704.55	372.02	2033.58	5162.22	580.77	2409.44	506.06	66.68
HDJB4-3	1076.25	300.23	1485.77	3293.91	364.19	1457.49	310.32	51.03
HDJB4-4	851.48	486.27	1936.78	5120.66	538.74	1878.20	273.90	61.54
HDJB4-5	1029.86	553.24	2192.15	5856.15	654.52	2405.99	335.26	54.39
HDJB4-6	831.07	424.92	2183.53	5285.82	578.66	2112.15	302.09	88.71
HDJB5-1	956.79	377.04	2121.60	6229.54	637.43	2008.82	263.41	67.43
HDJB5-2	889.29	460.88	2185.18	5784.18	603.67	2220.15	330.39	106.21
HDJB5-3	799.33	430.88	2037.61	5225.01	551.27	2001.23	302.17	94.96
HDJB5-4	1361.94	336.41	2049.15	5712.99	599.79	2195.25	409.95	65.18
HDJB5-5	3546.03	934.94	3422.05	12003.67	1628.63	7105.76	1336.71	180.27
HDJB5-6	2055.53	534.67	2783.95	8936.64	1174.31	4607.21	676.42	93.97
HDJB6-1	972.00	463.05	2089.17	5778.34	613.44	2228.74	352.87	86.88
HDJB6-2	1419.62	323.41	1826.56	5076.99	529.52	2121.32	431.63	61.53
HDJB6-3	931.10	287.46	1436.79	3278.04	349.14	1438.28	273.93	42.77
HDJB6-4	2159.54	376.99	2290.69	6740.93	827.75	3573.23	740.33	90.66
HDJB6-5	3860.43	514.15	2342.41	10003.31	1501.67	7085.01	1495.32	187.20
HDJB6-6	3104.90	21.38	672.98	3247.65	570.14	3003.90	874.69	113.75
HDJB7-1	1528.25	390.51	2216.78	5491.83	609.48	2367.46	470.36	67.88
HDJB7-2	1577.54	381.95	2093.11	5253.98	581.10	2363.60	480.55	66.45
HDJB7-3	794.34	259.74	1289.15	2614.81	279.47	1190.08	222.49	42.35
HDJB7-4	374.05	107.57	344.07	909.21	102.46	445.10	97.81	27.09
HDJB7-5	1333.22	442.63	2324.50	5751.80	612.73	2271.70	383.03	79.70
HDJB7-6	1099.77	539.41	2616.03	6089.62	690.95	2635.91	390.53	118.46
HDJB14-1	1028.35	436.13	2412.95	6965.50	730.76	2299.35	299.44	76.67
HDJB14-2	814.23	271.40	1380.95	3189.24	320.04	1270.31	243.47	42.64
HDJB14-3	876.04	302.97	1643.40	3526.29	362.17	1484.60	269.55	47.83
HDJB14-4	939.17	445.86	2234.96	6132.00	644.42	2299.71	352.40	109.77
HDJB14-5	930.11	465.83	2686.95	6653.12	657.39	2273.19	323.89	97.35
HDJB14-6	1111.99	535.67	2795.92	7184.32	732.68	2534.21	339.88	84.21
HDJB17-1	338.50	122.10	426.87	1059.87	109.05	452.02	92.90	26.39
HDJB17-2	354.11	91.90	237.48	694.16	87.88	407.43	91.65	25.81
HDJB17-3	315.49	80.33	175.08	528.58	65.28	339.94	82.46	19.32
HDJB17-4	931.53	460.19	2444.38	6292.99	654.61	2268.86	332.01	102.11
HDJB17-5	1015.31	473.66	2576.36	6660.52	672.02	2312.93	319.31	90.47
HDJB17-6	957.37	415.31	2119.06	5591.66	607.37	2023.53	266.53	62.08
HDJB20-1	892.72	531.76	2164.86	5254.16	569.03	2165.01	330.97	67.62
HDJB20-2	1164.07	568.99	2860.28	7408.09	829.10	3047.99	419.99	67.05
HDJB20-3	2866.60	787.91	4147.05	12733.13	1669.15	6660.56	1020.94	137.54
HDJB20-4	3031.94	877.15	4190.10	13007.83	1716.84	6945.05	1074.20	144.50
HDJB20-5	1500.09	591.28	2399.74	6953.89	855.68	3275.29	475.81	70.49
HDJB20-6	3697.86	902.60	3582.68	12086.24	1726.70	7486.89	1307.50	172.42
HDJB20-7	2872.30	572.25	3058.17	10282.52	1458.51	6142.64	1045.66	137.83
HDJB20-8	1068.65	529.78	2367.70	5826.68	654.25	2544.15	403.69	115.61
HDJB20-9	1010.13	555.90	2608.54	6317.44	696.98	2715.77	439.58	102.94
HDJB20-10	3790.68	981.46	4560.45	14542.32	2029.52	8398.74	1389.65	181.87
HDJB20-11	3529.56	1284.86	4486.19	14072.77	1900.50	7918.90	1276.92	163.15
HDJB20-12	1049.46	492.94	2835.06	6684.41	750.71	2963.21	455.87	114.34

Sample	Y ppm	Zr ppm	La ppm	Ce ppm	Pr ppm	Nd ppm	Sm ppm	Eu ppm
HDJB21-1	3799.09	714.55	3180.04	9949.68	1521.03	7124.80	1410.24	176.14
HDJB21-2	4614.66	1042.06	4852.21	14579.55	2172.50	9457.21	1661.94	199.17
HDJB21-3	1664.37	610.11	2629.04	7095.27	897.92	3541.36	520.24	73.26
HDJB21-4	6329.60	1334.30	4969.06	16221.74	2766.85	13747.44	2942.79	314.29
HDJB21-5	1230.55	610.14	2721.40	6644.82	769.75	2932.50	427.15	68.25
HDJB21-6	6535.70	1437.88	4622.88	15738.98	2711.15	13570.57	2948.19	326.38
HDJB21-7	2823.30	689.76	2455.82	7842.00	1255.79	6440.10	1415.34	177.34
HDJB21-8	3133.12	650.68	2899.44	9449.84	1375.40	5972.05	1051.83	133.92
HDJB21-9	2951.92	642.56	2810.04	9038.88	1288.66	5494.52	933.57	118.91
HDJB21-10	1287.59	584.68	2559.10	6041.24	717.41	2970.70	499.79	126.32
HDJB22-1	492.90	2568.40	6950.22	739.48	2433.53	318.08	82.74	270.78
HDJB22-2	865.96	561.42	2489.87	5961.76	628.95	2292.20	320.86	58.48
HDJB22-3	985.58	511.20	2144.51	5421.23	603.46	2321.62	357.72	107.39
HDJB22-4	951.12	509.24	2188.22	5412.04	597.05	2310.88	352.66	104.71
HDJB22-5	1115.37	516.70	2261.97	5620.05	623.69	2436.49	393.16	105.95
HDJB22-6	3183.17	592.61	3359.15	11377.73	1609.32	6835.23	1181.63	167.16
HDJB22-7	1998.54	454.35	2921.12	8737.00	1099.02	4341.32	675.58	98.02
HDJB22-8	1550.06	534.99	2556.08	6954.08	857.35	3593.38	639.82	118.88
HDJB23-1	2672.78	605.47	2815.92	9051.80	1251.66	5260.35	843.23	113.17
HDJB23-2	3411.62	1051.09	3445.27	10635.68	1512.43	6830.46	1314.30	172.01
HDJB23-3	3289.21	623.90	3097.18	10173.78	1479.49	6400.11	1102.99	141.69
HDJB23-4	3256.33	626.99	3033.07	9956.73	1441.16	6229.43	1073.34	138.54
HDJB23-5	3510.63	1038.80	5058.67	15133.64	2071.30	8632.70	1388.52	175.34
HDJB23-6	2357.20	597.58	2720.82	8526.21	1150.54	4693.10	744.73	100.92
HDJB23-7	2105.94	580.02	2877.84	8540.99	1114.60	4528.24	710.22	107.24
HDJB23-8	3227.75	903.09	4302.00	12963.58	1733.83	6994.57	1072.88	144.92
HDJB23-9	1118.29	517.31	2124.59	5197.12	579.73	2241.44	354.31	105.22
HDJB23-10	1377.45	576.17	2149.48	6221.77	780.24	3023.28	452.94	61.73
HDJB24-1	1044.05	472.37	2307.08	5842.06	611.59	2183.33	319.94	93.51
HDJB24-2	1081.42	461.00	2397.22	6193.96	642.20	2182.03	298.98	84.31
HDJB24-3	2628.59	591.95	2853.96	9583.72	1366.37	5910.25	1042.16	129.11
HDJB24-4	3454.88	637.76	3191.09	11436.44	1703.74	7704.84	1447.20	172.51
HDJB24-5	4022.39	802.95	4242.25	14346.42	2115.66	9450.90	1744.34	203.53
HDJB24-6	2935.20	587.58	2808.40	9498.82	1397.32	6618.33	1339.80	190.70
HDJB25-1	944.70	503.18	2207.73	5425.89	586.23	2198.78	332.65	94.52
HDJB25-2	2495.42	714.69	3817.31	11479.42	1443.82	5603.43	834.20	116.20
HDJB25-3	3020.50	627.14	3456.14	11438.52	1576.64	6704.86	1164.00	151.75
HDJB25-4	3497.26	990.00	3585.67	11746.96	1636.71	6964.79	1227.22	163.62
HDJB25-5	2843.24	669.32	2995.06	10018.87	1375.21	5695.84	933.04	125.47
HDJB25-6	2975.81	643.85	2921.52	9872.45	1471.29	7034.47	1429.68	195.00
HDJB25-7	3015.47	663.45	3067.94	10081.79	1452.79	6662.58	1291.47	174.52
HDJB25-8	1010.70	530.56	2201.12	5525.24	612.71	2392.09	373.46	109.27
HDJB26-1	968.25	513.54	2642.27	6342.47	651.37	2319.13	335.27	101.71
HDJB26-2	1124.23	535.12	2429.23	5903.91	661.83	2629.14	438.76	109.05
HDJB26-3	1183.29	534.25	2361.05	6073.37	705.84	2812.10	475.64	121.50
HDJB26-4	1213.68	542.92	2325.32	5953.35	698.54	2803.36	477.33	119.14
HDJB26-5	4204.31	966.80	4573.01	14800.75	2094.16	9125.43	1692.29	214.65
HDJB26-6	3242.94	647.58	3340.31	11292.49	1581.25	6800.03	1205.82	158.74
HDJB26-7	4163.83	1165.31	4596.77	14884.97	2096.80	9066.75	1644.59	203.82
HDJB26-8	1523.22	544.43	2593.58	7552.08	907.73	3463.05	506.76	74.79
HDJB26-9	951.16	572.06	2419.16	6049.24	665.73	2586.57	422.70	90.24
HDJB26-10	1122.99	780.17	3413.73	8323.06	857.16	3048.88	415.53	67.34
JB03-21_1	1553.36	610.13	2484.15	7332.59	947.58	3646.16	516.75	98.73
JB03-21_2	5875.58	671.29	2314.82	9131.11	1664.25	8970.89	2240.54	249.39

Sample	Y ppm	Zr ppm	La ppm	Ce ppm	Pr ppm	Nd ppm	Sm ppm	Eu ppm
JB03-21_3	2005.13	602.67	2653.90	8463.59	1154.18	4712.22	712.67	119.96
JB03-21_4	3993.39	687.56	2549.56	8823.48	1410.41	6740.41	1356.56	177.57
JB03-21_5	6586.27	686.50	2310.62	9199.64	1711.28	9398.99	2410.06	261.06
JB03-21_6	6450.81	676.70	2309.93	9340.16	1731.62	9531.49	2419.04	265.16
JB03-21_7	1179.39	552.25	2603.54	7393.40	881.39	3204.45	413.53	83.81
JB03-21_8	6245.59	681.51	2292.20	8932.19	1655.90	9100.90	2287.69	251.49
JB03-21_9	6605.00	677.97	2379.23	9704.90	1796.39	10010.57	2587.05	284.06
JB03-21_10	2061.81	611.49	2717.17	8569.52	1184.02	4866.21	747.46	127.19
JB03-21_11	1018.33	517.95	2211.87	5650.12	658.46	2331.73	306.15	70.12
JB03-21_12	5618.26	622.59	2257.72	8720.06	1587.13	8584.33	2134.58	237.33
JB03-21_13	6396.14	660.33	2334.64	9269.73	1740.90	9647.84	2512.43	275.51
JB03-21_14	1630.30	599.39	2575.26	7700.16	1033.88	4122.87	602.68	110.90
JB03-21_15	1092.38	504.70	2530.90	6751.74	778.54	2748.68	346.43	77.39
JB03-21_16	1552.60	591.98	2506.59	7230.98	934.50	3612.95	534.31	98.31
JB03-21_17	7014.75	72.92	116.78	1555.65	617.42	5107.36	2282.98	270.50
JB03-21_18	6609.55	679.89	2588.82	10023.62	1865.02	10111.44	2666.31	271.91
JB03-21_19	954.96	492.80	2223.99	5695.25	640.32	2266.06	300.33	69.58
JB03-21_20	7346.41	780.68	3701.90	13697.11	2529.06	13450.08	3414.83	333.57
JB03-21_21	6411.74	614.99	2392.12	9459.16	1781.30	9587.74	2475.62	271.83
JB03-21_22	1441.03	584.00	2767.45	7662.46	971.64	3647.47	496.47	95.32
JB03-21_23	1294.08	455.81	2497.19	5086.30	544.85	2096.26	360.17	64.33
JB03-21_24	6141.10	747.59	2480.52	9030.54	1711.25	9170.14	2290.61	247.63
JB03-21_25	2399.58	595.00	2625.08	8456.56	1201.53	5046.23	838.90	130.35
JB03-21_26	3512.64	711.64	3013.67	9909.45	1532.61	7006.96	1298.43	176.92
JB03-22_2_1	1017.11	426.81	2567.88	5367.69	558.54	1989.99	298.98	61.67
JB03-22_2_2	1074.17	502.24	2237.29	6019.41	678.33	2326.45	299.39	67.61
JB03-22_2_3	2291.39	607.95	2867.35	9327.34	1317.00	5423.19	856.06	136.76
JB03-22_2_4	1088.09	548.86	2355.12	6430.41	738.07	2569.51	326.51	72.11
JB03-22_2_5	2597.43	646.61	3558.98	11525.65	1586.79	6440.05	1005.28	158.39
JB03-22_2_6	2368.43	641.26	2796.73	9164.93	1299.25	5446.02	905.05	138.69
JB03-22_2_7	1137.85	527.53	2492.16	6850.37	787.37	2780.78	356.81	76.37
JB03-22_2_8	1961.91	619.92	2532.16	7814.91	1057.86	4162.26	632.21	111.19
JB03-22_2_9	2508.25	697.28	2999.88	9739.48	1390.73	6100.76	1067.88	155.56
JB03-22_2_10	3392.15	680.96	2822.36	9601.90	1472.32	6613.55	1219.10	165.92
JB03-22_2_11	1162.04	484.68	2239.23	6105.50	698.51	2444.09	315.77	69.39
JB03-22_2_12	1461.22	533.83	2338.55	7008.70	884.90	3338.01	468.80	89.02
JB03-22_2_13	3503.15	627.60	2545.02	9110.84	1431.80	6581.86	1276.64	170.17
JB03-22_2_14	5519.26	761.41	2568.22	9755.03	1697.93	8829.72	2109.69	238.90
JB03-22_2_15	2428.25	637.93	2721.89	8966.04	1260.80	5265.47	862.09	136.50
JB03-22_2_16	2793.46	641.21	2661.15	8935.35	1344.64	5960.15	1105.13	154.47
JB03-22_2_17	5254.38	639.70	2334.14	9191.33	1628.05	8393.51	2044.41	230.91
JB03-22_2_18	2240.47	591.11	2756.73	9179.55	1288.02	5269.85	848.83	134.20
JB03-22_2_19	1268.89	549.33	2377.39	7036.64	873.73	3234.08	437.78	84.33
JB03-22_3_1	3519.70	654.11	2648.79	9450.73	1433.81	6551.59	1263.39	168.74
JB03-22_3_2	6570.11	795.06	2729.94	10711.64	1867.07	9731.92	2427.27	265.70
JB03-22_3_3	2773.94	661.06	2784.67	9271.58	1334.31	5943.54	1087.09	155.33
JB03-22_3_4	1177.97	575.61	2595.85	7364.63	852.77	3066.45	406.05	81.22
JB03-22_3_5	4530.85	655.98	2560.79	9624.33	1570.70	7773.63	1765.03	211.47
JB03-22_3_6	6621.21	877.47	2524.77	10308.96	1811.86	9698.39	2529.38	270.08
JB03-22_3_7	7503.70	970.32	3432.90	13397.61	2354.75	12297.05	3082.03	325.65
JB03-22_3_8	5222.41	148.87	443.23	2729.06	712.61	4832.24	1660.85	199.99
JB03-22_3_9	5995.10	504.41	2028.46	8548.80	1569.50	8558.11	2270.33	258.58
JB03-22_3_12	6404.53	725.98	2463.01	9997.26	1760.14	9522.22	2466.32	264.19
JB03-22_3_13	6928.96	815.39	3006.96	11936.04	2099.80	11076.90	2824.47	302.07

Sample	Y ppm	Zr ppm	La ppm	Ce ppm	Pr ppm	Nd ppm	Sm ppm	Eu ppm
JB03-22_3_14	4135.00	608.69	2836.54	10526.28	1617.14	7584.65	1576.55	205.14
JB03-22_3_15	6396.90	629.01	2429.15	10010.58	1767.82	9344.75	2380.65	263.15
JB03-22_3_16	5682.10	631.17	2811.34	11370.73	1947.04	9975.50	2411.69	270.68
JB03-22_4_1	3143.80	482.55	2214.22	8507.02	1331.33	6201.52	1218.96	171.04
JB03-22_4_2	3449.43	638.27	2562.17	9370.91	1408.30	6405.98	1244.75	169.98
JB03-22_4_3	1204.30	560.82	2583.32	7465.44	869.82	3133.94	418.49	82.20
JB03-22_4_4	3533.85	680.95	3002.56	10704.77	1574.96	7018.07	1313.98	180.21
JB03-22_4_5	2292.95	627.21	2625.33	8664.13	1144.62	4623.06	744.92	123.76
JB03-22_4_6	1351.94	572.63	2520.09	7645.83	905.27	3353.58	462.65	90.68
JB03-22_4_7	2880.68	614.15	2642.69	9181.99	1327.75	5951.27	1105.02	152.32
JB03-22_4_8	6614.59	753.58	2594.76	10718.36	1872.40	9887.51	2533.53	276.94
JB03-22_4_9	3977.86	659.05	2570.17	9572.89	1474.05	7053.50	1500.22	190.65
JB03-22_4_10	6500.55	667.10	2379.75	10030.99	1770.19	9580.10	2510.86	273.52
JB03-22_1_1	7004.38	908.86	3111.95	12289.90	2137.51	11462.10	2919.56	305.50
JB03-22_1_2	2432.12	642.97	2681.57	8839.48	1209.10	4984.23	817.54	128.80
JB03-22_1_3	1247.46	580.90	2779.77	7882.38	930.41	3332.43	435.59	87.50
JB03-22_1_4	1490.50	605.27	2514.82	7522.42	932.62	3506.77	497.03	93.94
JB03-22_1_5	4171.56	847.13	3638.33	12659.87	1909.10	8587.59	1685.79	212.46
JB03-22_1_6	2073.61	619.97	2550.78	8310.25	1094.19	4355.50	674.37	116.24
JB03-22_1_7	2237.23	627.42	2584.46	8603.23	1154.32	4647.49	744.36	122.66
JB03-22_1_8	4983.25	817.00	3462.25	12376.94	1968.13	9495.99	2058.60	242.50
JB03-22_1_9	3728.22	683.62	2600.10	9348.59	1425.66	6653.50	1318.38	174.42
JB03-22_1_10	1092.25	522.66	2421.60	6586.66	733.48	2545.08	327.31	73.40
JB03-22_1_11	2227.09	615.99	2581.67	8449.18	1130.60	4551.53	731.11	120.93
JB03-22_1_12	6268.36	834.05	3165.80	12194.52	2087.83	10639.29	2545.58	275.71
JB03-22_1_13	5073.17	662.07	2267.90	8835.52	1486.11	7666.65	1861.35	212.45
JB03-22_1_14	3290.16	652.77	2606.61	9146.71	1367.81	6176.22	1184.90	160.98
JB03-22_1_15	2582.26	635.94	2683.70	8969.35	1244.60	5250.51	899.09	139.41
JB03-22_1_16	5690.37	649.35	3476.21	12995.94	2200.58	11055.95	2612.00	268.36
JB03-22_1_17	4727.21	670.30	2356.34	9044.04	1484.75	7487.30	1764.21	206.33
JB03-22_1_18	2762.37	637.16	2573.45	8569.27	1223.65	5397.39	994.16	141.95
JB03-22_1_19	2514.98	631.34	2667.84	8946.27	1226.22	5174.95	887.51	136.88
JB03-22_1_20	6482.46	780.63	2582.20	10594.53	1871.19	9839.89	2496.41	271.97
JB03-23_1_1	4059.33	677.36	2559.55	9539.99	1480.87	7156.85	1534.21	192.68
JB03-23_1_2	1035.21	463.79	2497.42	5556.23	571.61	2031.97	305.48	64.83
JB03-23_1_3	1001.48	508.26	2384.52	6507.99	716.18	2495.78	314.16	70.21
JB03-23_1_4	2445.33	586.40	2906.96	9751.27	1357.69	6100.69	1076.35	157.45
JB03-23_1_5	1213.04	267.83	1881.30	4442.66	486.81	1972.70	369.81	60.55
JB03-23_1_6	1648.54	334.85	2362.60	6819.66	814.14	3186.50	516.82	89.40
JB03-23_1_7	5498.13	616.97	2329.33	9400.21	1636.52	8666.32	2128.08	242.17
JB03-23_1_8	4822.20	647.85	2454.96	9450.94	1555.63	7997.49	1861.94	220.95
JB03-23_1_9	3728.84	751.20	3616.41	12388.37	1807.82	8062.79	1456.13	196.72
JB03-23_1_10	5754.47	591.66	2395.27	9997.34	1749.93	9280.11	2309.18	259.29
JB03-23_1_11	2238.71	593.39	2612.80	8797.02	1209.77	5062.89	818.67	131.45
JB03-23_2_1	5021.54	645.02	2663.52	10380.79	1723.53	8776.70	2044.22	243.58
JB03-23_2_2	7174.34	829.81	3390.78	13508.61	2375.68	12476.78	3141.59	330.60
JB03-23_2_3	5933.92	645.42	2344.44	9847.95	1737.89	9359.57	2413.74	262.37
JB03-23_2_4	5325.99	679.66	2655.56	10565.68	1768.05	9143.72	2145.09	251.84
JB03-23_2_5	5394.00	584.67	3338.39	12448.12	2087.81	10555.42	2428.24	254.44
JB03-23_2_6	5508.60	644.26	2627.03	10267.28	1771.16	9290.47	2235.38	251.26
JB03-23_2_7	4962.58	932.60	3528.05	12599.29	1972.94	9584.57	2042.87	246.61
JB03-23_2_8	3678.01	650.89	2818.01	10072.49	1542.63	7090.61	1357.77	183.80
JB03-23_2_9	2141.36	322.70	2361.57	6589.73	870.60	3821.13	720.14	105.13
JB03-23_2_10	2139.73	593.42	2468.93	8265.71	1108.32	4547.83	713.38	118.99

Sample	Gd ppm	Tb ppm	Dy ppm	Ho ppm	Er ppm	Tm ppm	Yb ppm	Lu ppm
HDJB1-1	348.37	42.93	238.30	42.70	123.55	16.83	127.87	19.06
HDJB1-2	463.51	60.59	344.15	61.30	175.15	23.00	164.17	24.16
HDJB1-3	318.11	41.89	230.84	41.45	117.29	15.75	110.59	16.68
HDJB1-4	271.04	31.91	177.71	33.78	104.59	15.71	127.36	20.15
HDJB1-5	296.28	32.98	176.84	33.53	106.58	16.92	141.20	21.57
HDJB1-6	261.49	30.31	175.20	30.22	113.45	16.68	112.88	19.47
HDJB4-1	358.15	46.49	263.44	46.59	132.68	18.46	141.74	20.40
HDJB4-2	454.27	59.39	344.25	60.01	174.59	23.36	176.66	25.50
HDJB4-3	254.07	32.30	203.39	34.31	104.71	14.78	116.10	18.42
HDJB4-4	224.75	24.91	138.38	25.64	79.09	12.08	103.68	15.79
HDJB4-5	272.45	31.13	166.59	31.42	97.02	14.94	119.59	17.89
HDJB4-6	236.43	27.61	156.68	26.72	81.64	11.28	93.09	14.82
HDJB5-1	230.21	25.36	140.74	27.88	89.51	14.08	119.01	18.20
HDJB5-2	285.42	31.15	166.02	30.79	89.04	12.70	97.25	14.64
HDJB5-3	246.41	29.07	151.18	27.13	81.99	11.54	84.15	12.51
HDJB5-4	358.86	45.54	254.55	46.12	132.48	18.55	142.18	20.57
HDJB5-5	1028.94	133.21	732.58	130.72	361.11	48.99	321.29	36.64
HDJB5-6	507.56	64.61	367.56	67.71	204.15	27.47	200.52	25.23
HDJB6-1	287.61	32.56	174.45	31.19	92.87	13.81	110.25	15.25
HDJB6-2	379.88	49.21	286.21	50.37	144.37	19.87	153.20	21.48
HDJB6-3	243.92	32.72	183.26	32.87	88.93	12.46	95.33	15.55
HDJB6-4	607.21	78.89	438.15	75.79	208.26	27.58	195.91	25.28
HDJB6-5	1144.76	151.95	831.42	141.88	383.53	49.90	320.28	34.21
HDJB6-6	786.76	117.11	705.38	122.42	322.90	40.76	264.80	27.85
HDJB7-1	417.58	53.73	300.37	53.44	147.86	20.28	149.18	21.24
HDJB7-2	430.61	56.37	315.11	56.23	157.82	21.30	156.87	23.48
HDJB7-3	211.74	26.08	141.61	26.52	75.07	10.01	78.16	11.82
HDJB7-4	95.19	12.49	71.34	13.21	37.18	4.90	35.92	5.74
HDJB7-5	343.17	41.78	235.31	43.79	132.77	19.59	159.44	24.54
HDJB7-6	334.08	40.53	205.56	35.35	105.76	15.22	106.33	16.61
HDJB14-1	263.71	28.61	157.35	31.11	97.13	13.97	109.28	16.79
HDJB14-2	217.50	27.68	153.25	28.22	81.04	11.13	82.49	13.02
HDJB14-3	237.30	31.95	169.30	29.91	87.48	11.63	85.40	12.94
HDJB14-4	291.53	32.00	169.80	30.80	90.01	12.97	101.76	14.94
HDJB14-5	279.89	30.83	161.79	30.21	93.44	13.99	112.05	17.20
HDJB14-6	275.96	33.24	176.86	34.82	120.74	19.42	141.86	22.15
HDJB17-1	88.49	11.37	64.35	11.91	33.81	4.49	32.96	5.37
HDJB17-2	91.88	12.38	68.97	12.57	35.75	4.64	32.94	5.32
HDJB17-3	83.78	11.36	54.10	10.63	30.52	3.88	28.92	4.69
HDJB17-4	276.18	30.47	163.08	30.01	88.75	12.74	100.73	15.13
HDJB17-5	281.93	30.96	166.70	32.18	101.51	15.89	128.69	19.82
HDJB17-6	245.38	25.19	152.34	28.84	94.55	13.75	116.37	17.43
HDJB20-1	269.97	30.69	161.77	29.56	88.55	12.74	99.97	15.95
HDJB20-2	331.69	35.92	193.73	36.66	110.10	16.59	129.84	19.48
HDJB20-3	767.30	94.16	519.34	96.25	283.51	40.34	277.30	34.99
HDJB20-4	816.85	100.62	557.58	101.95	298.02	41.18	285.94	35.12
HDJB20-5	369.43	43.80	247.63	47.05	146.57	21.42	161.48	21.74
HDJB20-6	1007.04	130.59	735.33	132.27	373.53	49.34	326.96	38.19
HDJB20-7	777.98	99.53	559.33	99.75	284.83	38.14	255.11	30.24
HDJB20-8	332.31	38.36	201.89	36.81	105.26	14.83	114.99	17.08
HDJB20-9	357.61	40.08	206.28	36.25	100.83	13.40	105.33	16.15
HDJB20-10	1041.17	131.45	730.60	131.40	375.18	50.20	330.11	38.86
HDJB20-11	951.70	121.06	676.87	122.07	349.02	47.65	319.82	38.37
HDJB20-12	357.28	40.58	213.20	37.32	103.28	13.86	106.19	15.17

Sample	Gd ppm	Tb ppm	Dy ppm	Ho ppm	Er ppm	Tm ppm	Yb ppm	Lu ppm
HDJB21-1	1122.68	143.70	796.91	137.85	379.83	49.62	318.09	37.67
HDJB21-2	1277.72	164.29	908.83	162.74	453.58	59.88	384.61	46.20
HDJB21-3	414.86	48.49	278.04	52.18	160.08	23.48	172.62	24.43
HDJB21-4	2262.96	291.05	1540.74	247.95	617.16	73.03	424.88	46.13
HDJB21-5	343.96	39.79	212.40	39.14	118.24	17.26	131.00	19.98
HDJB21-6	2272.65	295.67	1574.39	254.51	647.93	76.58	450.50	48.59
HDJB21-7	1096.02	132.80	697.40	110.93	278.48	33.42	208.57	25.28
HDJB21-8	818.27	105.98	604.59	109.12	313.76	43.25	287.53	34.91
HDJB21-9	717.09	94.50	543.54	100.54	294.02	40.79	275.48	33.70
HDJB21-10	412.01	47.96	257.88	44.84	128.00	17.72	133.24	19.70
HDJB22-1	30.65	172.06	33.25	108.76	16.17	120.39	17.98	46.50
HDJB22-2	262.41	28.59	153.47	28.38	83.34	12.37	95.63	14.87
HDJB22-3	298.99	34.26	185.29	33.43	96.81	13.85	106.87	15.44
HDJB22-4	286.39	32.76	175.35	32.17	93.16	13.52	103.46	15.54
HDJB22-5	324.16	37.78	208.72	37.73	110.32	15.94	124.53	18.80
HDJB22-6	879.66	111.86	623.70	110.80	314.16	42.44	284.43	33.36
HDJB22-7	514.42	63.91	358.13	66.43	197.60	28.01	204.31	26.38
HDJB22-8	503.33	61.12	323.55	56.50	154.56	20.44	141.70	18.64
HDJB23-1	645.32	83.52	478.01	88.65	262.44	36.38	249.68	30.64
HDJB23-2	1016.72	128.71	711.14	123.80	346.52	46.07	306.06	36.58
HDJB23-3	844.81	108.67	630.29	113.34	332.76	45.02	305.39	36.10
HDJB23-4	813.25	107.35	613.46	112.37	327.36	45.22	297.10	35.96
HDJB23-5	1032.06	129.35	711.31	124.38	351.29	45.85	297.33	33.84
HDJB23-6	571.96	71.07	411.51	76.97	232.35	32.34	229.02	29.58
HDJB23-7	541.69	67.38	376.49	69.72	203.03	29.04	203.44	25.24
HDJB23-8	801.53	100.07	566.69	107.40	316.80	43.64	306.89	38.40
HDJB23-9	295.63	34.73	192.94	35.90	110.37	16.76	133.19	20.80
HDJB23-10	343.41	42.17	235.48	44.78	135.91	19.06	142.28	18.38
HDJB24-1	267.32	30.20	171.52	32.22	101.99	15.72	134.71	20.57
HDJB24-2	253.51	29.14	166.82	32.10	105.78	17.00	146.35	22.90
HDJB24-3	773.22	96.80	541.21	93.36	265.76	34.13	227.02	26.53
HDJB24-4	1067.40	136.71	748.91	126.95	347.82	44.61	284.77	31.61
HDJB24-5	1282.03	163.01	881.51	150.11	404.86	50.97	322.32	36.82
HDJB24-6	1011.81	124.35	666.08	109.27	296.16	38.03	246.83	29.44
HDJB25-1	276.37	31.55	175.51	31.67	93.00	13.34	107.92	16.44
HDJB25-2	616.97	74.73	430.01	79.57	244.28	35.21	252.54	32.27
HDJB25-3	866.33	110.39	616.49	105.76	297.20	39.39	263.64	30.99
HDJB25-4	948.39	120.35	688.99	124.54	352.53	47.69	310.51	36.82
HDJB25-5	707.11	89.98	518.62	94.89	283.16	38.17	262.41	31.88
HDJB25-6	1074.39	132.64	698.44	113.88	292.67	36.35	230.38	26.77
HDJB25-7	985.08	121.57	659.39	110.45	301.49	39.70	257.25	30.13
HDJB25-8	309.16	35.54	190.66	34.19	99.79	14.37	109.67	16.53
HDJB26-1	278.71	31.62	169.34	31.33	96.29	14.32	115.24	17.92
HDJB26-2	359.37	41.29	219.57	38.64	110.87	16.32	120.73	16.90
HDJB26-3	378.83	44.91	240.87	41.57	118.33	15.92	119.97	17.12
HDJB26-4	387.73	45.71	245.15	42.48	120.48	16.34	116.04	16.87
HDJB26-5	1263.67	160.18	882.03	151.62	418.93	54.64	356.82	40.68
HDJB26-6	902.19	115.75	648.54	113.24	321.19	42.51	284.05	32.93
HDJB26-7	1230.49	156.01	867.59	148.39	414.03	54.77	353.30	40.10
HDJB26-8	386.81	45.83	257.19	48.07	145.75	21.18	158.18	21.57
HDJB26-9	334.87	37.24	193.62	33.66	92.96	12.45	91.18	13.36
HDJB26-10	329.55	35.74	192.19	35.01	107.82	15.91	128.19	19.44
JB03-21_1	396.65	46.00	258.27	48.72	149.89	22.45	173.68	24.61
JB03-21_2	1849.85	254.26	1381.63	228.57	579.40	68.66	409.20	44.31

Sample	Gd ppm	Tb ppm	Dy ppm	Ho ppm	Er ppm	Tm ppm	Yb ppm	Lu ppm
JB03-21_3	536.36	63.47	350.82	65.41	195.70	28.63	210.28	28.08
JB03-21_4	1102.52	140.86	788.00	139.02	388.77	51.17	352.05	42.71
JB03-21_5	2011.58	277.18	1545.06	254.03	653.13	78.31	471.79	50.05
JB03-21_6	2005.82	276.04	1523.00	250.85	642.22	77.14	459.06	49.27
JB03-21_7	328.12	34.78	189.66	36.32	110.65	16.50	129.84	19.09
JB03-21_8	1923.59	263.81	1462.05	242.03	622.03	73.54	441.74	47.69
JB03-21_9	2149.71	296.40	1618.40	261.45	655.26	78.48	461.94	48.15
JB03-21_10	553.72	66.65	370.05	68.61	201.84	30.08	216.45	28.71
JB03-21_11	253.21	29.22	164.56	31.85	99.23	14.26	108.58	15.63
JB03-21_12	1751.41	240.29	1316.85	216.77	554.31	66.39	400.88	43.53
JB03-21_13	2061.61	286.51	1559.44	252.20	636.58	76.58	451.93	47.70
JB03-21_14	455.28	53.06	285.77	52.83	161.31	22.86	169.01	22.97
JB03-21_15	282.03	30.44	172.56	32.90	105.95	16.53	134.50	20.24
JB03-21_16	400.30	46.28	258.72	49.31	150.02	21.88	170.26	24.25
JB03-21_17	2115.95	310.00	1740.63	281.72	710.99	83.08	486.84	49.42
JB03-21_18	2216.27	299.49	1613.39	262.48	654.05	77.95	461.53	49.22
JB03-21_19	248.17	28.24	158.49	30.40	93.29	13.45	96.65	14.33
JB03-21_20	2792.61	365.90	1938.76	303.46	734.44	82.49	460.30	46.38
JB03-21_21	2028.66	277.06	1531.71	250.82	638.85	76.46	452.08	47.83
JB03-21_22	382.40	42.79	237.07	45.65	139.39	20.53	154.69	22.52
JB03-21_23	324.43	41.12	240.81	43.91	131.08	18.40	136.33	21.09
JB03-21_24	1933.30	261.19	1438.74	238.55	603.60	71.05	424.51	47.46
JB03-21_25	623.85	76.33	430.50	78.67	236.74	33.90	249.89	32.10
JB03-21_26	1002.13	126.46	705.81	124.07	349.11	45.80	297.68	34.83
JB03-22_2_1	258.56	31.43	180.53	33.63	102.75	14.84	118.49	18.38
JB03-22_2_2	244.70	28.61	162.88	32.09	105.52	16.37	132.40	19.81
JB03-22_2_3	628.61	76.72	414.92	77.03	227.94	32.59	229.80	29.67
JB03-22_2_4	258.92	29.31	165.20	32.20	104.37	16.60	138.35	21.40
JB03-22_2_5	747.17	86.93	480.66	87.95	262.64	36.97	248.95	30.57
JB03-22_2_6	672.21	82.31	446.19	80.83	236.51	33.44	232.68	29.77
JB03-22_2_7	276.07	31.47	175.85	34.17	111.21	17.28	142.51	21.82
JB03-22_2_8	469.02	57.26	325.08	61.90	193.24	28.99	228.02	31.12
JB03-22_2_9	796.68	95.82	505.98	87.87	252.96	35.60	255.21	33.33
JB03-22_2_10	940.64	121.58	676.85	119.87	339.37	45.35	306.99	36.56
JB03-22_2_11	254.94	29.19	167.97	33.57	112.49	18.63	159.42	24.41
JB03-22_2_12	354.83	41.83	230.17	44.52	141.31	21.47	173.88	24.56
JB03-22_2_13	1003.62	127.05	701.03	125.28	351.24	47.09	307.99	36.53
JB03-22_2_14	1734.19	235.45	1277.39	212.52	549.76	66.64	407.31	44.35
JB03-22_2_15	649.86	77.93	434.96	79.82	241.47	35.15	258.27	33.18
JB03-22_2_16	841.66	105.60	571.63	99.34	275.99	35.97	252.57	32.19
JB03-22_2_17	1671.05	224.81	1216.85	202.34	522.31	63.76	385.55	42.11
JB03-22_2_18	613.45	74.62	412.21	74.67	221.70	31.27	223.39	28.56
JB03-22_2_19	336.81	38.45	209.15	40.04	122.78	18.21	141.92	20.31
JB03-22_3_1	979.36	125.63	701.15	123.20	342.50	46.68	312.89	37.75
JB03-22_3_2	2005.10	275.16	1515.01	254.86	652.78	77.71	455.70	48.66
JB03-22_3_3	830.53	102.65	566.29	97.84	271.29	36.74	256.59	33.44
JB03-22_3_4	308.77	34.31	190.01	36.33	112.65	17.55	133.64	19.57
JB03-22_3_5	1413.65	183.20	998.20	167.93	442.48	55.05	343.65	38.20
JB03-22_3_6	2063.53	288.28	1572.29	261.76	660.54	79.67	463.93	48.92
JB03-22_3_7	2512.20	338.82	1827.85	297.88	746.16	88.29	513.09	53.26
JB03-22_3_8	1437.79	214.77	1218.57	203.52	520.36	63.46	374.12	36.65
JB03-22_3_9	1860.15	255.61	1403.56	232.21	586.72	70.91	424.90	44.76
JB03-22_3_12	2030.26	278.71	1530.04	249.17	632.81	77.02	462.51	49.83
JB03-22_3_13	2293.46	311.53	1687.18	273.68	681.01	81.82	470.86	49.66

Sample	Gd ppm	Tb ppm	Dy ppm	Ho ppm	Er ppm	Tm ppm	Yb ppm	Lu ppm
JB03-22_3_14	1231.24	157.50	870.59	147.75	404.78	52.99	341.02	39.90
JB03-22_3_15	1949.27	269.81	1479.74	246.55	629.92	77.17	461.65	49.45
JB03-22_3_16	1932.52	257.35	1382.76	225.63	556.52	65.55	376.11	39.83
JB03-22_4_1	931.05	117.30	647.15	112.32	308.58	40.63	266.23	32.39
JB03-22_4_2	972.95	124.12	695.25	122.11	341.07	46.18	315.46	38.02
JB03-22_4_3	320.92	35.44	193.72	37.12	115.84	17.22	135.35	19.74
JB03-22_4_4	1012.43	128.67	712.62	126.38	348.55	46.10	301.71	35.46
JB03-22_4_5	552.60	68.34	385.66	73.45	225.68	33.58	257.13	34.43
JB03-22_4_6	348.07	39.87	219.69	41.80	130.95	19.51	152.96	21.62
JB03-22_4_7	837.41	105.33	582.17	102.86	280.40	35.29	224.88	27.24
JB03-22_4_8	2095.04	289.20	1588.14	260.68	657.78	79.06	458.65	47.90
JB03-22_4_9	1177.55	150.77	821.39	143.70	390.67	51.37	340.88	40.08
JB03-22_4_10	2064.48	285.92	1566.16	256.69	646.76	77.72	458.56	48.02
JB03-22_1_1	2380.55	323.12	1739.05	282.63	693.59	81.20	464.15	48.61
JB03-22_1_2	616.96	77.61	442.45	80.55	240.10	35.02	248.78	32.23
JB03-22_1_3	339.47	36.21	201.91	38.80	120.27	18.20	140.43	20.55
JB03-22_1_4	376.49	43.76	241.89	46.15	143.77	21.53	165.84	23.25
JB03-22_1_5	1302.05	160.15	877.18	151.98	413.70	53.04	329.24	37.06
JB03-22_1_6	502.96	61.29	349.75	65.03	202.90	31.43	237.33	31.93
JB03-22_1_7	551.93	67.78	380.67	70.88	218.85	33.35	255.08	33.17
JB03-22_1_8	1628.93	207.60	1115.42	187.76	491.24	60.85	363.20	41.11
JB03-22_1_9	1033.36	132.18	736.81	131.20	371.05	49.22	327.83	39.46
JB03-22_1_10	265.23	29.74	169.25	32.92	105.02	16.59	136.79	20.97
JB03-22_1_11	540.00	66.13	378.70	69.81	218.84	33.03	252.69	33.62
JB03-22_1_12	2049.33	276.66	1508.37	247.03	619.78	72.96	418.17	43.68
JB03-22_1_13	1499.68	204.95	1117.34	189.83	494.86	62.91	401.66	45.23
JB03-22_1_14	902.80	116.63	644.70	115.13	322.67	43.90	297.76	35.91
JB03-22_1_15	671.90	83.19	465.65	85.66	253.59	37.52	284.34	36.93
JB03-22_1_16	2018.66	263.79	1409.96	223.53	553.89	66.01	387.28	40.19
JB03-22_1_17	1405.50	187.59	1025.09	176.76	465.61	58.95	378.79	42.83
JB03-22_1_18	764.23	96.42	529.57	93.81	264.70	37.29	276.60	35.91
JB03-22_1_19	660.49	80.72	450.42	82.86	246.78	37.52	275.24	35.98
JB03-22_1_20	2070.81	283.82	1542.88	256.52	647.33	78.02	461.54	48.26
JB03-23_1_1	1201.13	154.71	846.34	146.23	400.35	53.63	356.78	41.56
JB03-23_1_2	259.86	31.61	180.95	34.13	100.41	15.01	115.50	18.46
JB03-23_1_3	244.79	27.07	152.44	30.06	95.43	14.98	127.04	20.02
JB03-23_1_4	802.07	95.81	503.51	86.58	244.77	35.01	250.90	31.80
JB03-23_1_5	314.69	40.37	229.54	42.41	120.85	16.60	123.85	17.64
JB03-23_1_6	404.54	50.06	286.51	53.60	163.37	24.33	181.97	25.82
JB03-23_1_7	1728.32	232.09	1259.64	208.32	535.82	65.59	392.88	43.23
JB03-23_1_8	1507.43	198.11	1070.70	179.06	470.22	58.70	363.47	39.98
JB03-23_1_9	1108.65	140.26	764.11	133.53	366.21	46.69	301.99	35.18
JB03-23_1_10	1861.13	253.17	1377.68	226.06	569.53	67.01	395.74	42.15
JB03-23_1_11	612.26	74.00	406.78	75.12	219.81	31.26	224.55	28.94
JB03-23_2_1	1629.47	211.78	1136.74	188.87	487.29	60.17	369.52	39.54
JB03-23_2_2	2533.11	341.28	1811.65	290.15	708.00	81.02	455.37	46.36
JB03-23_2_3	1947.86	264.52	1436.59	230.05	573.78	68.48	414.93	43.09
JB03-23_2_4	1716.40	227.55	1237.22	202.90	529.61	63.75	389.01	42.15
JB03-23_2_5	1883.65	244.07	1300.31	208.44	522.37	62.89	375.49	39.36
JB03-23_2_6	1810.13	240.93	1304.17	212.24	535.10	63.54	386.14	41.26
JB03-23_2_7	1602.32	205.05	1079.09	181.99	488.64	59.37	356.36	39.62
JB03-23_2_8	1041.44	133.80	751.05	131.53	365.91	47.54	309.59	36.85
JB03-23_2_9	594.70	74.66	418.17	75.04	214.31	29.04	201.75	26.55
JB03-23_2_10	535.75	65.93	368.73	68.05	211.05	30.85	234.41	30.60

APPENDIX D: EMP MAJOR AND TRACE ELEMENT DATA

Sample	Na_2O wt %	MgO wt %	Al_2O_3 wt %	SiO_2 wt %	CaO wt %
HDJB01-2_8_P108	0	0.001	1.332	29.848	27.274
HDJB01-2_8_P110	0	0	1.214	30.541	27.158
HDJB01-2_8_P111	0.006	0.007	1.271	30.731	27.372
HDJB01-2_8_P112	0.017	0.017	1.245	30.618	27.43
HDJB01-2_8_P113	0	0.145	1.239	30.881	26.094
HDJB01-2_8_P114	0	0.012	1.225	30.942	27.651
HDJB01-2_8_P115	0	0.014	1.018	30.575	27.66
HDJB01-2_8_P116	0.008	0.01	0.914	31.159	27.978
HDJB01-2_8_P117	0	0.013	1.092	30.839	27.216
HDJB01-2_8_P118	0.001	0.02	1.033	30.357	27.497
HDJB01-2_8_P119	0	0.017	0.981	30.989	28.014
HDJB01-2_8_P120	0.003	0.003	0.838	31	28.564
HDJB01-2_8_P121	0.001	0.009	0.88	31.247	28.025
HDJB01-2_8_P122	0.006	0.017	1.002	31.954	28.448
HDJB01-2_8_P123	0.015	0	0.943	31.389	28.06
HDJB01-2_8_P124	0.003	0.01	0.934	31.13	28.287
HDJB01-2_8_P125	0.012	0	0.578	31.683	28.81
HDJB01-2_8_P126	0.013	0.008	1.056	31.649	28.711
HDJB01-2_8_P127	0	0.013	1.135	30.877	26.93
HDJB01-2_8_P128	0.002	0	0.813	31.293	28.343
JB03-21_P1	0.005	0.006	1.539	30.803	25.313
JB03-21_P2	0	0.014	1.553	30.453	25.317
JB03-21_P3	0	0.005	1.533	30.634	25.47
JB03-21_P4	0	0.009	1.523	30.253	25.477
JB03-21_P9	0	0.017	1.142	31.365	27.056
JB03-21_P11	0	0.028	1.435	30.36	26.335
JB03-21_P12	0	0.01	1.539	30.073	25.649
JB03-21_P13	0	0.018	1.232	29.447	25.438
JB03-21_P14	0	0.011	1.422	29.332	25.666
JB03-21_P15	0	0.006	1.129	30.408	26.395
JB03-21_P16	0.019	0.003	1.114	30.636	26.968
JB03-21_P17	0	0.022	1.243	29.04	24.95
JB03-21_P18	0.001	0.01	1.008	29.422	26.275
JB03-21_P19	0	0.015	1.061	29.954	25.877
JB03-21_P20	0.008	0.008	1.118	30.88	27.14
JB03-21_P21	0	0.006	1.219	30.254	26.785
JB03-21_P22	0	0.005	1.356	29.75	26.031
JB03-21_P23	0.001	0	0.884	30.297	27.172
JB03-21_P24	0	0	1.21	30.649	27.021
JB03-21_P25	0	0.017	1.402	29.663	25.589
JB03-21_P26	0.001	0.021	1.319	29.72	24.928
JB03-21_P27	0	0.02	1.434	29.702	25.976
JB03-21_P28	0.007	0.008	1.068	30.728	27.244
JB03-21_P29	0	0	1.141	30.62	27.388
JB03-21_P30	0	0.024	1.294	29.834	25.356
JB03-21_P31	0	0.01	1.262	29.985	25.237
JB03-21_P32	0	0.005	1.367	30.243	26.077
JB03-21_P33	0	0.016	1.475	30.058	25.886
JB03-22_1_P51	0.008	0.007	1.258	31.033	27.247
JB03-22_1_P52	0.011	0.005	1.125	30.524	27.463
JB03-22_1_P53	0.009	0.002	1.137	30.182	27.455
JB03-22_1_P54	0	0.014	1.182	29.555	27.027
JB03-22_1_P55	0.011	0.012	1.168	29.762	27.605
JB03-22_1_P56	0.021	0.017	1.16	30.151	27.615

Sample	Na_2O wt %	MgO wt %	Al_2O_3 wt %	SiO_2 wt %	CaO wt %
JB03-22_1_P57	0.02	0.014	1.28	29.979	26.959
JB03-22_1_P58	0.012	0.022	1.135	28.847	26.438
JB03-22_1_P59	0	0.009	1.298	29.391	26.874
JB03-22_1_P60	0	0.003	1.231	29.917	27.557
JB03-22_1_P61	0.008	0.013	1.138	30.079	27.71
JB03-22_1_P62	0.016	0	1.155	30.714	27.923
JB03-22_1_P63	0	0.011	1.115	29.948	26.719
JB03-22_1_P64	0	0.012	1.107	29.994	26.99
JB03-22_1_P65	0.004	0.01	1.061	30.033	26.777
JB03-22_1_P66	0	0	1.198	30.5	27.661
JB03-22_1_P67	0.003	0.018	1.118	29.26	26.467
JB03-22_1_P68	0.01	0	1.176	30.3	26.794
JB03-22_1_P69	0	0.001	1.053	30.343	27.429
JB03-22_1_P70	0	0.005	1.149	30.723	27.753
JB03-22_1_P71	0.001	0.016	1.501	30.075	26.468
JB03-22_1_P72	0	0.013	1.199	29.79	26.436
JB03-22_1_P73	0	0.005	1.395	29.847	27.008
JB03-22_1_P74	0.004	0.002	1.232	30.594	27.774
JB03-22_1_P75	0	0.007	1.262	29.687	25.967
JB03-22_1_P77	0	0.013	1.238	29.506	26.416
JB03-22_1_P78	0.013	0.011	1.322	29.716	26.219
JB03-22_1_P79	0.001	0.009	1.304	30.118	26.331
JB03-22_1_P80	0	0.024	1.295	30.168	25.977
JB03-22_1_P81	0.009	0.008	1.246	30.017	26.388
JB03-22_1_P82	0	0.005	1.232	29.96	26.344
JB03-22_1_P83	0	0.026	1.169	29.874	26.378
JB03-22_1_P84	0.002	0.025	1.191	30.39	26.276
JB03-22_1_P85	0.007	0.016	1.015	30.822	27.32
JB03-22_1_P86	0	0.01	1.208	31.149	27.893
JB03-23_1_P87	0	0.013	1.364	30.72	27.343
JB03-23_1_P88	0	0	0.932	30.36	28.455
JB03-23_1_P89	0	0.011	1.509	30.148	27.371
JB03-23_1_P91	0	0.004	1.578	30.17	26.963
JB03-23_1_P92	0	0.009	1.37	30.621	27.257
JB03-23_1_P93	0	0	1.034	30.967	28.114
JB03-23_1_P94	0	0.018	1.486	30.283	26.915
JB03-23_1_P95	0	0.026	1.491	30.04	26.785
JB03-23_1_P96	0	0.006	1.299	30.672	26.61
JB03-23_1_P97	0	0.001	1.269	30.745	26.574
JB03-23_1_P98	0.002	0.006	1.207	30.361	26.815
JB03-23_1_P99	0	0.004	1.325	29.774	26.409
JB03-23_1_P100	0.01	0.012	1.33	30.321	26.601
JB03-23_1_P101	0.007	0.01	1.352	29.68	26.284
JB03-23_1_P102	0	0.016	1.489	30.295	27.194
JB03-23_1_P103	0	0.017	1.369	29.624	26.386
JB03-23_1_P104	0	0.003	1.023	30.331	27.569
JB03-23_1_P105	0	0	0.947	30.724	27.887
JB03-23_1_P106	0	0.021	1.439	30.267	27.358
JB03-23_1_P107	0	0.021	1.317	30.211	26.585
JB03-22_3_P34	0.018	0.008	1.065	30.499	27.647
JB03-22_3_P35	0	0.012	1.475	30.347	26.067
JB03-22_3_P36	0	0	1.076	31.189	27.536
JB03-22_3_P38	0	0	1.02	31.102	27.158
JB03-22_3_P39	0	0.016	1.323	30.971	26.539

Sample	Na_2O wt %	MgO wt %	Al_2O_3 wt %	SiO_2 wt %	CaO wt %
JB03-22_3_P40	0.007	0	1.147	31.653	27.603
JB03-22_3_P41	0	0.001	1.276	31.529	26.828
JB03-22_3_P42	0	0.004	0.922	31.545	27.594
JB03-22_3_P43	0.005	0.014	1.212	30.564	26.172
JB03-22_3_P44	0	0.01	1.223	30.426	25.831
JB03-22_3_P45	0.005	0.013	1.004	30.799	26.57
JB03-22_3_P46	0	0.009	1.281	30.694	25.609
JB03-22_3_P47	0.006	0.008	1.3	30.825	25.564
JB03-22_3_P48	0	0.002	1.296	30.596	25.668
JB03-22_3_P50	0.01	0.007	1.122	31.236	27.251
JB01-12_1-P70	0.013	0	1.132	29.986	27.066
JB01-12_1-P71	0	0.017	1.06	29.851	26.706
JB01-12_1-P72	0.002	0.02	1.1	29.872	26.771
JB01-12_1-P73	0.004	0.016	1.104	30.04	27.122
JB01-12_1-P74	0	0.009	1.068	30.155	27.115
JB01-12_1-P75	0	0.012	0.946	29.847	27.107
JB01-12_1-P76	0.003	0.017	1.071	30.079	27.201
JB01-12_1-P77	0.001	0.012	1.031	29.852	27.039
JB01-12_1-P78	0.009	0.01	1.1	30.094	27.324
JB01-12_1-P79	0	0.017	1.072	30.001	27.303
JB01-12_1-P80	0.005	0.017	1.101	29.888	26.876
JB01-12_1-P81	0.004	0.023	1.105	30.024	27.119
JB01-12_1-P82	0.003	0.004	1.08	29.79	26.913
JB01-12_1-P83	0.002	0.024	1.075	29.95	26.89
JB01-12_1-P84	0	0.008	1.066	29.834	27.122
JB01-12_2-P85	0	0.02	1.115	29.974	26.949
JB01-12_2-P86	0.002	0.004	1.154	29.755	26.294
JB01-12_2-P87	0	0.019	1.082	29.711	26.82
JB01-12_2-P88	0.003	0.017	1.089	29.741	26.534
JB01-12_2-P89	0.006	0.008	1.161	29.683	26.627
JB01-12_2-P90	0.01	0.017	1.198	29.443	26.102
JB01-12_2-P91	0	0.006	0.994	30.042	26.926
JB01-12_2-P92	0.007	0.013	1.078	30.022	26.848
JB01-12_2-P93	0	0.007	0.88	29.859	26.608
JB01-12_2-P94	0	0.005	0.976	29.826	26.513
JB01-12_2-P95	0.005	0.016	0.987	29.543	26.244
JB01-12_2-P96	0.002	0.011	0.936	30.026	27.039
JB01-12_2-P97	0.015	0.014	1.177	29.905	26.698
JB01-12_2-P98	0.008	0.014	1.14	29.883	26.792
JB01-12_2-P99	0.009	0.011	1.127	30.029	26.618
JB01-12_2-P100	0	0	1.129	30.04	26.603
JB01-12_2-P101	0.006	0.013	0.986	29.724	26.437
JB01-12_2-P102	0	0.013	1.108	29.95	26.743
JB01-12_2-P103	0.015	0.017	1.094	29.909	27.038
JB01-12_2-P104	0	0.015	0.929	29.968	26.879
JB01-12_2-P105	0.003	0.015	0.803	29.826	26.622
JB01-12_2-P106	0	0.013	1.168	29.924	26.555
JB01-12_2-P107	0.003	0.017	0.967	29.39	25.472
JB01-12_3-P108	0	0.006	1.154	30.142	26.955
JB01-12_3-P109	0.001	0.006	1.036	30.068	27.013
JB01-12_3-P110	0.006	0.023	0.931	29.653	26.201
JB01-12_3-P111	0.003	0.025	1.052	29.79	26.462
JB01-12_3-P112	0.016	0.009	0.863	30.035	26.949
JB01-12_3-P113	0.014	0.021	1.16	30.005	26.944

Sample	Na_2O wt %	MgO wt %	Al_2O_3 wt %	SiO_2 wt %	CaO wt %
JB01-12_3-P114	0.001	0.014	1.166	29.974	27.18
JB01-12_3-P115	0.067	0.006	0.909	30.58	26.821
JB01-12_3-P116	0.007	0.01	0.98	29.621	26.241
JB01-12_3-P117	0	0.002	1.636	29.881	26.478
JB01-12_3-P118	0	0.01	1.071	29.801	26.69
JB01-12_3-P119	0	0.009	1.103	29.715	26.242
JB01-12_3-P120	0	0	0.96	30.008	27.454
JB01-12_3-P121	0.01	0.003	0.788	29.88	26.79
JB01-12_3-P122	0.002	0.022	0.909	29.679	26.046
JB01-12_3-P123	0.013	0.005	4.174	28.817	26.069
JB01-21_1-P1	0.004	0.003	1.151	29.543	25.311
JB01-21_1-P2	0	0.007	0.968	30.155	26.779
JB01-21_1-P3	0.002	0.003	1.16	29.708	25.542
JB01-21_2-P4	0	0.018	1.095	30.114	26.326
JB01-21_2-P5	0	0.002	1	30.225	26.895
JB01-21_2-P6	0	0.012	1.072	29.836	26.031
JB01-21_2-P7	0	0.018	1.228	29.973	26.061
JB01-21_2-P8	0	0.011	1.126	29.955	26.047
JB01-21_2-P9	0	0.008	0.98	29.589	25.447
JB01-21_2-P10	0.003	0.019	1.126	29.803	25.884
JB01-21_2-P11	0	0.01	1.222	29.833	25.936
JB01-21_2-P12	0	0	1.085	29.849	26.188
JB01-21_2-P13	0	0.018	1.052	30.112	26.272
JB01-21_2-P14	0	0	1.065	30.16	26.862
JB01-21_2-P15	0.006	0.013	1.179	30.042	26.483
JB01-21_2-P16	0.008	0.008	1.077	30.094	26.922
JB01-21_2-P17	0.02	0.001	0.898	30.004	26.602
JB01-21_3-P39	0	0.012	1.024	29.941	26.995
JB01-21_3-P40	0.003	0.015	1.017	29.934	27.023
JB01-21_3-P41	0.006	0.01	0.894	29.621	26.608
JB01-21_3-P42	0	0.014	1.184	29.52	26.205
JB01-21_3-P43	0	0.019	1.234	29.446	25.687
JB01-21_3-P44	0	0.009	1.097	29.15	25.4
JB01-21_3-P45	0	0.025	1.294	29.646	26.011
JB01-21_3-P46	0.002	0.009	1.146	29.822	26.698
JB01-21_3-P47	0.008	0.004	1.026	29.866	27.039
JB01-21_3-P48	0.005	0.015	1.207	29.759	26.446
JB01-21_3-P49	0.004	0.009	0.995	29.961	27.075
JB01-21_3-P50	0	0.031	1.096	29.674	26.653
JB01-21_3-P51	0.004	0.019	1.065	29.555	25.994
JB01-21_3-P52	0.013	0.02	1.094	29.782	26.541
JB01-21_4-P39	0	0.012	1.033	30.164	26.711
JB01-21_4-P40	0.004	0.011	1.064	30.257	26.902
JB01-21_4-P41	0.001	0.013	1.128	29.648	25.766
JB01-21_4-P42	0.002	0.006	1.135	29.452	25.451
JB01-21_4-P43	0.014	0	0.771	30.043	26.847
JB01-21_4-P44	0.013	0.012	0.648	30.333	27.444
JB01-21_4-P45	0	0.013	0.793	30.127	26.976
JB01-21_4-P46	0.004	0.008	1.133	29.448	25.737
JB01-21_4-P47	0.005	0.005	1.262	30.159	26.849
JB01-21_4-P48	0.009	0	0.922	30.319	27.546
JB01-21_4-P49	0	0.013	1.049	30.13	26.823
JB01-21_4-P50	0.001	0.015	1.037	30.039	26.933
JB01-21_4-P51	0.013	0	1.032	29.995	26.938

Sample	Na_2O wt %	MgO wt %	Al_2O_3 wt %	SiO_2 wt %	CaO wt %
JB01-21_4-P52	0.014	0.005	1.081	29.996	26.783
JB01-21_4-P53	0.003	0.005	1.076	29.713	26.181
JB01-21_4-P54	0.004	0.012	1.059	29.758	26.265
JB01-21_4-P55	0.002	0.015	1.093	29.733	26.198
JB01-21_4-P53	0.006	0.013	1.027	30.048	26.837
JB01-21_4-P54	0	0.007	1.098	29.524	25.886
JB01-21_4-P55	0	0.005	1.115	29.4	25.681
JB01-21_4-P56	0	0	0.763	29.88	26.702
JB01-21_4-P57	0.005	0.001	0.675	30.239	27.408
JB01-21_4-P58	0.009	0.011	0.934	30.211	27.399
JB01-21_4-P59	0	0.009	1.176	30.213	27.003
JB01-21_5-P60	0	0.013	1.155	29.963	26.788
JB01-21_5-P61	0	0.012	1.155	29.977	26.675
JB01-21_5-P62	0	0.007	0.938	29.776	26.226
JB01-21_5-P63	0.008	0.002	0.902	29.867	26.075
JB01-21_5-P64	0	0.013	1.248	29.718	25.781
JB01-21_5-P65	0.009	0.008	0.86	30.113	26.799
JB01-21_5-P66	0	0.007	1.129	29.904	26.408
JB01-21_5-P67	0.011	0.014	1.096	30.086	26.752
JB01-21_5-P68	0	0.012	1.146	30.042	26.692
JB01-21_5-P69	0.002	0.004	1.102	29.316	25.388

Sample	TiO_2 wt %	MnO wt %	FeO wt %	P_2O_5 wt %
HDJB01-2_8_P108	34.997	0.012	1.86	0.078
HDJB01-2_8_P110	35.401	0.006	1.651	0.07
HDJB01-2_8_P111	35.377	0.002	1.683	0.106
HDJB01-2_8_P112	35.735	0.013	1.636	0.117
HDJB01-2_8_P113	35.701	0.015	1.637	0.1
HDJB01-2_8_P114	35.879	0.022	1.547	0.112
HDJB01-2_8_P115	35.972	0.004	1.338	0.162
HDJB01-2_8_P116	36.594	0.003	1.171	0.167
HDJB01-2_8_P117	35.537	0.012	1.488	0.099
HDJB01-2_8_P118	35.963	0.002	1.453	0.122
HDJB01-2_8_P119	36.143	0.007	1.359	0.087
HDJB01-2_8_P120	37.182	0.011	0.76	0.027
HDJB01-2_8_P121	36.748	0.013	1.159	0.056
HDJB01-2_8_P122	36.817	0.002	1.234	0.074
HDJB01-2_8_P123	36.561	0.012	1.152	0.168
HDJB01-2_8_P124	36.946	0.006	1.165	0.11
HDJB01-2_8_P125	38.065	0.002	0.655	0.015
HDJB01-2_8_P126	36.342	0.016	1.171	0.064
HDJB01-2_8_P127	34.718	0.007	1.569	0.146
HDJB01-2_8_P128	36.494	0.016	1.055	0.067
JB03-21_P1	34.472	0.003	1.921	0.092
JB03-21_P2	34.309	0.01	1.923	0.083
JB03-21_P3	34.118	0.005	1.936	0.069
JB03-21_P4	33.984	0.01	1.932	0.069
JB03-21_P9	36.519	0.007	1.235	0.069
JB03-21_P11	35.226	0.009	1.677	0.061
JB03-21_P12	34.406	0	1.908	0.083
JB03-21_P13	34.912	0.01	1.655	0.141
JB03-21_P14	34.413	0.008	1.732	0.067
JB03-21_P15	36.067	0.005	1.315	0.092
JB03-21_P16	36.293	0	1.358	0.052
JB03-21_P17	34.62	0	1.612	0.143
JB03-21_P18	35.87	0	1.242	0.101
JB03-21_P19	35.576	0.007	1.351	0.089
JB03-21_P20	36.035	0.001	1.277	0.06
JB03-21_P21	35.523	0.012	1.494	0.071
JB03-21_P22	34.633	0.008	1.707	0.071
JB03-21_P23	36.83	0.009	0.728	0.019
JB03-21_P24	37.121	0	0.437	0.006
JB03-21_P25	34.634	0.018	1.819	0.093
JB03-21_P26	34.585	0.011	1.76	0.151
JB03-21_P27	34.8	0.013	1.775	0.07
JB03-21_P28	36.203	0.007	1.27	0.052
JB03-21_P29	36.089	0.007	1.384	0.06
JB03-21_P30	35.205	0.006	1.433	0.132
JB03-21_P31	34.73	0.008	1.707	0.151
JB03-21_P32	34.847	0.006	1.847	0.079
JB03-21_P33	34.384	0.003	1.924	0.09
JB03-22_1_P51	35.98	0	1.407	0.069
JB03-22_1_P52	36.394	0	1.302	0.054
JB03-22_1_P53	36.061	0.003	1.295	0.067
JB03-22_1_P54	36.209	0.005	1.192	0.077
JB03-22_1_P55	35.874	0.013	1.538	0.023
JB03-22_1_P56	36.194	0	1.326	0.054

Sample	TiO_2 wt %	MnO wt %	FeO wt %	P_2O_5 wt %
JB03-22_1_P57	35.975	0.012	1.471	0.074
JB03-22_1_P58	35.508	0.002	1.433	0.152
JB03-22_1_P59	35.097	0.007	1.498	0.076
JB03-22_1_P60	35.729	0.004	1.471	0.062
JB03-22_1_P61	36.208	0.016	1.342	0.02
JB03-22_1_P62	36.278	0.008	1.441	0.043
JB03-22_1_P63	35.801	0.012	1.367	0.146
JB03-22_1_P64	35.864	0.007	1.343	0.13
JB03-22_1_P65	35.684	0.008	1.338	0.135
JB03-22_1_P66	37.094	0	0.624	0.02
JB03-22_1_P67	35.395	0	1.388	0.135
JB03-22_1_P68	35.796	0.007	1.463	0.108
JB03-22_1_P69	36.386	0.005	0.801	0.039
JB03-22_1_P70	35.908	0.009	1.345	0.053
JB03-22_1_P71	34.559	0.003	1.801	0.063
JB03-22_1_P72	34.976	0.014	1.563	0.124
JB03-22_1_P73	35.24	0.012	1.639	0.069
JB03-22_1_P74	36.092	0.007	1.416	0.063
JB03-22_1_P75	34.594	0.005	1.651	0.118
JB03-22_1_P77	34.631	0.007	1.702	0.141
JB03-22_1_P78	34.722	0.002	1.411	0.158
JB03-22_1_P79	34.702	0.013	1.427	0.166
JB03-22_1_P80	34.36	0.009	1.671	0.169
JB03-22_1_P81	34.878	0.008	1.604	0.162
JB03-22_1_P82	34.963	0.007	1.561	0.135
JB03-22_1_P83	35.24	0.01	1.534	0.123
JB03-22_1_P84	35.077	0.006	1.595	0.133
JB03-22_1_P85	35.99	0.001	1.3	0.135
JB03-22_1_P86	35.871	0.013	1.361	0.054
JB03-23_1_P87	35.445	0.006	1.703	0.071
JB03-23_1_P88	37.192	0.004	0.885	0.017
JB03-23_1_P89	34.456	0.01	2.005	0.085
JB03-23_1_P91	34.864	0.003	1.942	0.053
JB03-23_1_P92	35.133	0.006	1.751	0.083
JB03-23_1_P93	36.398	0.012	1.2	0.102
JB03-23_1_P94	34.763	0.011	1.849	0.073
JB03-23_1_P95	34.681	0.001	1.86	0.115
JB03-23_1_P96	35.2	0.007	1.702	0.164
JB03-23_1_P97	35.238	0.006	1.607	0.112
JB03-23_1_P98	35.415	0	1.644	0.093
JB03-23_1_P99	34.66	0.012	1.703	0.16
JB03-23_1_P100	35.158	0.012	1.531	0.162
JB03-23_1_P101	34.75	0.002	1.749	0.135
JB03-23_1_P102	34.998	0.013	1.84	0.091
JB03-23_1_P103	35.077	0.006	1.71	0.166
JB03-23_1_P104	36.385	0.007	1.338	0.042
JB03-23_1_P105	36.203	0.01	1.188	0.031
JB03-23_1_P106	34.883	0.008	1.811	0.089
JB03-23_1_P107	34.982	0.002	1.665	0.154
JB03-22_3_P34	36.525	0.008	1.295	0.071
JB03-22_3_P35	34.947	0	1.773	0.065
JB03-22_3_P36	37.799	0	0.498	0.016
JB03-22_3_P38	36.733	0.003	0.727	0.011
JB03-22_3_P39	35.184	0.009	1.545	0.085

Sample	TiO_2 wt %	MnO wt %	FeO wt %	P_2O_5 wt %
JB03-22_3_P40	36.394	0.014	1.291	0.065
JB03-22_3_P41	35.668	0.009	1.388	0.086
JB03-22_3_P42	37.597	0.011	0.549	0.025
JB03-22_3_P43	35.567	0.003	1.513	0.077
JB03-22_3_P44	35.538	0.013	1.404	0.108
JB03-22_3_P45	36.223	0.006	1.297	0.096
JB03-22_3_P46	34.872	0.007	1.648	0.151
JB03-22_3_P47	34.971	0	1.686	0.162
JB03-22_3_P48	34.951	0.009	1.63	0.149
JB03-22_3_P50	36.616	0.009	0.589	0.044
JB01-12_1-P70	34.516	0.004	1.429	0.043
JB01-12_1-P71	34.627	0	1.413	0.063
JB01-12_1-P72	34.529	0.006	1.477	0.054
JB01-12_1-P73	35.279	0.012	1.349	0.046
JB01-12_1-P74	35.378	0.014	1.293	0.069
JB01-12_1-P75	35.167	0.004	1.242	0.092
JB01-12_1-P76	34.924	0.003	1.321	0.049
JB01-12_1-P77	35.685	0.011	1.263	0.101
JB01-12_1-P78	35.373	0.01	1.323	0.076
JB01-12_1-P79	35.377	0.004	1.275	0.076
JB01-12_1-P80	34.777	0.01	1.443	0.055
JB01-12_1-P81	34.923	0.02	1.363	0.049
JB01-12_1-P82	34.896	0.01	1.371	0.06
JB01-12_1-P83	35.096	0.011	1.462	0.056
JB01-12_1-P84	35.508	0.006	1.378	0.059
JB01-12_2-P85	35.171	0.007	1.261	0.049
JB01-12_2-P86	34.521	0.011	1.59	0.064
JB01-12_2-P87	34.761	0.005	1.448	0.052
JB01-12_2-P88	34.276	0.013	1.485	0.068
JB01-12_2-P89	34.04	0.004	1.641	0.077
JB01-12_2-P90	33.876	0.002	1.647	0.065
JB01-12_2-P91	35.008	0.007	1.338	0.056
JB01-12_2-P92	35.032	0.012	1.363	0.057
JB01-12_2-P93	35.14	0.007	1.209	0.078
JB01-12_2-P94	34.618	0.02	1.365	0.078
JB01-12_2-P95	34.644	0.01	1.446	0.096
JB01-12_2-P96	35.381	0.009	1.135	0.156
JB01-12_2-P97	34.314	0.001	1.629	0.065
JB01-12_2-P98	34.72	0.009	1.515	0.057
JB01-12_2-P99	34.636	0.01	1.52	0.059
JB01-12_2-P100	34.551	0.002	1.559	0.055
JB01-12_2-P101	34.502	0.009	1.432	0.079
JB01-12_2-P102	34.316	0.008	1.507	0.05
JB01-12_2-P103	34.67	0.009	1.462	0.058
JB01-12_2-P104	35.291	0.008	1.281	0.097
JB01-12_2-P105	35.678	0	1.123	0.132
JB01-12_2-P106	35.01	0	1.521	0.091
JB01-12_2-P107	34.76	0.004	1.558	0.094
JB01-12_3-P108	34.744	0.004	1.292	0.053
JB01-12_3-P109	34.622	0.015	1.251	0.059
JB01-12_3-P110	34.446	0.006	1.411	0.099
JB01-12_3-P111	35.132	0.007	1.37	0.141
JB01-12_3-P112	35.849	0.012	1.084	0.1
JB01-12_3-P113	34.828	0.009	1.625	0.082

Sample	TiO_2 wt %	MnO wt %	FeO wt %	P_2O_5 wt %
JB01-12_3-P114	34.842	0.013	1.596	0.078
JB01-12_3-P115	35.482	0.009	1.175	0.115
JB01-12_3-P116	35.092	0.012	1.374	0.091
JB01-12_3-P117	34.931	0.006	1.416	0.104
JB01-12_3-P118	34.735	0.013	1.517	0.052
JB01-12_3-P119	34.731	0.013	1.534	0.062
JB01-12_3-P120	35.336	0.004	1.289	0.095
JB01-12_3-P121	35.805	0.017	1.086	0.111
JB01-12_3-P122	34.748	0.011	1.401	0.089
JB01-12_3-P123	34.525	0.01	1.436	0.104
JB01-21_1-P1	33.636	0.002	1.639	0.09
JB01-21_1-P2	34.92	0.004	1.295	0.08
JB01-21_1-P3	33.623	0.002	1.663	0.074
JB01-21_2-P4	34.586	0.007	1.163	0.109
JB01-21_2-P5	34.989	0.012	1.234	0.094
JB01-21_2-P6	33.793	0	1.454	0.082
JB01-21_2-P7	33.379	0.008	1.68	0.065
JB01-21_2-P8	33.282	0.002	1.588	0.079
JB01-21_2-P9	33.534	0.005	1.51	0.114
JB01-21_2-P10	33.582	0.004	1.683	0.08
JB01-21_2-P11	33.543	0.011	1.711	0.086
JB01-21_2-P12	33.979	0.006	1.49	0.079
JB01-21_2-P13	33.943	0.006	1.5	0.087
JB01-21_2-P14	34.357	0.01	1.583	0.07
JB01-21_2-P15	33.864	0.003	1.454	0.081
JB01-21_2-P16	34.295	0.005	1.282	0.054
JB01-21_2-P17	34.123	0.013	1.172	0.058
JB01-21_3-P39	35.174	0.008	1.315	0.088
JB01-21_3-P40	35.26	0.005	1.351	0.101
JB01-21_3-P41	35.534	0	1.177	0.177
JB01-21_3-P42	34.189	0.008	1.604	0.077
JB01-21_3-P43	34.024	0.01	1.594	0.143
JB01-21_3-P44	34.024	0.001	1.491	0.16
JB01-21_3-P45	33.886	0.013	1.71	0.078
JB01-21_3-P46	34.457	0.007	1.479	0.083
JB01-21_3-P47	35.321	0.012	1.194	0.072
JB01-21_3-P48	34.243	0.007	1.477	0.071
JB01-21_3-P49	35.271	0.003	1.219	0.042
JB01-21_3-P50	34.939	0.008	1.451	0.078
JB01-21_3-P51	34.778	0.013	1.205	0.122
JB01-21_3-P52	34.854	0.01	1.411	0.087
JB01-21_4-P39	34.786	0.001	1.246	0.056
JB01-21_4-P40	35.048	0.011	1.248	0.046
JB01-21_4-P41	34.112	0	1.441	0.109
JB01-21_4-P42	34.382	0	1.476	0.17
JB01-21_4-P43	35.718	0.009	1.092	0.036
JB01-21_4-P44	36.227	0.02	0.914	0.078
JB01-21_4-P45	35.341	0.013	1.008	0.069
JB01-21_4-P46	33.588	0.016	1.553	0.147
JB01-21_4-P47	34.049	0.01	1.539	0.069
JB01-21_4-P48	35.864	0.001	0.932	0.098
JB01-21_4-P49	34.935	0.004	1.333	0.061
JB01-21_4-P50	35.11	0.007	1.31	0.038
JB01-21_4-P51	34.883	0.009	1.275	0.053

Sample	TiO_2 wt %	MnO wt %	FeO wt %	P_2O_5 wt %
JB01-21_4-P52	35.149	0.001	1.305	0.064
JB01-21_4-P53	34.567	0.001	1.226	0.103
JB01-21_4-P54	34.614	0.013	1.293	0.091
JB01-21_4-P55	34.462	0.001	1.287	0.118
JB01-21_4-P53	34.594	0.01	1.217	0.056
JB01-21_4-P54	34.241	0.007	1.43	0.124
JB01-21_4-P55	34.025	0.005	1.4	0.167
JB01-21_4-P56	35.599	0.015	1.062	0.062
JB01-21_4-P57	36.305	0.016	0.929	0.092
JB01-21_4-P58	36.291	0.006	0.951	0.108
JB01-21_4-P59	34.708	0.009	1.417	0.073
JB01-21_5-P60	34.667	0.013	1.295	0.083
JB01-21_5-P61	34.491	0.02	1.339	0.099
JB01-21_5-P62	34.846	0.012	1.238	0.149
JB01-21_5-P63	34.746	0.007	1.689	0.149
JB01-21_5-P64	34.084	0.011	1.59	0.093
JB01-21_5-P65	35.733	0.008	0.968	0.08
JB01-21_5-P66	35.123	0.006	1.453	0.098
JB01-21_5-P67	35.085	0.006	1.282	0.09
JB01-21_5-P68	35.022	0.014	1.235	0.088
JB01-21_5-P69	34.058	0	1.481	0.13

Sample	Nd ppm	Ce ppm	Y ppm	Zr ppm	La ppm	Gd ppm
HDJB01-2_8_P108	5347.68	9861.39	3014.21	540.2	2550.47	1649.2
HDJB01-2_8_P110	5570.5	11073.786	2998.47	547.6	2721.07	1762.04
HDJB01-2_8_P111	4953.46	10629.81	2841.07	732.6	2712.54	1588.44
HDJB01-2_8_P112	4593.52	10638.348	2927.64	791.8	2499.29	1631.84
HDJB01-2_8_P113	4773.49	10262.676	1928.15	636.4	2405.46	1388.8
HDJB01-2_8_P114	3839.36	9562.56	2447.57	865.8	2371.34	1206.52
HDJB01-2_8_P115	4679.22	10655.424	2156.38	888	2883.14	1432.2
HDJB01-2_8_P116	2905.23	8538	1817.97	606.8	2541.94	1232.56
HDJB01-2_8_P117	5347.68	12320.334	2919.77	710.4	3130.51	1718.64
HDJB01-2_8_P118	4859.19	12217.878	2770.24	592	3181.69	1588.44
HDJB01-2_8_P119	3205.18	9041.742	1676.31	488.4	2379.87	989.52
HDJB01-2_8_P120	2973.79	5105.724	1967.5	199.8	528.86	746.48
HDJB01-2_8_P121	3719.38	7940.34	1991.11	466.2	1953.37	1137.08
HDJB01-2_8_P122	1971.1	7223.148	1054.58	377.4	2064.26	807.24
HDJB01-2_8_P123	2339.61	8922.21	1290.68	717.8	2746.66	998.2
HDJB01-2_8_P124	2365.32	8742.912	1030.97	740	2840.49	963.48
HDJB01-2_8_P125	1928.25	3978.708	1125.41	407	366.79	434
HDJB01-2_8_P126	1474.04	6215.664	873.57	236.8	1791.3	633.64
HDJB01-2_8_P127	6461.78	13293.666	3447.06	932.4	3429.06	2161.32
HDJB01-2_8_P128	2091.08	6480.342	1762.88	399.6	1859.54	894.04
JB03-21_P1	6907.42	9024.666	5327.99	592	1586.58	2039.8
JB03-21_P2	6641.75	9161.274	5509	503.2	1740.12	2065.84
JB03-21_P3	6778.87	8990.514	5556.22	510.6	1595.11	1892.24
JB03-21_P4	6838.86	8853.906	5351.6	540.2	1731.59	1883.56
JB03-21_P9	1465.47	5669.232	763.39	384.8	1424.51	555.52
JB03-21_P11	4824.91	8708.76	3297.53	614.2	1876.6	1553.72
JB03-21_P12	6418.93	8947.824	5209.94	569.8	1714.53	1944.32
JB03-21_P13	7533.03	10049.226	6217.3	777	1910.72	2265.48
JB03-21_P14	6736.02	9135.66	5312.25	606.8	1723.06	1979.04
JB03-21_P15	3119.48	8307.474	1345.77	525.4	2081.32	1076.32
JB03-21_P16	1782.56	6932.856	897.18	377.4	1808.36	607.6
JB03-21_P17	8647.13	11893.434	6052.03	629	2260.45	2647.4
JB03-21_P18	4550.67	9741.858	2801.72	592	2243.39	1458.24
JB03-21_P19	5973.29	9767.472	4108.14	510.6	2081.32	1926.96
JB03-21_P20	1242.65	5609.466	889.31	481	1518.34	633.64
JB03-21_P21	3496.56	8452.62	2203.6	562.4	2013.08	980.84
JB03-21_P22	6076.13	9041.742	4840.05	606.8	1808.36	1866.2
JB03-21_P23	3385.15	2544.324	4777.09	333	127.95	1015.56
JB03-21_P24	3325.16	2595.552	5863.15	0	59.71	1345.4
JB03-21_P25	7207.37	9878.466	5446.04	503.2	2064.26	2352.28
JB03-21_P26	9152.76	13199.748	6225.17	740	2780.78	2916.48
JB03-21_P27	7044.54	9443.028	5351.6	495.8	1842.48	2265.48
JB03-21_P28	1902.54	6770.634	834.22	569.8	1816.89	746.48
JB03-21_P29	1285.5	5805.84	881.44	525.4	2106.91	529.48
JB03-21_P30	8184.35	12286.182	4958.1	540.2	2806.37	2343.6
JB03-21_P31	8672.84	11859.282	6311.74	917.6	2422.52	2847.04
JB03-21_P32	6247.53	9135.66	4722	599.4	1833.95	1987.72
JB03-21_P33	6624.61	9110.046	5579.83	673.4	1808.36	2074.52
JB03-22_1_P51	2219.63	6847.476	1086.06	436.6	1833.95	859.32
JB03-22_1_P52	1328.35	6096.132	810.61	444	1714.53	624.96
JB03-22_1_P53	1971.1	6668.178	857.83	488.4	1859.54	659.68
JB03-22_1_P54	2819.53	8341.626	1841.58	547.6	1816.89	789.88
JB03-22_1_P55	1739.71	4875.198	1652.7	392.2	1450.1	720.44
JB03-22_1_P56	1431.19	5643.618	905.05	444	1851.01	598.92

Sample	Nd ppm	Ce ppm	Y ppm	Zr ppm	La ppm	Gd ppm
JB03-22_1_P57	3059.49	8205.018	2211.47	599.4	1748.65	1111.04
JB03-22_1_P58	5107.72	10049.226	3045.69	606.8	2448.11	1492.96
JB03-22_1_P59	4310.71	8478.234	2337.39	673.4	1953.37	1232.56
JB03-22_1_P60	2348.18	7035.312	1204.11	599.4	1833.95	824.6
JB03-22_1_P61	1525.46	6121.746	952.27	421.8	1748.65	763.84
JB03-22_1_P62	1431.19	5387.478	1243.46	236.8	1501.28	616.28
JB03-22_1_P63	5124.86	10322.442	3148	614.2	2388.4	1423.52
JB03-22_1_P64	5047.73	10237.062	2864.68	658.6	2311.63	1657.88
JB03-22_1_P65	4936.32	9767.472	2911.9	740	2311.63	1406.16
JB03-22_1_P66	3710.81	6224.202	2628.58	495.8	665.34	998.2
JB03-22_1_P67	5450.52	11184.78	3187.35	769.6	2831.96	1770.72
JB03-22_1_P68	4670.65	9562.56	2604.97	643.8	2072.79	1449.56
JB03-22_1_P69	4130.74	8435.544	2589.23	606.8	1543.93	1267.28
JB03-22_1_P70	2013.95	6352.272	849.96	451.4	1893.66	668.36
JB03-22_1_P71	6238.96	8802.678	4470.16	695.6	1808.36	1918.28
JB03-22_1_P72	6590.33	9665.016	5516.87	821.4	1910.72	2143.96
JB03-22_1_P73	4764.92	8964.9	3525.76	562.4	1782.77	1466.92
JB03-22_1_P74	2013.95	7154.844	1015.23	436.6	1919.25	720.44
JB03-22_1_P75	8235.77	11645.832	6429.79	703	2328.69	2621.36
JB03-22_1_P77	8150.07	11765.364	6233.04	584.6	2431.05	2551.92
JB03-22_1_P78	7790.13	11919.048	4784.96	710.4	2772.25	2413.04
JB03-22_1_P79	7481.61	11509.224	4840.05	636.4	2729.6	2421.72
JB03-22_1_P80	8072.94	11372.616	6052.03	954.6	2559	2664.76
JB03-22_1_P81	7190.23	11372.616	5359.47	917.6	2294.57	2360.96
JB03-22_1_P82	7207.37	11389.692	5076.15	962	2456.64	2473.8
JB03-22_1_P83	7053.11	11176.242	4903.01	547.6	2490.76	2430.4
JB03-22_1_P84	7198.8	11526.3	4533.12	888	2755.19	2360.96
JB03-22_1_P85	4010.76	9178.35	2227.21	680.8	2439.58	1171.8
JB03-22_1_P86	2185.35	7197.534	1274.94	651.2	1833.95	894.04
JB03-23_1_P87	5313.4	8819.754	3887.78	658.6	1944.84	1683.92
JB03-23_1_P88	3128.05	2783.388	4611.82	0	102.36	1128.4
JB03-23_1_P89	6993.12	9588.174	5516.87	621.6	1816.89	2265.48
JB03-23_1_P91	6744.59	9169.812	5619.18	562.4	1731.59	2187.36
JB03-23_1_P92	6736.02	9536.946	5351.6	636.4	1765.71	2187.36
JB03-23_1_P93	3368.01	8631.918	1959.63	621.6	2089.85	1128.4
JB03-23_1_P94	6907.42	9494.256	5312.25	606.8	1833.95	2222.08
JB03-23_1_P95	7430.19	10424.898	5666.4	717.8	2183.68	2404.36
JB03-23_1_P96	8192.92	12585.012	5509	777	2934.32	2777.6
JB03-23_1_P97	8398.6	11799.516	5839.54	651.2	2405.46	2621.36
JB03-23_1_P98	7987.24	10954.254	5705.75	658.6	2175.15	2604
JB03-23_1_P99	8955.65	12388.638	5839.54	747.4	2789.31	2725.52
JB03-23_1_P100	8312.9	12192.264	5036.8	599.4	2678.42	2569.28
JB03-23_1_P101	8758.54	12337.41	6107.12	917.6	2738.13	2968.56
JB03-23_1_P102	6376.08	9391.8	5115.5	503.2	1833.95	2074.52
JB03-23_1_P103	8390.03	12234.954	6335.35	828.8	2516.35	2630.04
JB03-23_1_P104	5030.59	9024.666	3431.32	340.4	1833.95	1536.36
JB03-23_1_P105	3805.08	7692.738	2715.15	251.6	2106.91	1145.76
JB03-23_1_P106	5681.91	8298.936	4391.46	688.2	1646.29	1718.64
JB03-23_1_P107	7293.07	11662.908	5359.47	1050.8	2576.06	2465.12
JB03-22_3_P34	1422.62	5677.77	763.39	458.8	1492.75	677.04
JB03-22_3_P35	5973.29	8956.362	4761.35	606.8	1680.41	1874.88
JB03-22_3_P36	2082.51	1784.442	5548.35	14.8	0	1024.24
JB03-22_3_P38	4190.73	3039.528	5587.7	680.8	119.42	1275.96
JB03-22_3_P39	4002.19	8512.386	2785.98	695.6	1902.19	1145.76

Sample	Nd ppm	Ce ppm	Y ppm	Zr ppm	La ppm	Gd ppm
JB03-22_3_P40	1645.44	6881.628	1015.23	584.6	1944.84	789.88
JB03-22_3_P41	2785.25	8000.106	1991.11	451.4	1842.48	1041.6
JB03-22_3_P42	2828.1	3517.656	2817.46	0	85.3	876.68
JB03-22_3_P43	6067.56	9511.332	4729.87	532.8	1671.88	2057.16
JB03-22_3_P44	6873.14	10809.108	4965.97	473.6	2337.22	2187.36
JB03-22_3_P45	4559.24	9349.11	3037.82	629	2030.14	1527.68
JB03-22_3_P46	8047.23	11440.92	6162.21	673.4	2311.63	2690.8
JB03-22_3_P47	7970.1	11867.82	6280.26	703	2524.88	2760.24
JB03-22_3_P48	7978.67	11671.446	6225.17	651.2	2396.93	2621.36
JB03-22_3_P50	4404.98	3133.446	5933.98	0	136.48	1623.16
JB01-12_1-P70	1191.23	5336.25	417.11	407	1970.43	338.52
JB01-12_1-P71	2236.77	6172.974	936.53	592	1765.71	677.04
JB01-12_1-P72	2571	6113.208	1149.02	599.4	1646.29	781.2
JB01-12_1-P73	1936.82	5763.15	889.31	458.8	1560.99	807.24
JB01-12_1-P74	1594.02	4849.584	692.56	518	1433.04	659.68
JB01-12_1-P75	2296.76	5720.46	936.53	451.4	1535.4	755.16
JB01-12_1-P76	1568.31	4969.116	787	540.2	1458.63	703.08
JB01-12_1-P77	1388.34	4192.158	448.59	458.8	1364.8	581.56
JB01-12_1-P78	848.43	3850.638	377.76	547.6	1160.08	546.84
JB01-12_1-P79	797.01	3859.176	275.45	481	1194.2	329.84
JB01-12_1-P80	2253.91	5472.858	944.4	569.8	1646.29	633.64
JB01-12_1-P81	1534.03	4866.66	676.82	473.6	1407.45	503.44
JB01-12_1-P82	2211.06	5592.39	936.53	651.2	1586.58	711.76
JB01-12_1-P83	1945.39	5515.548	731.91	577.2	1552.46	720.44
JB01-12_1-P84	1628.3	5259.408	794.87	547.6	1569.52	651
JB01-12_2-P85	1482.61	4969.116	621.73	407	1595.11	581.56
JB01-12_2-P86	3308.02	7129.23	1558.26	569.8	1748.65	980.84
JB01-12_2-P87	2125.36	5882.682	1007.36	555	1714.53	633.64
JB01-12_2-P88	2862.38	6480.342	1172.63	547.6	1893.66	954.8
JB01-12_2-P89	2665.27	6394.962	1172.63	562.4	1663.35	894.04
JB01-12_2-P90	4739.21	8008.644	2305.91	629	1740.12	1397.48
JB01-12_2-P91	1276.93	4943.502	700.43	436.6	1535.4	503.44
JB01-12_2-P92	1696.86	5131.338	818.48	577.2	1458.63	607.6
JB01-12_2-P93	2502.44	6804.786	1054.58	599.4	1868.07	711.76
JB01-12_2-P94	3153.76	7410.984	1267.07	599.4	2013.08	920.08
JB01-12_2-P95	4319.28	8170.866	1912.41	540.2	2081.32	1380.12
JB01-12_2-P96	1431.19	4277.538	598.12	421.8	1501.28	512.12
JB01-12_2-P97	2245.34	6463.266	1109.67	555	1782.77	928.76
JB01-12_2-P98	1945.39	5822.916	983.75	473.6	1688.94	737.8
JB01-12_2-P99	2091.08	6096.132	1054.58	451.4	1808.36	824.6
JB01-12_2-P100	2271.05	6138.822	1093.93	421.8	1671.88	668.36
JB01-12_2-P101	3599.4	7146.306	1581.87	629	1748.65	1050.28
JB01-12_2-P102	2365.32	6121.746	936.53	466.2	1799.83	746.48
JB01-12_2-P103	1654.01	5404.554	787	614.2	1748.65	529.48
JB01-12_2-P104	1602.59	5225.256	613.86	621.6	1902.19	590.24
JB01-12_2-P105	1945.39	7078.002	810.61	762.2	2456.64	746.48
JB01-12_2-P106	2185.35	5942.448	1101.8	732.6	1671.88	772.52
JB01-12_2-P107	6770.3	10416.36	2959.12	629	2456.64	1926.96
JB01-12_3-P108	1714	5302.098	668.95	362.6	1518.34	694.4
JB01-12_3-P109	1696.86	5447.244	873.57	555	1578.05	512.12
JB01-12_3-P110	4327.85	7965.954	1636.96	695.6	2047.2	1345.4
JB01-12_3-P111	2519.58	7854.96	1030.97	614.2	2405.46	1041.6
JB01-12_3-P112	1791.13	5524.086	779.13	377.4	1535.4	494.76
JB01-12_3-P113	1088.39	4653.21	362.02	540.2	1415.98	546.84

Sample	Nd ppm	Ce ppm	Y ppm	Zr ppm	La ppm	Gd ppm
JB01-12_3-P114	1242.65	4781.28	472.2	429.2	1381.86	425.32
JB01-12_3-P115	719.88	4465.374	393.5	547.6	1424.51	425.32
JB01-12_3-P116	4216.44	8913.672	1542.52	599.4	2234.86	1163.12
JB01-12_3-P117	2459.59	6616.95	1086.06	429.2	1808.36	711.76
JB01-12_3-P118	2605.28	6668.178	912.92	503.2	1799.83	833.28
JB01-12_3-P119	4027.9	7530.516	1841.58	436.6	1953.37	1302
JB01-12_3-P120	522.77	3816.486	212.49	495.8	1202.73	269.08
JB01-12_3-P121	1825.41	6497.418	692.56	547.6	1970.43	677.04
JB01-12_3-P122	4576.38	9084.432	1778.62	577.2	2226.33	1223.88
JB01-12_3-P123	1491.18	4687.362	598.12	310.8	1373.33	529.48
JB01-21_1-P1	6513.2	10382.208	3085.04	577.2	2354.28	1848.84
JB01-21_1-P2	1516.89	5635.08	810.61	510.6	1697.47	572.88
JB01-21_1-P3	6564.62	10348.056	3258.18	629	2294.57	1866.2
JB01-21_2-P4	2091.08	5925.372	1684.18	473.6	1543.93	937.44
JB01-21_2-P5	1276.93	4781.28	550.9	525.4	1347.74	460.04
JB01-21_2-P6	3599.4	7880.574	1660.57	577.2	2055.73	1163.12
JB01-21_2-P7	4113.6	8205.018	1841.58	695.6	2030.14	1275.96
JB01-21_2-P8	4353.56	8367.24	1991.11	540.2	2013.08	1371.44
JB01-21_2-P9	6307.52	10126.068	3061.43	643.8	2286.04	1953
JB01-21_2-P10	4542.1	8444.082	2148.51	547.6	1978.96	1397.48
JB01-21_2-P11	4413.55	8759.988	2085.55	643.8	1970.43	1267.28
JB01-21_2-P12	3702.24	7940.34	1692.05	503.2	2004.55	1050.28
JB01-21_2-P13	2896.66	7462.212	1314.29	569.8	2115.44	963.48
JB01-21_2-P14	1259.79	5156.952	645.34	658.6	1450.1	486.08
JB01-21_2-P15	2519.58	6523.032	1455.95	503.2	1748.65	963.48
JB01-21_2-P16	1122.67	4747.128	716.17	288.6	1535.4	477.4
JB01-21_2-P17	1551.17	5080.11	1164.76	325.6	1851.01	564.2
JB01-21_3-P39	1628.3	5174.028	763.39	555	1492.75	564.2
JB01-21_3-P40	1345.49	5080.11	731.91	569.8	1467.16	538.16
JB01-21_3-P41	2588.14	7983.03	1125.41	614.2	2396.93	972.16
JB01-21_3-P42	3522.27	7410.984	1629.09	473.6	1978.96	1163.12
JB01-21_3-P43	4867.76	9408.876	2447.57	725.2	2379.87	1588.44
JB01-21_3-P44	5861.88	11534.838	2675.8	910.2	2976.97	1683.92
JB01-21_3-P45	4482.11	8367.24	2046.2	488.4	2141.03	1223.88
JB01-21_3-P46	2459.59	6172.974	1109.67	577.2	1663.35	911.4
JB01-21_3-P47	1088.39	4158.006	653.21	481	1236.85	572.88
JB01-21_3-P48	2451.02	6480.342	1644.83	370	1535.4	885.36
JB01-21_3-P49	1028.4	4704.438	590.25	421.8	1569.52	364.56
JB01-21_3-P50	2528.15	6403.5	1196.24	518	1671.88	598.92
JB01-21_3-P51	4216.44	10501.74	1566.13	532.8	3036.68	1449.56
JB01-21_3-P52	3042.35	6531.57	1392.99	703	1578.05	1006.88
JB01-21_4-P39	1516.89	5285.022	787	421.8	1586.58	624.96
JB01-21_4-P40	1105.53	5276.484	826.35	384.8	1560.99	494.76
JB01-21_4-P41	4919.18	9519.87	2699.41	695.6	2081.32	1536.36
JB01-21_4-P42	5827.6	10450.512	3029.95	569.8	2644.3	1788.08
JB01-21_4-P43	1285.5	5071.572	826.35	251.6	2089.85	546.84
JB01-21_4-P44	282.81	1656.372	31.48	96.2	452.09	43.4
JB01-21_4-P45	1431.19	4712.976	724.04	362.6	1620.7	468.72
JB01-21_4-P46	4190.73	10843.26	1991.11	1272.8	3147.57	1397.48
JB01-21_4-P47	1816.84	5993.676	920.79	392.2	1731.59	581.56
JB01-21_4-P48	0	2219.88	0	340.4	631.22	78.12
JB01-21_4-P49	1508.32	4926.426	692.56	251.6	1697.47	572.88
JB01-21_4-P50	1216.94	5105.724	661.08	370	1688.94	555.52
JB01-21_4-P51	1482.61	5370.402	771.26	333	1757.18	633.64

Sample	Nd ppm	Ce ppm	Y ppm	Zr ppm	La ppm	Gd ppm
JB01-21_4-P52	1636.87	5532.624	826.35	310.8	1637.76	555.52
JB01-21_4-P53	3787.94	7231.686	1959.63	555	1927.78	1275.96
JB01-21_4-P54	3582.26	7180.458	1951.76	621.6	1868.07	1154.44
JB01-21_4-P55	3445.14	6932.856	1699.92	562.4	1833.95	1163.12
JB01-21_4-P53	1456.9	5336.25	802.74	370	1782.77	494.76
JB01-21_4-P54	5047.73	9306.42	2660.06	532.8	2431.05	1614.48
JB01-21_4-P55	5510.51	10194.372	2896.16	673.4	2669.89	1675.24
JB01-21_4-P56	2159.64	5865.606	1078.19	414.4	1782.77	798.56
JB01-21_4-P57	8.57	1536.84	55.09	59.2	426.5	0
JB01-21_4-P58	205.68	2424.792	62.96	421.8	707.99	95.48
JB01-21_4-P59	728.45	3936.018	362.02	259	1245.38	295.12
JB01-21_5-P60	1534.03	5413.092	873.57	429.2	1450.1	468.72
JB01-21_5-P61	2219.63	5831.454	1164.76	481	1603.64	789.88
JB01-21_5-P62	3350.87	7863.498	1487.43	481	2260.45	1128.4
JB01-21_5-P63	3633.68	8324.55	1715.66	495.8	2576.06	1249.92
JB01-21_5-P64	5664.77	8683.146	3037.82	488.4	2089.85	1527.68
JB01-21_5-P65	2211.06	5652.156	920.79	325.6	1612.17	815.92
JB01-21_5-P66	3110.91	6856.014	1550.39	569.8	1791.3	998.2
JB01-21_5-P67	1988.24	6096.132	1101.8	510.6	1671.88	781.2
JB01-21_5-P68	2116.79	5874.144	1196.24	429.2	1526.87	685.72
JB01-21_5-P69	6898.85	11099.4	3384.1	466.2	2618.71	2031.12

REFERENCES

Ackerson, M.R., 2011, Trace element partitioning between titanite groundmass in silicic volcanic systems [M.S. Thesis]: University of North Carolina, Chapel Hill, 69 p.

Albarede, F., and Bottinga, Y., 1972, Kinetic disequilibrium in trace element partitioning between phenocrysts and host lava: Geochimica et Cosmochimica Acta, v. 36, p. 141–156, doi: 10.1016/0016-7037(72)90003-8.

Allègre, C.J., Provost, A., and Jaupart, C., 1981, Oscillatory zoning: a pathological case of crystal growth: Nature, v. 294, p. 223–228.

Bachmann, O., Dungan, M.A., and Lipman, P.W., 2002, The Fish Canyon Magma Body, San Juan Volcanic Field, Colorado: Rejuvenation and Eruption of an Upper-Crustal Batholith: Journal of Petrology, v. 43, p. 1469–1503, doi: 10.1093/petrology/43.8.1469

Bateman, P.C., 1992, Plutonism in the central part of the Sierra Nevada Batholith, California. US Geological Survey Professional Paper 1483

Beane, R., and Wiebe, R.A., 2012, Origin of quartz clusters in Vinalhaven granite and porphyry, coastal Maine: Contributions to Mineralogy and Petrology, v. 163, p. 1069–1082, doi: 10.1007/s00410-011-0717-1.

Blundy, J., and Wood, B., 2003, Partitioning of trace elements between crystals and melts: Earth and Planetary Science Letters, v. 210, p. 383–397, doi: 10.1016/S0012-821X(03)00129-8.

Cherniak, D.J., 2010, Diffusion in accessory minerals: zircon, titanite, apatite, monazite and xenotime: Reviews in Mineralogy and Geochemistry, v. 72, p. 827–869, doi: 10.2138/rmg.2010.72.18.

Cicconi, R.M., Giuli, G., Paris, E., Ertel-Ingrisch, W., Ulmer, P., and Dingwell, D.B., 2012, Europium oxidation state and local structure in silicate glasses: American Mineralogist, v. 97, p. 918–929, doi: 10.2138/am.2012.4041.

Coleman, D.S., Bartley, J.M., Glazner, A.F., and Pardue, M.J., 2012, Is chemical zonation in plutonic rocks driven by changes in source magma composition or shallow-crustal differentiation ? Geosphere, v. 8, p. 1568–1587, doi: 10.1130/GES00798.1.

Coleman, D.S., Gray, W., and Glazner, A.F., 2004, Rethinking the emplacement and evolution of zoned plutons: Geochronologic evidence for incremental assembly of the Tuolumne Intrusive Suite, California: Geology, v. 32, p. 433, doi: 10.1130/G20220.1.

Colombini, L.L., Miller, C.F., Gualda, G.A.R., Wooden, J.L., and Miller, J.S., 2011, Sphene and zircon in the Highland Range volcanic sequence (Miocene, southern Nevada, USA): Elemental partitioning, phase relations, and influence on evolution of silicic magma: Mineralogy and Petrology, v. 102, p. 29–50, doi: 10.1007/s00710-011-0177-3.

Coombs, D.S., Nakamura, Y., and Vuagnat, M., 1976, Pumpellyite-actinolite facies schists of the Taveyanne Formation near Loèche, Valais, Switzerland: Journal of Petrology, v. 17, p. 440–471, doi: 10.1093/petrology/17.4.440.

Deer, W. A., Howie, R. A. & Zussman, J. 1982, Orthosilicates, Rock- forming Minerals, vol. 1A, 2nd ed., 443-66. London: Longman Group Limited.

Drake, M.J., and Weill, D.F., 1975, Partition of Sr, Ba, Ca, Y, Eu^{2+}, Ee^{3+}, and other REE between plagioclase feldspar and magmatic liquid : An experimental study: Geochimica et Cosmochimica Acta, v. 39, p. 689–712, doi: 10.1016/0016-7037(75)90011-3.

Frost, B.R., Chamberlain, K.R., and Schumacher, J.C., 2000, Sphene (titanite): phase relations and role as a geochronometer: Chemical Geology, v. 172, p. 131–148.

Gao, X.Y., Zheng, Y.F., Chen, Y.X., and Guo, J., 2012, Geochemical and U-Pb age constraints on the occurrence of polygenetic titanites in UHP metagranite in the Dabie orogen: Lithos, v. 136-139, p. 93–108, doi: 10.1016/j.lithos.2011.03.020.

Gast, P.W., 1968, Trace element fractionation and the origin of tholeiitic and alkaline magma types: Geochimica et Cosmochimica Acta, v. 32, p. 1057–1086, doi: 10.1016/0016-7037(68)90108-7.

Glazner, A. F., Bartley, J. M., Law, B., and Coleman, D. S., 2011, The granite aqueduct and advection of water and heat through plutonic terranes: Abstract V14B-05 presented at 2011 Fall Meeting, AGU.

Glazner, A.F., and Johnson, B.R., 2013, Late crystallization of K-feldspar and the paradox of megacrystic granites: Contributions to Mineralogy and Petrology, v. 166, p. 777–799, doi: 10.1007/s00410-013-0914-1.

Graham, A.L., and Ringwood, A.E., 1971, Lunar basalt genesis: the origin of the europium anomaly: Earth and Planetary Science Letters, v. 13, p. 105–115, doi: 10.1016/0012-821X(71)90111-7.

Gray, W., 2003, Chemical and thermal evolution of the late Cretaceous Tuolumne Intrusive Suite, Yosemite National Park, California [Ph. D thesis]: University of North Carolina, Chapel Hill, 202 p.

Green, T.H., 1994, Experimental studies of trace-element partitioning applicable to igneous petrogenesis --Sedona 16 years later: Chemical Geology, v. 117, p. 1–36.

Green, T.H., and Pearson, N.J., 1986, Rare-earth element partitioning between sphene and coexisting silicate liquid at high pressure and temperature: Chemical Geology, v. 55, p. 105–119, doi: 10.1016/0009-2541(86)90131-2.

Gromet, L., and Silver, L.T., 1983, Rare earth element distributions among minerals in a granodiorite and their petrogenetic implications: Geochimica et Cosmochimica Acta, v. 47, p. 925–939, doi: 10.1016/0016-7037(83)90158-8.

Heinrich, C.A., Pettke, T., Halter, W.E., Aigner-Torres, M., Audétat, A., Günther, D., Hattendorf, B., Bleiner, D., Guillong, M., and Horn, I., 2003, Quantitative multi-element analysis of minerals, fluid and melt inclusions by laser-ablation inductively-coupled-plasma mass-spectrometry: Geochimica et Cosmochimica Acta, v. 67, p. 3473–3496, doi: 10.1016/S0016-7037(03)00084-X.

Higgins, J.B., and Ribbe, P.H., 1976, The crystal chemistry and space groups of natural and synthetic titanites: American Mineralogist, v. 61, p. 878–888.

Jarosewich, E., 2002, Smithsonian microbeam standards: Journal of Research of the National Institute of Standards and Technology, v. 107, p. 681–685, doi: 10.6028/jres.107.054.

L'Heureux, I., and Fowler, A.D., 1996, Isothermal constitutive undercooling as a model for oscillatory zoning in plagioclase: The Canadian Mineralogist, v. 34, p. 1137–1147.

Lipman, P.W., 1971, Iron-titanium oxide phenocrysts in compositionally zoned ash-flow sheets from Southern Nevada: The Journal of Geology, v. 79, p. 438–456.

Mahood, G., and Hildreth, W., 1983, Large partition coefficients for trace elements in high-silica rhyolites: Geochimica et Cosmochimica Acta, v. 47, p. 11–30.

McIntire, W.L., 1963, Trace element partition coefficients—a review of theory and applications to geology: Geochimica et Cosmochimica Acta, v. 27, p. 1209–1264, doi: 10.1016/0016-7037(63)90049-8.

Mutchler, S.R., Fedele, L., and Bodnar, R.J., 2008, Analysis Management System (AMS) for reduction of Laser Ablation ICM-MS data: Mineralogical Association of Canada Short Course Series, v. 40, p. 318–327.

Nakada, S., 1991, Magmatic processes in titanite-bearing dacites, central Andes of Chile and Bolivia: American Mineralogist, v. 76, p. 548–560.

Olin, P.H., and Wolff, J. a., 2012, Partitioning of rare earth and high field strength elements between titanite and phonolitic liquid: Lithos, v. 128-131, p. 46–54, doi: 10.1016/j.lithos.2011.10.007.

Pamukcu, A.S., Carley, T.L., Gualda, G.A.R., Miller, C.F., and Ferguson, C.A., 2013, The evolution of the Peach Spring giant magma body: evidence from accessory mineral textures and compositions, bulk pumice and glass geochemistry, and Rhyolite-MELTS modeling: Journal of Petrology, v. 54, p. 1109–1148, doi: 10.1093/petrology/egt007.

Paterson, B. A., and Stephens, W.E., 1992, Kinetically induced compositional zoning in titanite: implications for accessory-phase/melt partitioning of trace elements: Contributions to Mineralogy and Petrology, v. 109, p. 373–385, doi: 10.1007/BF00283325.

Perugini, D., De Campos, C.P., Ertel-Ingrisch, W., and Dingwell, D.B., 2012, The space and time complexity of chaotic mixing of silicate melts: Implications for igneous petrology: Lithos, v. 155, p. 326–340, doi: 10.1016/j.lithos.2012.09.010.

Petford, N., 2003, The rheology of granitic magmas during ascent and emplacement: Annual Review of Earth and Planetary Sciences, v. 31, p. 399–427, doi: 10.1146/annurev.earth.31.100901.141352.

Piccoli, P., Candela, P., and Rivers, M., 2000, Interpreting magmatic processes from accessory phases: titanite—a small-scale recorder of large-scale processes: Transactions of the Royal Society of Edinburgh: Earth Sciences, v. 91, p. 257–267, doi: 10.1017/S0263593300007422.

Prowatke, S., and Klemme, S., 2005, Effect of melt composition on the partitioning of trace elements between titanite and silicate melt: Geochimica et Cosmochimica Acta, v. 69, p. 695–709, doi: 10.1016/j.gca.2004.06.037.

Ribbe, P. H. 1982. Titanite. In Ribbe, P. H. ed. Reviews in Mineralogy, vol. 5, Orthosilicates, 2nd ed., 137-54. Washington, D.C.: Mineralogical Society of America.

Rollinson, Hugh R. Using Geochemical Data: Evaluation, Presentation, Interpretation. Harlow, Essex, England: Longman Scientific & Technical, 1993.

Sahama, T., 1946, On the chemistry of the mineral titanite: Bulletin de la Commission Geologique de Finlande, v. 138, p. 88–120.

Smith, A.L., 1970, Sphene, perovskite and coexisting Fe-Ti oxide minerals: American Mineralogist, v. 55, p. 264–269.

Sun, S. -s., and McDonough, W.F., 1989, Chemical and isotopic systematics of oceanic basalts: implications for mantle composition and processes: Geological Society, London, Special Publications, v. 42, p. 313–345, doi: 10.1144/GSL.SP.1989.042.01.19.

Taylor, S.R., and McLennan, S.M., 1995, The geochemical evolution of the continental crust: Reviews of Geophysics, v. 33, p. 241–265, doi: 10.1029/95RG00262.

Tiepolo, M., Oberti, R., and Vannucci, R., 2002, Trace-element incorporation in titanite: constraints from experimentally determined solid/liquid partition coefficients: Chemical Geology, v. 191, p. 105–119, doi: 10.1016/S0009-2541(02)00151-1.

Vogt, J.H.L., 1921, The Physical Chemistry of the Crystallization and Magmatic Differentiation of Igneous Rocks: The Journal of Geology, v. 29, p. 318–350.

Watson, E.B., 1976, Two-liquid partition coefficients: Experimental data and geochemical implications: Contributions to Mineralogy and Petrology, v. 56, p. 119–134, doi: 10.1007/BF00375424.

Watson, E.B., and Liang, Y., 1995, A simple model for sector zoning in slowly grown crystals : Implications for growth rate and lattice diffusion, with emphasis on accessory minerals in crustal rocks: American Mineralogist, v. 80, p. 1179–1187.

Watson, E.B., and Müller, T., 2009, Non-equilibrium isotopic and elemental fractionation during diffusion-controlled crystal growth under static and dynamic conditions: Chemical Geology, v. 267, p. 111–124, doi: 10.1016/j.chemgeo.2008.10.036.

Whitney, J.A., and Stormer, J.C., 1985, Mineralogy, petrology, and magmatic conditions from the Fish Canyon Tuff, Central San Juan Volcanic Field, Colorado: Journal of Petrology, v. 26, p. 726–762, doi: 10.1093/petrology/26.3.726.

Wiebe, R.A., 1968, Plagioclase stratigraphy: a record of magmatic conditions and events in a granite stock: American Journal of Science, v. 266, p. 690–703.

Wones, D.R., 1989, Significance of the assemblage titanite+magnetite+quartz in granitic rocks: American Mineralogist, v. 74, p. 744–749.

Vance, J.A., 1969, On Synneusis: Contributions to Mineralogy and Petrology, v. 24, p. 7–29.